NATIONAL AERONAUTICS AND SPACE ADMINISTRATION

Space Programs Summary No. 37-32, Volume VI

for the period January 1, 1965 to February 28, 1965

Space Exploration Programs and Space Sciences

jpl   JET PROPULSION LABORATORY
CALIFORNIA INSTITUTE OF TECHNOLOGY
PASADENA, CALIFORNIA

March 31, 1965

NATIONAL AERONAUTICS AND SPACE ADMINISTRATION

Space Programs Summary No. 37-32, Volume VI

for the period January 1, 1965 to February 28, 1965

Space Exploration Programs and Space Sciences

JET PROPULSION LABORATORY
CALIFORNIA INSTITUTE OF TECHNOLOGY
PASADENA, CALIFORNIA

March 31, 1965

Preface

The *Space Programs Summary* is a six volume, bimonthly publication designed to report on JPL space exploration programs, and related supporting research and advanced development projects. The subtitles of all volumes of the *Space Programs Summary* are:

Vol. I. The Lunar Program (Confidential)

Vol. II. The Planetary–Interplanetary Program (Confidential)

Vol. III. The Deep Space Network (Unclassified)

Vol. IV. Supporting Research and Advanced Development (Unclassified)

Vol. V. Supporting Research and Advanced Development (Confidential)

Vol. VI. Space Exploration Programs and Space Sciences (Unclassified)

The *Space Programs Summary*, Volume VI consists of an unclassified digest of appropriate material from Volumes I, II, and III; an original presentation of the JPL (1) quality assurance and reliability efforts, and (2) environmental- and dynamic-testing facility-development activities; and a reprint of the space science instrumentation studies of Volumes I and II. This instrumentation work is conducted by the JPL Space Sciences Division and also by individuals of various colleges, universities, and other organizations. All such projects are supported by the Laboratory and are concerned with the development of instruments for use in the NASA space flight programs.

W. H. Pickering, *Director*
Jet Propulsion Laboratory

Contents

Contents (Cont'd)

LUNAR PROGRAM

I. *Ranger* Project

A. Introduction

The *Ranger* Project was established to develop a space flight technology for transporting engineering and scientific instruments to the Moon and planets. Of the nine *Ranger* launchings, using *Atlas D–Agena B* vehicles, now planned, eight flights have been made.

Rangers I and *II* (Block I) were not lunar-oriented, but were engineering evaluation flights to test the basic systems to be employed in later lunar and planetary missions. Several scientific experiments were carried on a noninterference basis. Both spacecraft performed satisfactorily within the constraints of the obtained satellite orbit. *Rangers III, IV,* and *V* (Block II) carried a gamma-ray instrument, a TV camera, and a rough-landing seismometer capsule; each of these flights experienced failures.

The objective of the *Ranger* Block III (*Rangers VI, VII, VIII,* and *D*)[1] flights is to obtain pictures of the lunar surface, at least an order of magnitude better than those obtainable with Earth-based photography, which will be

of benefit to both the scientific program and the U.S. manned lunar flight program. The *Ranger VI* spacecraft, which was launched from the Air Force Eastern Test Range (AFETR) on January 30, 1964, and impacted the Moon essentially on target on February 2, 1964, did not accomplish the primary flight objective due to a failure of the TV subsystem to transmit pictures. An extensive analysis of the TV subsystem failure was conducted, new and reworked hardware was assembled as the *Ranger VII* TV subsystem, and extensive testing of the reassembled TV subsystem was performed. The *Ranger VII* spacecraft was launched from the AFETR on July 28, 1964, and impacted the Moon on target on July 31, 1964. The mission flight objective was accomplished. The outstanding events of the mission were the precision of the trajectory correction and the transmission of 4304 video pictures of the lunar surface. The *Ranger VIII* spacecraft was launched from the AFETR on February 17, 1965, and impacted the Moon on target on February 20, 1965. The mission flight objective was again accomplished, and approximately 7000 high-quality video pictures of the lunar surface were transmitted from the spacecraft. The final calculated impact point represented a miss of only 15 miles from the originally selected aiming point. At the end of the reporting period, *Ranger D* was undergoing preflight testing at the AFETR; all operations were on schedule.

---

[1] *Ranger D* is the designation for the spacecraft which completes the *Ranger* Block III Project.

B. Spacecraft Assembly and Test Operations

1. Ranger VIII

The *Ranger C (Ranger VIII)* spacecraft was prepared for shipment to the AFETR after the final electrical test at JPL was completed on December 30, 1964. A six-van convoy carrying the spacecraft, flight spares, and operational support equipment (OSE) left Pasadena on January 4, 1965, and arrived at Building AO (Spacecraft Checkout Facility 2) at the AFETR on January 8. Setup of the OSE was performed from January 9 to 13. The Explosive Safe Facility (ESF) equipment trailer and OSE arrived January 12. This equipment was shipped separately because it was needed for the *Ranger D* dummy run tests at JPL. *Ranger C* test operations at the AFETR were performed in the following sequence:

Initial test and assembly operations at Building AO (January 8–24): TV operational checkout (no 890-Mc RF interference observed); TV turn-on backup clock test; installation of gyros, gyro electronics, midcourse accelerometer modules, and the Case VI instrumentation accelerometer; installation of TV subsystem on spacecraft bus; backup functions system test; RF-link no-cables test; solar panel checkout; and antenna yoke and Sun shade actuation test.

Initial test and assembly operations at the ESF (January 25–31): attitude-control high-pressure leak test; installation of midcourse motor; checkout of ESF dummy run trailer; TV subsystem full-power test; autopilot test; midcourse motor transducer checkout; matchmate of *Agena* adapter and shroud to spacecraft; determination of gap from omni-antenna to shroud omni-antenna coupler; pressurization of attitude-control gas subsystem for the joint flight-acceptance composite test (J-FACT); and electrical test of the spacecraft before movement to Launch Complex 12.

Initial tests at Launch Complex 12 (February 1, 2): spacecraft mate to *Atlas–Agena* launch vehicle; precountdown and countdown dummy run tests; J-FACT; and demate from *Atlas–Agena*.

Final test and assembly operations at Building AO (February 3–8): midcourse motor and TV subsystem demate; TV camera final calibration and alignment checks; hydraulic timer, Earth detector, and solar panel damper bench checks; thermal-control-surface cleaning and di-mension checks; spacecraft bus inspection; thermal-control-surface emissometer checkout; TV subsystem quality-assurance inspection; TV subsystem functional test; TV subsystem mate to spacecraft bus; final system test; and demate of TV subsystem and midcourse motor.

Final test and assembly operations at the ESF (February 9–14): battery continuity checkout; secondary Sun sensor checkout; installation of flight jet nozzles; installation and test of high-gain antenna; midcourse motor fueling; thermal shield installation; pyrotechnics checkout; midcourse motor and TV subsystem installation; TV full-power test; autopilot test; midcourse motor transducer checkout; solar panel pinpuller installation; weight and center-of-gravity determination; final spacecraft matchmate to *Agena* adapter and shroud; final flight pressurization of attitude-control gas subsystem; final ESF mechanical assembly verification and inspection; and final ESF electrical test.

Final tests and countdown operations at Launch Complex 12 (February 15–17): spacecraft mate to *Atlas–Agena* launch vehicle; precountdown test; dummy run countdown; and launch countdown.

Ranger VIII (Ranger C) was successfully launched on February 17, 1965, at 17:05:00.795 GMT at the beginning of the launch window. No holds resulted from spacecraft malfunction.

2. Ranger D

The precountdown and countdown dummy runs for the *Ranger D* spacecraft were satisfactorily completed at JPL on December 30. A discrepancy in the communications automatic-gain-control value noted during the tests was investigated on December 31 and January 2. The methods used to measure the receiver sensitivity and the external test equipment used were found to be the causes of the discrepancy.

On January 4 and 5, attitude-control gas subsystem and midcourse motor pressure transducer calibrations were performed. The $-x$ solar panel/TV arm microswitch assembly was replaced as a result of its shaft being bent during mechanical fit checks of the spare solar panels. The spacecraft gyros and gyro electronics were removed and bench-checked in the attitude-control laboratory because of an uncertainty concerning their calibration. A

new circulator was installed in the communications subsystem to provide better electrical isolation between the omni-antenna and directional antenna cavities.

During a pyrotechnics verification test performed January 6, the flight-type pyrotechnics were actuated in a simulated normal flight sequence during which all OSE cables were disconnected. A weight and center-of-gravity test was satisfactorily completed on January 7.

Vibration tests were performed at the Environmental Test Laboratory, JPL Building 144, from January 8 to 13. The test sequence was as follows: x-axis modal verification, x-axis vibration, y-axis vibration, torsional vibration, z-axis vibration, and x-axis modal vibration. The only anomalies noted during the sequence were slight overtests during the y-axis noise vibration (about 2% too high for 20 sec) and during the sinusoidal y-axis vibration (0.5 g too high at 20 cps for 15 sec). The effect of the over-tests was investigated, and System Test 4, the postvibration system test, was then performed on January 14 without incident.

After several days of preparation, the spacecraft was moved to JPL Building 150 for a series of mission tests in the 25-ft Space Simulator. The premission verification test and high- and low-temperature mission tests were performed from January 18 to 25. The following problems were noted during both mission tests:

(1) A small offset was noted on the hardline monitor of the pitch and yaw Sun sensor error signals before central computer and sequencer (CC&S) Command A-4. Investigations in the CC&S laboratory and on the proof test model indicated that the offset was normal even though it had not been observed previously.

(2) Fluctuations in communications automatic gain control were observed and determined to be caused by test transmitter variations, changes in the air link to the omni-antenna, and a connector failure of the 960-Mc omni-antenna probe cable due to temperature variation during the first mission test.

On January 26, the spacecraft was removed from the 25-ft Space Simulator and prepared for the RF-link test. Upon completion of a solar simulation lamp intensity measurement and a verification test of the spacecraft, the RF-link test was performed on January 27 and 28. The only problem encountered was a failure of the 890-Mc probe cable OSE. The directional antenna deploy/TV

RF-interference test was performed on January 30 at the Spacecraft Assembly Facility (SAF). No interference with TV pictures resulting from spacecraft bus RF radiation was observed.

Postenvironmental inspection of the spacecraft was performed by quality-assurance personnel at the SAF between February 1 and 10. During this period a number of subsystem laboratory tests and calibrations were also performed, including an attitude-control gas subsystem leak test; a secondary Sun sensor checkout; measurement of the voltage standing-wave ratio of the omni-antenna, directional antenna, and associated cables; and a test of the TV subsystem shutter operation against a 1-g field (TV subsystem turned upside down).

System Test 5, the preshipment system test, was performed at the SAF on February 11. Higher-than-desired 3.5-kc noise was observed on TV Camera F_a. This noise had been observed previously, and, as a result of an investigation of the problem on February 12, it was determined that the noise was not the result of spacecraft failure.

The *Ranger D* spacecraft left JPL in a two-van convoy on February 18 and arrived at the AFETR on February 22. Upon arrival at the AFETR, the spacecraft bus was unloaded at the ESF and was inspected for damage in shipment. The midcourse motor was removed from the spacecraft, and the attitude-control gas subsystem was pressurized for a leak test. The TV subsystem and its OSE were unloaded at Building AO.

During a TV subsystem postshipment test performed February 23, camera shutter operation was verified while the subsystem was rightside up and upside down. In addition, the flight TV subsystem batteries were checked for mechanical fit, and the TV backup clock was started for the 66-hr clock test. The attitude-control leak test on February 25 revealed that the gas subsystem leak rate was less than 30 cm^3/hr. On February 25, the spacecraft bus was moved from the ESF to Building AO, where Case II, gyros, gyro electronics, and accelerometers were installed and emissometer tests of the thermal-control surfaces were begun. The midcourse motor and system-test batteries were installed on February 26, and a test of the TV subsystem indicated normal operation of Cameras F and P. Installation of the Teflon thermal shield and preflight installation of the top hat, omni-antenna, TV subsystem, and attitude-control nitrogen tanks were completed February 27.

C. Space Flight Operations

1. Preflight Preparation for the Ranger VIII Mission

During January and February 1965, the *Ranger* Space Flight Operations (SFO) System conducted all of its testing in preparation for the *Ranger VIII* mission. An extensive test schedule was possible due to the large time span between the *Ranger VII* mission and the beginning of *Ranger VIII* (*Ranger C*) spacecraft testing. The SFO tests may be categorized as follows:

Compatibility test. The SFO Facility–*Ranger VIII* spacecraft compatibility test, conducted December 28, 1964, proved valuable in familiarizing the Spacecraft Data Analysis Team (SDAT) with *Ranger VIII* data from the "live" spacecraft.

Acceptance tests. Acceptance Tests 1 and 2 were designed to ensure the acceptability of the SDAT and Flight Path Analysis and Command (FPAC) Group programs throughout the data-processing system. Both tests proved satisfactory, and only a few minor program problems were encountered and were subsequently resolved.

Acceptance Tests 3 and 4 were designed to familiarize the SDAT and FPAC Group with the SFO Facility and data-processing procedures. These also proved satisfactory, with only minor procedural problems experienced.

Acceptance Tests 5, 6, and 7 were designed to train the Goldstone Echo, Woomera, and Johannesburg Tracking Station personnel in *Ranger* tracking and telemetry-processing. All stations performed quite satisfactorily, and adequate support for the *Ranger VIII* mission was indicated.

For Acceptance Test 8, the command procedures test, each station was exercised six times in the receipt, verification, and transmission of spacecraft commands. All stations performed well, but a serious communications problem caused partial loss of the command message during transmission to the Johannesburg Tracking Station. The problem was later found to have been caused by an equipment failure at an overseas relay site.

Acceptance Test 9 was designed and performed by the SFO Facility communications personnel to exercise transmission lines to and from the Air Force Eastern Test Range (AFETR), Woomera Tracking Station, and Johannesburg Tracking Station with *Ranger* tracking and telemetry data.

Integration tests. Integration Tests 1 and 2 were in-house training tests for the combined SDAT and FPAC Group. SDAT procedural problems experienced in Test 1 were well resolved in Test 2.

Integration Tests 3 and 4 were performed with Deep Space Instrumentation Facility participation. Performance by all units was generally good, but corrective work was required in some areas. Data simulation caused several minor problems which were expected to be resolved for future tests.

Verification tests. Scheduling difficulties were experienced during Verification Test 1, causing AFETR support for Phases I and II to be cancelled for 24 hr. Phases II (without AFETR support), III, and IV were performed on the scheduled date, and all systems functioned very well. The AFETR data transmission test on the following day did not prove satisfactory, and it was hoped that AFETR performance would be satisfactory in Verification Test 2. Although the AFETR was still somewhat slow in providing computed data during Verification Test 2, performance was satisfactory in all areas.

It was decided in late-January that the SFO Facility would support the AFETR simulated launch for *Ranger VIII*, which was to be followed by an AFETR data transmission test. However, the AFETR cancelled the simulated launch due to booster vehicle difficulties, and only the data transmission test was conducted. All problems and procedural difficulties were satisfactorily resolved by this test.

It was felt that the test philosophy used for the preparation of *Ranger VIII* mission readiness was more than adequate in preparing all systems for the flight. Each test accomplished its objectives and pointed out deficiencies which were resolved prior to subsequent tests. The SFO Director concluded that the SFO System was prepared to support the mission by the successful conclusion of the last verification test.

D. *Ranger VIII* Power Subsystem Performance

The three major elements of the power subsystem—silver–zinc batteries, solar panel arrays, and the conversion equipment—operated as predicted throughout the

various phases of the mission. The batteries provided system power from launch to initial Sun acquisition and also during part of the midcourse maneuver. Spacecraft power was supplied by the solar panels during the remaining portions of the mission. The conversion equipment transformed the system input power to the voltage and current requirements of the individual spacecraft subsystems.

Solar panels. Shroud ejection at 17:10:14 GMT was indicated by an increase in solar panel voltages resulting from exposure to ambient space illumination. The amount of incident energy on the panels was enough to provide a change in the telemetry transducer, but was insufficient to provide any significant power to the spacecraft.

The raw power load supplied by the solar panels during the cruise portions of the flight was 138 w. Telemetry data showed a slight unbalance in the solar panel currents (0.3 amp), which agrees with the preflight test measurements performed on each panel.

At approximately 1 hr prior to impact, the panel temperatures began to increase due to intercepted radiant energy reflected from the lunar surface. Just prior to impact, the panel temperatures were reading 16°F higher than the cruise temperatures. These data were in close agreement with data from the *Ranger VII* flight.

Batteries. Battery capacity at launch was 86 amp-hr, and 10 amp-hr was used during the flight. As in the *Ranger VI* and *VII* missions, only a small percentage of the available capacity was utilized: approximately 15.5%. This amount of usage did not provide sufficient data to determine actual maximum capacity.

II. *Surveyor* Project

A. Introduction

The *Surveyor* Project will be the next step in developing lunar technology. It will attempt soft landings on the Moon with a group of test missions whose objective is to demonstrate successful soft landing by post-landing spacecraft operation. An engineering payload including elements of redundancy, increased diagnostic telemetry, touchdown instrumentation, and survey TV will be used.

Following the test missions, the general objective is to conduct lunar exploration to extend our knowledge of the nature of the Moon and to discover and verify the suitability of sites for *Apollo* spacecraft landings. These flights will carry a scientific payload consisting of the following experiments: two-camera TV, micrometeorite ejecta, single-axis seismometer, alpha-particle scattering, soil properties (surface sampler), and touchdown dynamics.

The spacecraft will be injected into the lunar trajectory using *Atlas–Centaur* vehicles. A 50-m/sec midcourse correction capability will exist.

Surveyor Mission A is scheduled for launch during the latter part of 1965. The primary objective for this flight will be to demonstrate successful operation of the launch vehicle, spacecraft, space flight operations, Deep Space Instrumentation Facility, and ground communications from launch through the completion of the midcourse maneuver. The secondary objective will be the successful operation of the spacecraft from the midcourse maneuver through landing. The tertiary objective will be to accomplish spacecraft functions after landing.

Hughes Aircraft Company (HAC) is under contract to develop and manufacture the first seven flight spacecraft.

B. Systems Testing

1. T-21 Prototype System-Test Spacecraft

In preparation for solar-thermal-vacuum testing at HAC, thermal instrumentation was installed on the T-21 prototype vehicle, the main retrorocket dummy and the altitude marking radar were mated to the vehicle, and the vehicle was installed on the vacuum chamber end bell. Power was applied to the vehicle, and power-on calibration of the vehicle and associated test equipment was performed.

A system readiness test and a dry-run mission sequence were initiated. Numerous problems were encountered, primarily with the test equipment; e.g., a failure of the power profile monitor resulted in damage to the boost regulator. Considerable difficulty was also encountered with closed-loop simulation of terminal descent. This simulation was the first attempt at closing the loops around both the flight-control and the radar altimeter and doppler velocity sensors. Several minor design changes were necessary before a successful run was achieved.

Compartment covers, thermal switches, shadow shrouds, and other equipment were then installed. Pump-down was initiated, and the functional environmental test followed immediately. This test consisted of a 66-hr real-time mission simulation, a 12-hr thermal test, a 30-hr mission sequence at high temperature, and a 30-hr mission sequence at low temperature. The test was completed, even though a malfunction of the flight-control electronics unit caused some difficulty. Preliminary results showed that most temperatures were within the predicted ranges.

2. SC-1 Flight Spacecraft

The SC-1 flight spacecraft completed upgrading operations at HAC and was readied for system testing. Group tests, in which the various subsystems are individually tested with their associated test equipment, were completed. No major spacecraft problems were encountered. System-test-equipment-assembly–spacecraft interface problems were all resolved. The next test phase, initial system checkout, is under way. This test phase involves the integration of the various spacecraft subsystems, e.g., spacecraft power with flight control.

3. SC-2 Flight Spacecraft

System testing of the SC-2 flight spacecraft (Fig. 1) was conducted at HAC. Group tests were completed on the power subsystem, the TV cameras, and the command decoder unit utilizing spacecraft power. No major spacecraft problems were encountered. System-test-equipment-assembly–spacecraft interface problems were all resolved.

4. T-2 Descent-Test Vehicles

The descent-test program involving the release of a test spacecraft from a tethered balloon at the Air Force Missile Development Center (AFMDC) was reoriented, and a program plan incorporating revised test objectives
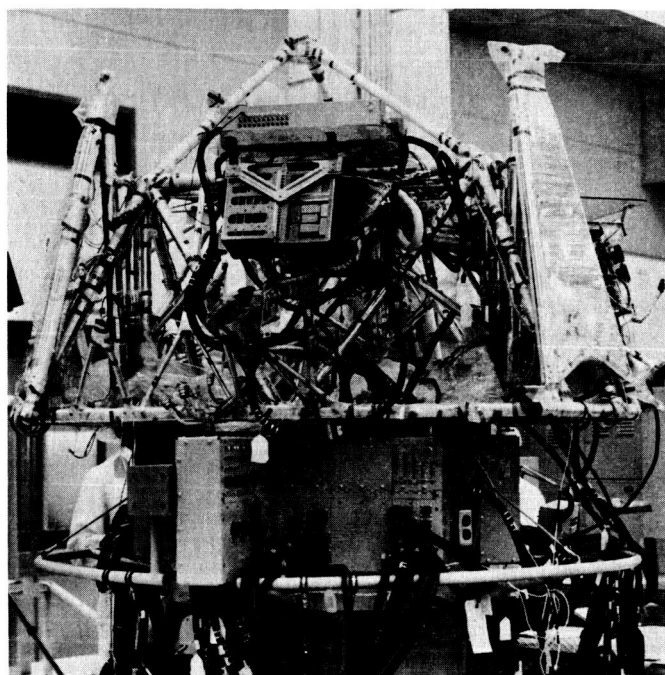
Fig. 1. SC-2 flight spacecraft

was prepared. The revised program will employ the T-2NR recovery-test vehicle [a modified T-2S (T-2 spare) configuration] and two new descent-test vehicles, T-2N-1 and T-2N-2.

5. SD-1 Dynamics-Test Flight Model

The integrated combined system test and flight-acceptance composite test of the SD-1 vehicle were completed at General Dynamics/Astronautics. Calibration of instrumentation, vehicle cleanup, and final acceptance tests were performed. The vehicle was then shipped to the Air Force Eastern Test Range on January 21, 1965. Postshipment inspection revealed no damage to the vehicle resulting from shipment.

6. S-2B Test Model

The S-2B test model is the S-2 spaceframe with the latest SC-1 payload installations. After the completion of upgrading operations, static testing will be conducted on the S-2B test model to: (1) demonstrate the capability of the *Surveyor* spacecraft to meet the specified functional requirements dependent on structural load deformations, and (2) verify the adequacy of structural subsystems under critical load conditions that were not simulated during the type-approval vibration or drop tests.

C. Flight Control

1. Acceleration-Control-Loop Structural Coupling

The spacecraft structural qualification vehicle S-2A was used to measure the extent of structural coupling into the acceleration control loop during vernier-engine firing. The attitude-control loops are not significantly affected due to the use of gyros as position-sensing elements and the low control-loop gain at structural frequencies.

Transmissibility levels were measured from the vernier-engine mounting brackets to the accelerometer in the inertial reference unit to determine if structural resonances provided an equivalent control system gain increase of sufficient magnitude to cause an unstable condition. The S-2A vehicle was supported by means of an elastic suspension system, and input forces were applied at each of the three vernier-engine mounting brackets with modal shakers capable of supplying up to 7 lb(f). Data were obtained with the vehicle in the terminal-descent configuration (no retro-engine) for various positions of the planar array and solar panel.

Additional tests are planned to simulate the effect of unsymmetrical engine thrust and to better define the problem.

2. Acquisition Sun Sensor

Flight-acceptance tests were completed on the first flight model of the acquisition Sun sensor. The unit was integrated into the sensor-group wiring harness and is undergoing additional tests as part of the flight-control sensor group.

Since extensive circuit modifications of the flight-control programmer are required, it was decided to use the solar-panel-deployment signal for the initiation of automatic Sun acquisition on the first two flight models of the sensor group. (Originally it was planned to use a signal generated within the programmer.) The necessary programmer changes will be incorporated in the third and subsequent flight models of the sensor group. The acquisition sequence for the first two spacecraft will be as follows:

(1) The separation signal will cause the solar panel to be stepped to the transit position and locked.

(2) Completion of this sequence will result in a solar-panel-deployment indication signal generated in the boost regulator.

(3) Upon receipt of this signal, the flight-control programmer will supply a signal to the logic circuits initiating a negative roll maneuver.

(4) The roll maneuver will continue until the acquisition Sun sensor cells are illuminated, at which time a positive yaw maneuver will be commanded until the primary Sun sensor lock-on signal is generated.

3. Gas Jet Subsystem

Excessive pressure regulator valve leakage occurred following type-approval vibration tests along the thrust axis. An engineering model incorporating a new valve design successfully met performance requirements following exposure to type-approval vibrations. Type-approval tests on a flight-quality regulator with the new type of valve are in progress.

The final 90-day storage cycle test on the pressure relief valve was successfully completed. Results indicate that the valve is not affected by storage. Flight-acceptance tests were completed on seven flight-quality jet valves available for installation on spacecraft. A thrust-vector test made on one jet valve indicated that the thrust vector is within the specification limit of 1 deg.

The nitrogen manifold flexible line test for cleanliness after vibration and flexure was terminated. During the test, the line was flexed 5 times and vibrated on one axis perpendicular to the plane of the line. The total vibration time was equivalent to that required for a three-axis vibration test. Results of the cleanliness test showed that the amount of particulate matter per cubic foot of gas exhausting from the line was within specification.

A nitrogen manifold cleanliness test was conducted on the S-2 vehicle after vehicle vibration with the legs in the stowed position, followed by normal leg deployment. The amount of particulate matter per cubic foot of gas exhausting at each jet valve connection was within the specification limit.

D. Thermal Control

1. Subsystem Thermal Analysis and Design

Thermal predictions for the T-21 gold-plated vernier thrust chamber assembly (TCA) were completed. The

predictions were compared with the predictions for the previous design utilizing vapor-deposited aluminum. The data indicate: (1) an increased gradient in the barrel of the thrust chamber utilizing the gold plating, and (2) greater uncertainty tolerances for the gold-plated assembly. Furthermore, the redefined location of the solar collector in the second vernier engine added to the increased gradient through the barrel.

All effort was stopped on the present TCA thermal design. A solar reflector which directs solar energy onto the engine extension cone is being incorporated into the design. By this modification, the demand for thermal energy from the head end of the engine will be reduced, thereby reducing the temperature gradient along the TCA above the barrel/extension cone interface. Updating of the analytical thermal model and a parametrically oriented design study are under way.

2. T-21 System-Test Support

The T-21 thermal-control evaluation phase was redefined in accordance with present program plans. The purposes of the program were to demonstrate thermal-control acceptance criteria, perform a radar altimeter and doppler velocity sensor (RADVS) thermal development test, and determine thermal performance during nonstandard mission events. The redefined program has a 12-hr thermal test phase instead of the 75-hr thermal-control evaluation phase of the original program. This phase is performed after the completion of the functional test, but without returning the chamber to ambient conditions between the functional test and special thermal test. In addition, the RADVS thermal development test and a solar eclipse phase are being performed concurrently with the functional test. Most of the objectives of the original thermal phase will be realized using the modified test program.

3. Spacecraft Analysis and Command Support

The thermal-management-program transit analog model was used to provide temperature–time profiles of the spacecraft thermal sensors. The program utilized electrical power dissipations generated by the power management program. The Space Flight Operations Plan for Mission A was used as a basis for generating the power and thermal data. These will be used to generate simulated telemetry data that will, in turn, be used during checkout and testing of the spacecraft analysis and command computer programs and procedures.

E. Electrical Power Supply

Solar-panel design changes are being made to bond the titanium sockets to the lower end of the panel support brackets to provide an interface for dampener rods. Following completion of the design changes, retrofit of the T-21 panel, the type-approval panel, and three flight panels will be initiated.

Solar-panel design changes are also being made to attach the static ground straps from the solar-panel substrate facing to the panel mounting brackets to provide static-charge ground continuity. Laboratory tests were conducted using silver-filled conductive epoxy to bond copper foil straps to the panel. The results were satisfactory, and the ground straps will be incorporated into existing hardware concurrently with retrofit installation of the dampener rod sockets.

F. Scientific Experiments

1. Seismological Experiment

Since failures were experienced during type-approval testing, certain changes were made to the seismometer sensor design. The new configuration is shown in Fig. 2.

The prototype instrument underwent a successful unit functional test using the seismological-experiment bench test set. As expected, high ambient acoustical noise levels caused the instrument amplifier to saturate on the high-gain setting, even with the sensor caged. Calibrate pulses were observable on the low-gain setting only.

2. Alpha Scattering Experiment

The prototype instrument completed a successful unit functional test using the alpha-scattering-experiment bench test set. A test source consisting of Cm-244 and Pu-239 radioactive materials was used to stimulate the instrument sensor head. Instrument output data were processed satisfactorily through all associated test equipment. Data records were obtained in the form of typewritten data, punched tape data, and photographs of oscilloscope-displayed analog data.

A portable 18-in. bell-jar vacuum system underwent a satisfactory checkout and test in the HAC Payload Systems Laboratory. This vacuum system is required for tests employing flight-strength radioactive sources.
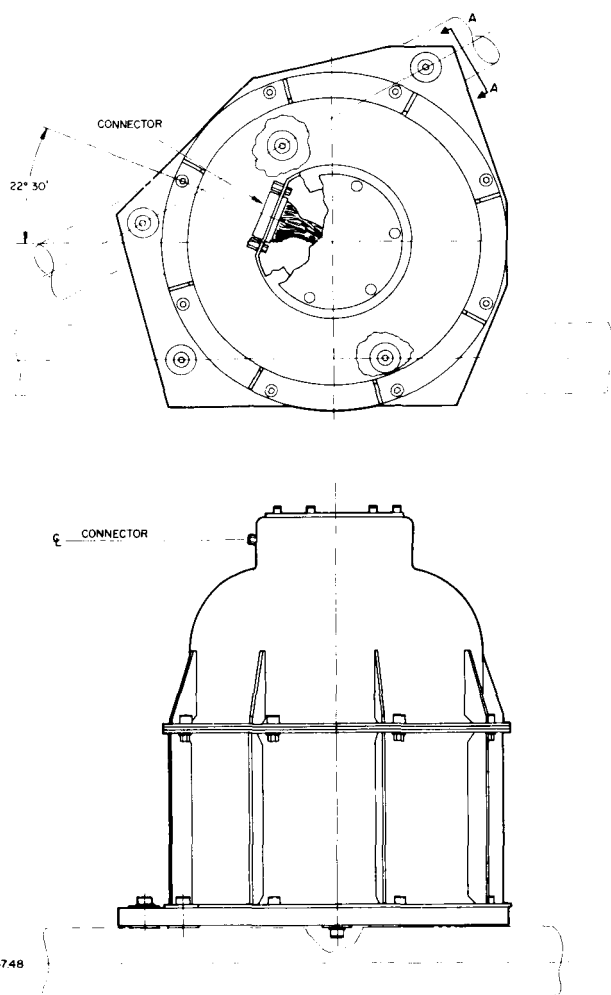
Fig. 2. Modified seismometer sensor

3. Soil Mechanics/Surface Sampling Experiment

Two modifications to the soil mechanics/surface sampler interface specification will have significant effects on equipment design: (1) changing elevation coverage from 72 to 67 deg will allow strengthening of the elevation yoke, and (2) changing the required acceleration measuring system frequency response from a 20- to 50,000-cps range to a 10- to 30,000-cps range will allow a wider latitude in the selection of telemetry transmission parameters.

Methods of adding an automatic (tape-programmed) command capability to the HAC Payload Systems Laboratory test equipment were investigated. The proposed system will utilize the existing tape reader and will closely simulate the command and data console automatic tape mode.

4. Touchdown Dynamics Experiment

An investigation of the technical problems and program implications associated with integrating a touchdown dynamics experiment subsystem into the *Surveyor* payload was completed. Experiment objectives require that the subsystem have a capability of retrieving, storing, and transmitting 31 groups of spacecraft dynamic history developed immediately prior to and during a *Surveyor* spacecraft landing. Study report findings indicate that it is possible to integrate the proposed subsystem into the A-21A (scientific payload) series spacecraft and meet the experiment specification requirements. Equipment location on the *Surveyor* spacecraft is indicated in Fig. 3.

G. Propulsion

1. Vernier Propulsion Subsystem

A program was initiated by JPL to perform limited environmental tests of selected upstream system components for the purpose of evaluating, on an independent basis, the capability of these components to meet *Surveyor* requirements. A helium regulator on loan from HAC has become the first test object in the program. It is planned to test the life-cycle capability of the regulator, as well as its flow, regulation, and lockup characteristics under vibration and under high- and low-temperature extremes. Thus far, the regulator's flow and lockup characteristics under ambient conditions have been checked to provide a baseline for reference. Additional runs just completed have dealt with the effects of temperature extremes. Results of the ambient and temperature-extreme tests have indicated that the regulator exhibits regulation deficiencies. These deficiencies were also noted by HAC. A redesign of the regulator was accomplished, and the characteristics of the regulator were satisfactorily improved.

2. Thrust Chamber Assembly

A test program was initiated at the JPL Edwards Test Station to provide design verification data for the *Surveyor* vernier-propulsion-system thrust chamber under development at the Reaction Motors Division of Thiokol Chemical Corporation. The over-all objective of the program is to develop backup information which will increase confidence in the ability of the engine to fulfill the requirements
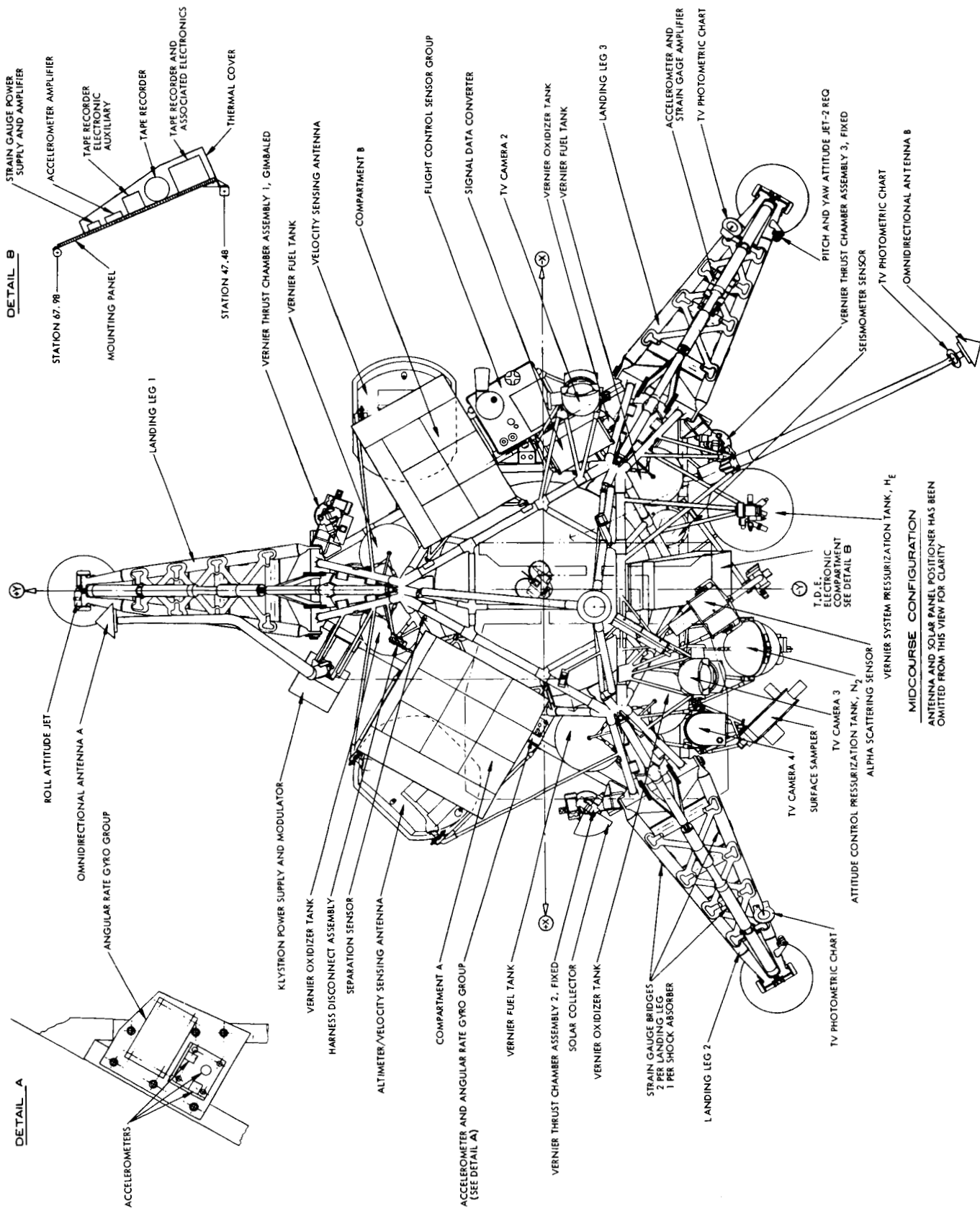
Fig. 3. Surveyor spacecraft configuration showing touchdown dynamics experiment subsystem

of the *Surveyor* mission. Two tests have been performed thus far:

(1) The first test, a checkout of the facility, was entirely successful. The engine was fired at sea-level conditions for 73 sec, using an acceptance-test profile which involved operation at three different thrust levels, 5-cps cycling, and several throttling rates.

(2) The second test involved operation at maximum thrust for 40 sec, a hold period of 1 hr, and a cycling (10-cps) restart at mid-thrust. The primary purpose was to investigate the restart characteristics (phase lag, gain attenuation, etc.) of the chamber after a margin limit midcourse firing of extended duration at maximum thrust. The results of this test are currently being analyzed.

PLANETARY–INTERPLANETARY PROGRAM

III. *Mariner* Project

A. Introduction

The early objective of the Planetary–Interplanetary Program is the initial probing of the planets Mars and Venus by unmanned spacecraft. The initial probing of Venus was successfully accomplished by *Mariner II*. The next operation directed toward this objective is the initial probing of Mars by the *Mariner IV* spacecraft, which is now in transit.

The primary objective of the *Mariner C* missions (*Mariner* Mars 1964 Project) is to conduct closeup (flyby) scientific observations of the planet Mars during the 1964–1965 opportunity and to transmit the results of these observations back to Earth. The planetary observations should, to the greatest practical extent, provide maximum information about Mars. TV and cosmic dust experiments and a reasonable complement of field- and particle-measuring experiments are being carried by *Mariner IV*. In addition, an Earth occultation experiment is planned.

A secondary objective is to provide experience and knowledge about the performance of the basic engineer-ing equipment of an attitude-stabilized flyby spacecraft during a long-duration flight in space farther away from the Sun than the Earth. Field and/or particle measure-ments will be made in interplanetary space during the trip and in the vicinity of Mars.

The *Mariner IV* (*Mariner C-3*) spacecraft was success-fully injected into a Mars encounter orbit about the Sun on November 28, 1964. *Mariner IV* is continuing in the cruise phase of flight, and all subsystems are performing as planned, except for the solar plasma instrument and the 10311 Geiger tube. A failure occurred in the power supply of the solar plasma instrument after approximately 1 wk in flight, resulting in degraded and uncalibrated data from the spacecraft. The probable failure mode has been determined, and, by recalibration of the instrument, there is good probability that much of the received data can still be utilized. The 10311 Geiger tube is a com-panion instrument to the ion chamber, both covering basically the same radiation energy levels. The apparent failure of this tube, which occurred a few days after the solar flare of February 5, 1965, has not affected the ion chamber data or any other spacecraft subsystem.

During January and February, the *Mariner C-1 (Mariner proof test model)* was tested to aid in the evaluation of *Mariner IV* in-flight anomalies and projected mission-control procedures.

B. *Mariner IV* Mission Operations

A scheduled telemetry bit rate switch from 33⅓ to 8⅓ bps to permit the long-range communications required for the *Mariner IV* mission occurred at 16:59:56 GMT on January 3, 1965, without incident. This was a programmed change timed to take place prior to the received telemetry falling below the ground-receiver sensitivity threshold. The data encoder was commanded by the central computer and sequencer to make the switch, which increases the time interval of the Data Mode II data frame from 12.6 to 50.4 sec. This data rate will be maintained for the remainder of the mission.

A number of roll transients have occurred, but none have caused loss of Canopus lock. It is believed that these transients are the result of dust particles passing through the field of view of the Canopus sensor. Direct Command 15, sent to the spacecraft in December to remove the sensitivity limits of the Canopus sensor intensity circuits, is still in effect.

A Class II solar flare occurred at 18:00 GMT on February 5. The event was immediately detected because real-time data were being transmitted from the Johannesburg Tracking Station. The particle experiments on the spacecraft first detected high-energy particles from this event at approximately 18:50 GMT and detected the rate increase over the following 3 hr. The ion chamber showed an increase in count rate of about a factor of 200. The trapped-radiation-detector background reading increased from approximately 30 to approximately 1400 data numbers on the Geiger tube channels. Analysis of the response of the cosmic-ray telescope requires more extended computation, but its response was qualitatively consistent with the increased activity. Response from the magnetometer and plasma experiments, which often accompanies such disturbances, will be anticipated in the data analysis.

Beginning at 03:29 GMT on February 11, a series of 12 ground commands was sent to the spacecraft to open the TV optics cover. During the same operation, the TV scan platform was positioned such that it is now in an optimum pointing angle to "see" the planet Mars during encounter. This was a precautionary measure taken in case the platform would fail to start scanning at the appointed time during the start of the encounter sequence.

The first updating of the Canopus cone angle was commanded by the central computer and sequencer on February 27, and the event took place without incident.

Deep Space Network coverage has been continuous during this reporting period, except for approximately 20 days when the Johannesburg Tracking Station was released for *Ranger* operations. The *Mariner IV* spacecraft was unmonitored for about 7 hr during each of these 20 days. The Tidbinbilla Tracking Station has assumed prime status for *Mariner IV*, replacing the Woomera Station, which was released for *Ranger* and other Deep Space Network commitments.

The *Mariner* operations in the JPL Space Flight Operations Facility have been combined and are basically all in one mission support area. The *Mariner* support team will occupy this area for the duration of the mission.

C. *Mariner IV* Power Subsystem Performance

Operation of the *Mariner IV* power subsystem continues to be normal. On December 13 (15 days after launch), the spacecraft radio system changed from cavity-amplifier operation to traveling-wave-tube operation. This resulted, as expected, in an increase in solar-panel loading from 154 to 182 w.

Eight of the 12 commands sent to the spacecraft on December 10 to check encounter science equipment and to turn off the battery charger directly affected the power subsystem. Direct-command inputs to the power distribution assembly were exercised, and all functioned properly. The sequence terminated with turn-off of the battery charger, which decreased the solar-panel loading to its present value of 166 w. This load is expected to remain constant until encounter, at which time the load will increase to approximately 205 w.

Solar-panel operation has been normal since launch. The panel capability at Mars will exceed the power demand by approximately 100 w. This margin is considered entirely adequate.

D. Life-Testing Activities

1. Gyro Control Assembly

The type-approval gyro control assembly (GCA) has been undergoing life testing since March 1964. By mid-February 1965, this GCA had accumulated 6800 hr of operation under various environmental conditions. The initial phase of the life test involved an automatic test set which carried the electronic portion of the GCA through a series of 10 cyclic commands starting with power turn-on. Response to these commands was measured by a voltage comparator which sent a *go, no-go* impulse to the corresponding impulse recording counters. This test phase lasted approximately 780 hr, and no failures in 27,000 complete cycles were recorded. The gyros were operated continuously during this phase. At its conclusion, the gyros were removed from the test setup and were subjected to two runs of an 8-position heading test to determine the four important gyro performance parameters of torquer scale factor, reaction torque, spin-axis mass unbalance, and input-axis mass unbalance. Extended observation of these parameters can give an over-all picture of long-term gyro wear-out phenomena.

At approximately 2300 hr of operating time, the entire GCA was placed in a vacuum-temperature chamber and allowed to operate for 1038 hr at a gyro temperature of 165°F, which is 30°F higher than the maximum expected temperature in the spacecraft. Tests were run through the vacuum chamber interface at regular intervals to check for any gross failures or malfunctions, and none were observed.

Since the conclusion of the vacuum-temperature run, the GCA has been running continuously under typical room ambient conditions with periods of down-time for further heading tests. The last of these tests shows conclusive evidence of gyro motor bearing wear on at least two gyros, pitch and yaw. The spin- and input-axis mass unbalances have increased considerably over their initial values. In the case of the pitch gyro, the spin motor input power has decreased, indicating a reduction of bearing preload (another sign of bearing wear).

Although the running time is now over 6800 hr, no additional heading tests have been run since the 4600-hr test. Life testing of the GCA will continue until a complete failure of some vital component part occurs or until future programs require additional laboratory space or equipment.

2. Pyrotechnic Control Assembly

A thermal-vacuum life test of the *Mariner C* pyrotechnic control assembly was begun August 31, 1964, and will continue until 10,000 operating hr are reached or until a failure occurs. By this test, it is hoped to determine:

(1) Any failures or gradual degradation of components due to long-term exposure to normal operating voltages at an elevated temperature and a moderate vacuum.

(2) Any spontaneous operation of an output channel without a command having been initiated.

The pyrotechnic control assembly within the chamber may be seen in Fig. 1. Pressure is maintained at less than 15×10^{-3} mm Hg. Component temperature is maintained at $65 \pm 2°C$ and is monitored by means of six thermocouples. Degradation of the electronic components involved is normally accelerated at this elevated temperature.

The subsystem is normally in the cruise mode, with weekly simulation of pyrotechnic events. Operating power and the command function are provided by special bench-test equipment which enables simulation of flight operation. Through the first 4300 hr of operation, no anomalies or changes have been noted in the parameters being monitored, and no spurious events have occurred.
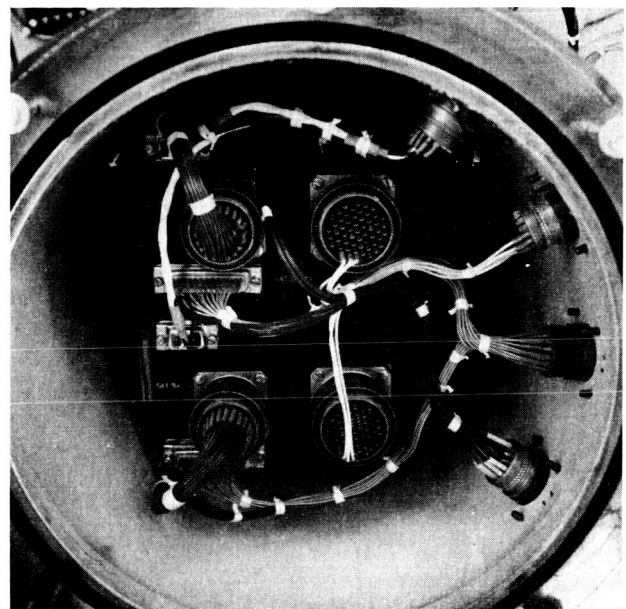

Fig. 1. Pyrotechnic control assembly within thermal-vacuum chamber

3. Propulsion System

During the propulsion system life storage test described in *SPS 37-31*, Vol. VI, p. 20, a temperature limitation became apparent. At ambient temperatures in excess of 100°F, decomposition of hydrazine (caused by the bladder) caused an appreciable rate-of-pressure increase in the propellant tank. Inspection of the bladder following the completion of the life test revealed that gross changes had occurred. Thousands of small bubbles had formed inside the bladder membrane in those areas where the bladder had contacted the propellant tank (Fig. 2). A leakage test showed that the bladder was still integral and could contain a gas under pressure in its degraded condition; therefore, mission performance capability had not been reduced.

It is not expected that the *Mariner IV* bladder is developing bubbles in the bladder membrane, since spacecraft interior temperatures have been 75°F or lower. Should these bubbles develop, they should not affect the performance capability of the propulsion system.

0.200 in.
(ORIGINALLY 0.050 in.)
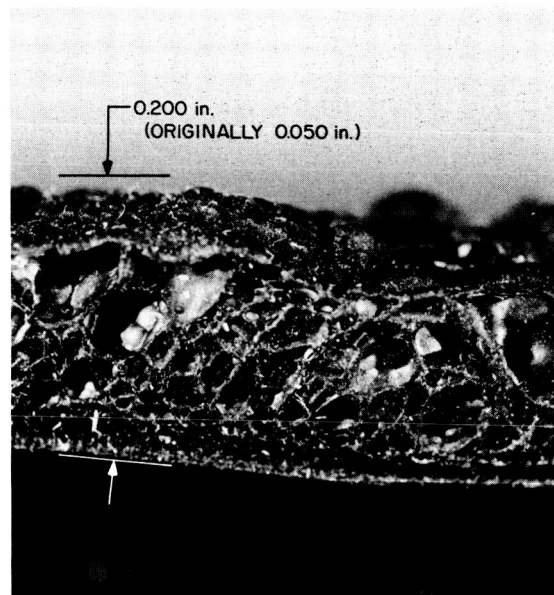
Fig. 2. Sectioned bladder membrane following life testing

DEEP SPACE NETWORK

IV. Deep Space Instrumentation Facility

A. Introduction

The Deep Space Instrumentation Facility (DSIF) utilizes large antennas, low-noise phase-lock receiving systems, and high-power transmitters located at stations positioned approximately 120 deg around the Earth to track, command, and receive data from deep space probes. The DSIF stations are:

Station	Location
Goldstone Pioneer	Goldstone, California
Goldstone Echo	Goldstone, California
Goldstone Venus (research and development)	Goldstone, California
Goldstone Mars (under construction)	Goldstone, California
Woomera	Island Lagoon, Australia
Tidbinbilla	Canberra, Australia
Johannesburg	Johannesburg, South Africa
Madrid (under construction)	Madrid, Spain
Spacecraft Monitoring	Cape Kennedy, Florida
Spacecraft Guidance and Command (under construction)	Ascension Island

To improve the data rate and distance capability, a 210-ft-diameter Advanced Antenna System is under construction at the Goldstone Mars Station, and two additional antennas of this size are scheduled for installation at overseas stations. Overseas stations are generally operated by personnel of the respective countries.

It is the policy of the DSIF to continuously conduct research and development of new components and systems and to engineer them into the DSIF to maintain a state-of-the-art capability.

B. Tracking Stations Engineering and Operations

1. Goldstone Pioneer Station

Tracking activities for the *Mariner IV* mission have progressed to the efficiency of routine operation, with the S-band tracking system requiring only periodic adjustments. A continual flow of spacecraft engineering and scientific data is being recorded and forwarded to JPL for reduction and analysis.

Preparations for the *Surveyor* mission are continuing. All cabling between the *Surveyor* control room and the Pioneer S-band building has been completed, and the

interim compatibility tests between the *Surveyor* installation and the Pioneer S-band system have been performed.

The Pioneer Station was scheduled to participate in the *Atlas–Centaur 5* mission in early-March. A special discriminator was installed in the analog instrumentation system, and the RF subsystem was modified to enable the No. 2 S-band receiver to angle-track. Tests in preparation for the tracking support included an integration test between the Pioneer and Venus Stations and the JPL Space Flight Operations Facility (SFOF). A final operational readiness test was held in February.

Since the Pioneer S-band system was designated the original development system, new equipment and operating techniques are operationally tested there prior to incorporation into other systems. Assembly of all S-band systems continues at the Pioneer Station, with limited operational testing being performed, when possible, by the operating personnel of the station involved. The Madrid Station S-band system was shipped during January; however, most of the Madrid Station personnel remained at the Pioneer Station until late-February in order to acquire additional operating experience by participation in the *Mariner IV* tracking operations.

The Pioneer L-band receiver was installed in the new west wing of the control building, while the backup video equipment remained in the original location. Tests were performed to determine the time necessary to remove the hyperbola and change the antenna feed from S- to L-band so that the *Mariner IV* spacecraft could be tracked until just before impact of *Ranger VIII*. Pioneer made the S- to L-band change prior to acquisition and provided full backup for the entire third pass of *Ranger VIII*.

2. Goldstone Venus Station

The Venus Station was originally programmed to provide high-power command transmission to the *Mariner IV* spacecraft. However, it was decided that a full receive capability should also be provided as a backup for operations at the Pioneer Station. This required the installation of a traveling wave maser, the addition of two RF switches, and associated waveguide changes in the *Mariner IV* cassegrain cone assembly (Fig. 1). The 2295-Mc maser at the Echo Station was removed for installation at the Venus Station. The control instrumentation and closed-cycle refrigerator compressor were installed adjacent to the Venus Station cone storage area. A new noise box was fabricated to provide the voltage-standing-wave-ratio load measurement capability. This system can be operated in
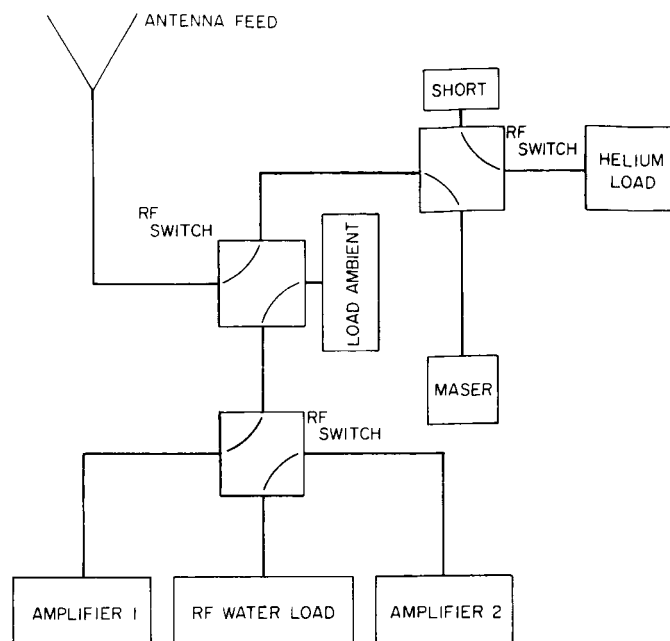

Fig. 1. Mariner IV cassegrain cone in receive-capability configuration

the Venus Station cone storage area with the original DSIF instrumentation or on the antenna with the research-and-development cable installation and instrumentation in the control room.

An immediate requirement existed to receive *Mariner IV* telemetry at the Venus Station during periods when the Pioneer Station would be committed to other programs, such as backup support for *Ranger VIII*. To provide this support, a "suitcase" telemetry receiver was installed in the *Mariner* cassegrain cone. The telemetry output of the receiver is transmitted to the Venus Station control building by cable link and then to the Pioneer Station over microwave link. At this point, the telemetry is demodulated and transmitted to the SFOF at JPL by microwave link. This installation was completed and tested.

The Venus Station provided the prime receiving system at Goldstone on February 20, 1965, when the Pioneer Station provided the backup support for *Ranger VIII*.

3. Goldstone Echo Station

Equipment preparation and minor subsystem testing for the *Ranger VIII* mission began in December 1964. With the completion of the *Mariner IV* midcourse maneuver, additional personnel were available for comprehensive testing and operation of the Echo Station L-band system. No major changes were made to the system after the

Ranger VII mission, and testing consisted primarily of ensuring full operational capability. Six tests simulating full tracking operation were conducted: one acceptance test, one command procedures test, two SFOF/DSIF integration tests, and two operational readiness tests. These tests indicated that the L-band system was in good condition and the Echo Station, except for minor peaking adjustments, was ready for the *Ranger VIII* launch.

Ranger VIII was launched at 17:05:00 GMT on February 17, 1965, and impacted the Moon's Sea of Tranquility at 09:57:38 GMT (Echo-recorded time) on February 20. Both video channels turned on at the same time, and photographs were received simultaneously by the Echo and Pioneer Stations for 23 min (from 09:34:34 GMT until impact). Except for the erratic signal levels during the midcourse maneuver of the first Echo Station pass, a normal tracking mission was accomplished.

Equipment for the Echo Station S-band system is being delivered. Testing has been limited to power turn-on for the units, but full operational tests will be conducted after final installation of the equipment. Meanwhile, construction of the S-band wing of the Echo Station control building is nearing completion.

4. Spacecraft Monitoring Station

Construction of the control building at the Spacecraft Monitoring Station is continuing. Equipment has been checked out at Goldstone and is scheduled for shipment to Cape Kennedy, Florida, in March. The station is scheduled to be operational with the new equipment by early-May.

5. Spacecraft Guidance and Command Station

The new space communications station at Ascension Island will provide guidance and command functions and data acquisition support for spacecraft launched from Cape Kennedy whenever the injection point is sufficiently uprange to permit the station to obtain early acquisition information. This station will not normally be used when other DSIF stations can perform the same functions. The system will be composed of Goldstone Duplicate Standard S-band equipment, except for the antenna which will have a 30-ft azimuth-elevation mount and the microwave subsystem which must be modified because of the difference in the antennas.

Approximately 60% of all major equipment items have been procured. The equipment will be delivered

to Goldstone and integrated as a system, using a 30-ft mockup antenna being procured for this purpose. When the integration and testing activities have been completed, the system will be shipped to Ascension Island. The station is scheduled to be operational by March 1966.

6. Ranger VIII Tracking Operations

The tracking of *Ranger VIII* was different than the usual tracking for other missions in that another spacecraft, *Mariner IV*, was being tracked simultaneously from Goldstone. In Australia, the Woomera Tracking Station had released tracking responsibility for the *Mariner IV* mission to the new Tidbinbilla Station in January. Just prior to the launch of *Ranger VIII*, the Johannesburg Station left the *Mariner* track and converted from S- to L-band for final testing and participation in the *Ranger VIII* mission. Removal of the Johannesburg Station from the *Mariner* track caused a non-view period of approximately 7 hr between the end of the Tidbinbilla view period and the start of the Pioneer Station view period.

Since the Pioneer Station would be used to back up the Echo Station during the third view period of *Ranger VIII*,
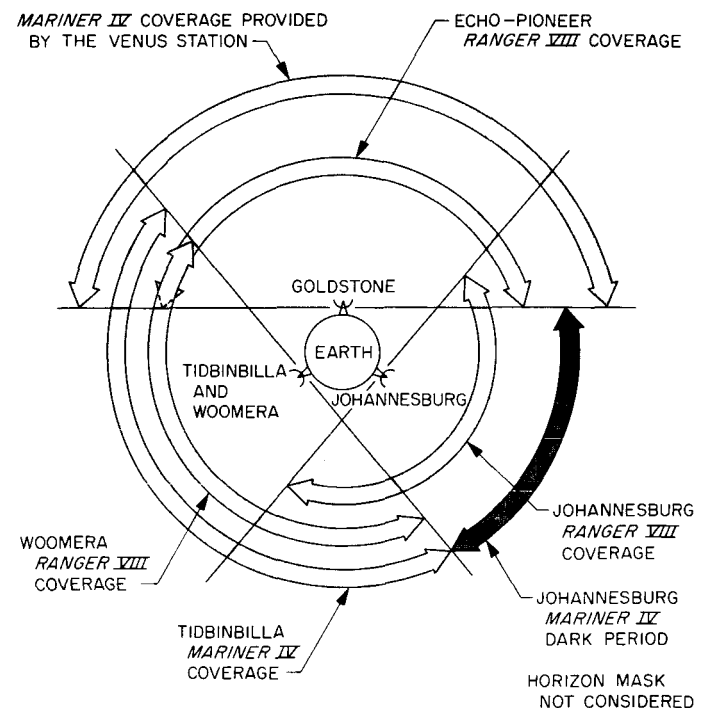

Fig. 2. DSIF tracking coverage for the *Mariner IV* and *Ranger VIII* missions during the third and last view period of *Ranger VIII*

its removal from the *Mariner* track could add an additional 10 hr of non-view to the Johannesburg 7 hr, for a total non-view period of approximately 17 hr. The Venus Station, using the "suitcase" receiver assembly, assumed the Pioneer Station track of *Mariner IV*. Thus, *Ranger VIII* received full coverage from the three DSIF

stations, and *Mariner IV* had only a 7-hr non-view period caused by the absence of tracking by the Johannesburg Station. Fig. 2 illustrates the tracking coverage provided for the two missions during the third and last view period of *Ranger VIII*.
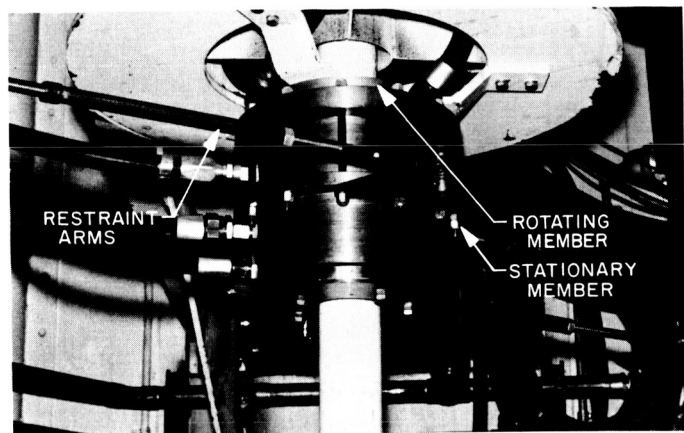
Fig. 3. Rotary joint installation on 30-ft antenna

C. Developmental and Testing Activities

1. Antenna Servo System

Dynamic testing and installation of the redesigned high-pressure hydraulic rotary joint for the Venus Station 30-ft antenna are now complete. The installation of the joint on the azimuth axis of the antenna is shown in Fig. 3. The cable wrap-up and the servo system were both designed to accept a torque component of 500 ft-lb from the rotary joint. The test results show a maximum value of 300 ft-lb, well below the allowable maximum value.

Fig. 4. Receiver–exciter subsystem

2. S-Band Receiver–Exciter Subsystem

Ten Deep Space Network (DSN) 1964 S-band RF receiver–exciter subsystems (Fig. 4) have been produced; seven have been assigned to the DSN and three to the Manned Space Flight Network (MSFN). Certain modifications to the subsystem have been designed which are required to make it adequate for MSFN pur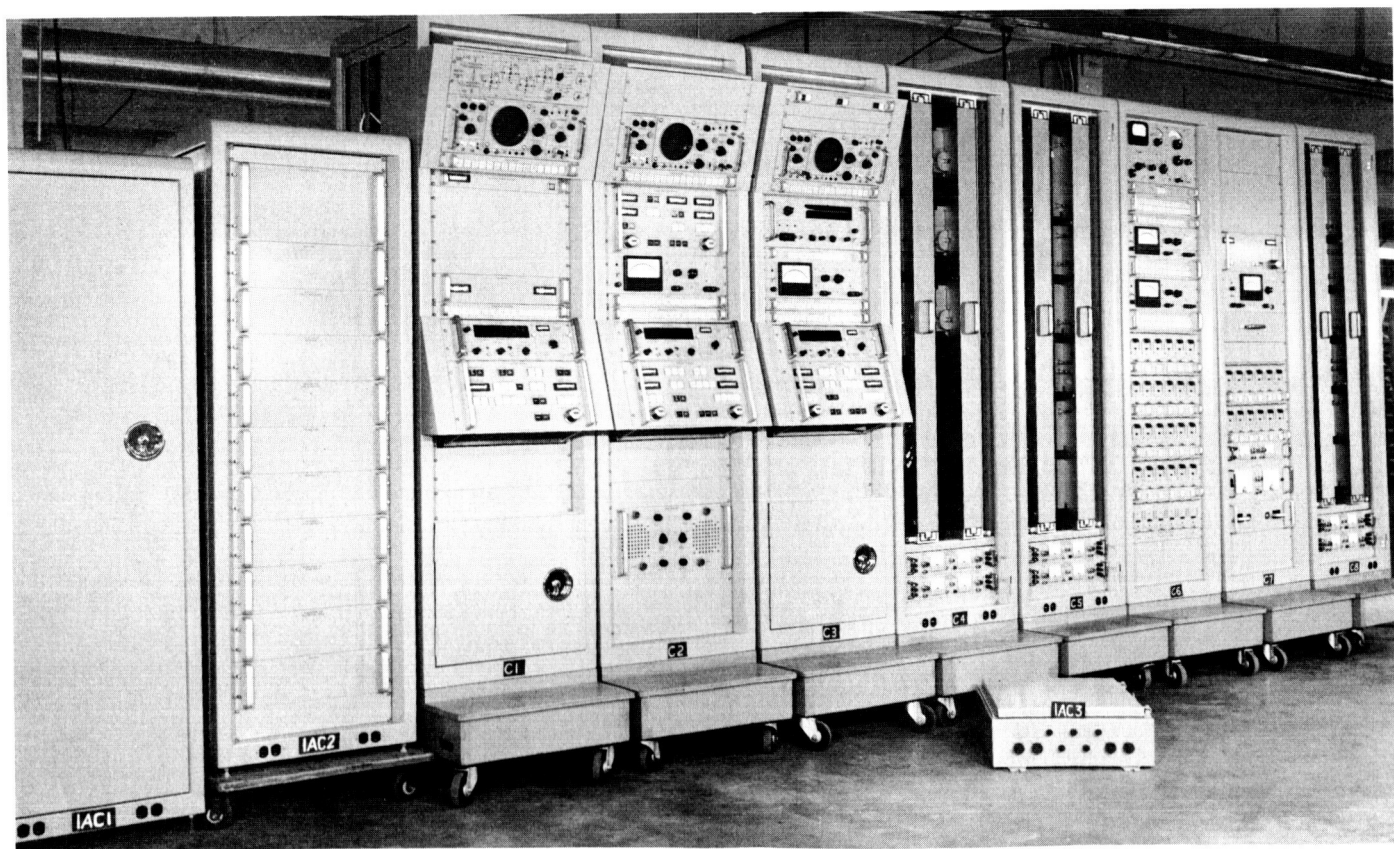poses. These design modifications are being incorporated into a subsequent MSFN subsystem and, since they are also applicable to the DSN, they will be included in subsequent DSN subsystems. Except for frequency channel assignments and loop noise bandwidths, the DSN and MSFN subsystems will be essentially identical.

Certain discrepancies between performance data for the subsystem and the specification requirements do not adversely affect the performance of the subsystem in supporting existing or anticipated programs; therefore, it was decided not to effect any design change until a major redesign effort, such as the incorporation of the MSFN modifications, has begun.

Adequate alignment and testing of the RF subassemblies or modules require special test equipment in addition to some other subassemblies and commercial test equipment. A set of ten fixtures developed by JPL will be used to maintain the equipment; these, or similar fixtures, will also be used during the production phase. This specialized RF test equipment is contained in two primary subassemblies: the test transmitter and the test transponder. These subassemblies, with associated equipment, provide the capability of: (1) accurate signal level calibration of the DSN receiver, and (2) simulation of the spacecraft-to-ground link or two-way link between the spacecraft and ground.

One set of these two subassemblies is mounted in the antenna racks of the receiver–exciter subsystem, and, when connected by transmission lines to this subsystem, one- and two-way tests over cable can be performed. Another set is mounted in the collimation tower for similar tests over a space link. In addition, the test transponder can be installed in an aircraft for acquisition tests, doppler and range measurements, and operator training.

3. S-Band Cassegrain Monopulse (SCM) Feed

The prototype SCM feed was a dual-polarization monopulse feed utilizing a multimode matching section to propagate both sum and difference modes through a single, square-cross-section, pyramidal horn. Although the performance of this feed was acceptable and, in fact, represented a considerable improvement over the performance of previous feeds, the S-band development schedule permitted further research to be carried out before the design of the complete SCM cone assembly was finalized. A contract was awarded to Hughes Aircraft Company to explore the possibility of utilizing higher-order wave-
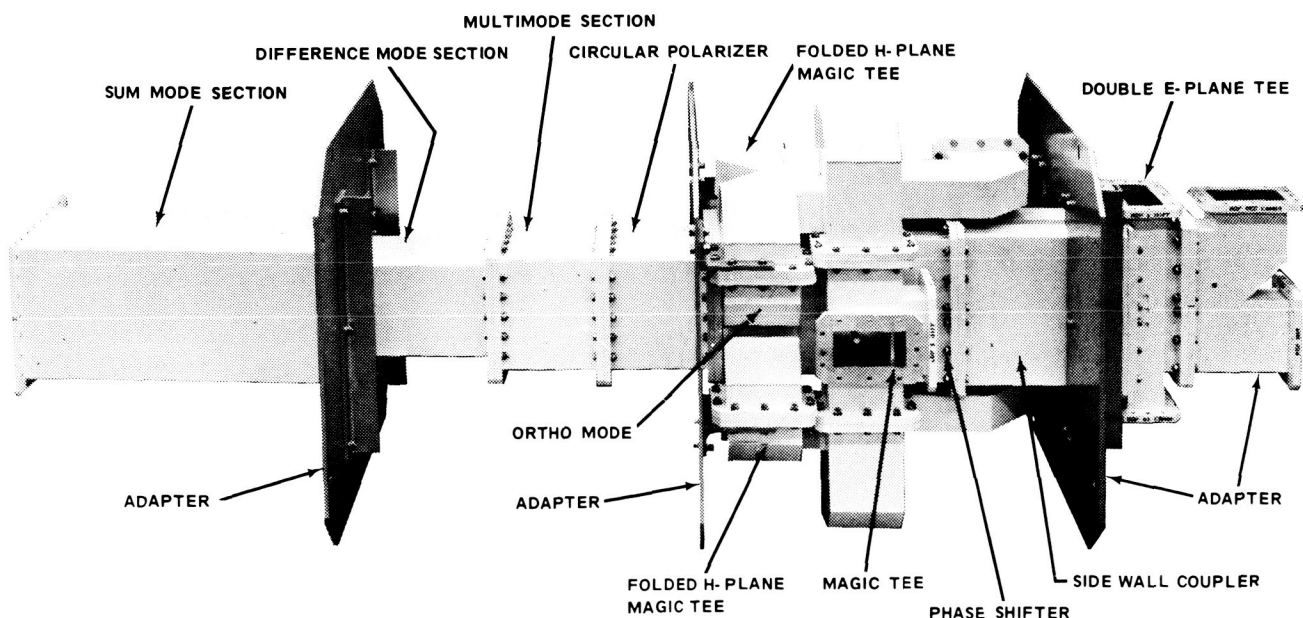

Fig. 5. SCM feed assembly

guide modes for the sum channel in order to achieve partial or complete sidelobe suppression comparable to that obtained at JPL for a circular-cross-section listening feed. This research program resulted in the development of a dual-frequency (2110 and 2295 Mc), dual-polarization (right and left circular), diplexed, monopulse (simultaneous lobing) tracking feed that utilizes higher-order waveguide modes to: (1) achieve sidelobe suppression in the sum channel, and (2) obtain dual-plane error channels from a single feed horn. The assembled feed (except for the horn, which connects directly to the sum mode control section) is shown in Fig. 5.

D. Advanced Antenna System

1. Cassegrain Feed Cone Assembly

A new configuration for the cassegrain feed cone assembly has been defined. The new configuration (Fig. 6) consists of the originally conceived bottom two cone sections, an adapter section, and an upper cone section which is structurally identical to the existing 85-ft antenna feed cone, thereby allowing interchangeability of feed systems with the DSIF 85-ft antennas and also providing for direct use of existing feed technology. Three of these upper assemblies are being procured: a DSIF tracking assembly; a low-noise 2295-Mc listening assembly for evaluation tests; and an ultrahigh-performance 2295-/2388-Mc listening assembly, which will be a DSIF prototype for use in research-and-development experiments.

An analytical technique for synthesis of ultrahigh-performance non-optical cassegrain-type feed systems has been developed and programmed for the IBM 7094 computer. This technique analytically develops a prescribed subreflector surface and a prescribed feed-horn radiation pattern to produce ultimate over-all antenna performance. The IBM 7094 synthesis program was used to generate a subreflector surface and physically realizable required feed-horn radiation characteristics for a high-quality feed having central-region reduced radiation. Very high performance was indicated.

Because the dual-mode horn is an existing high-performance feed horn, and since the generation and control of higher-order waveguide modes necessary for the production of the ideal four-mode horn pattern have presented difficulties, the dual-mode horn is the Advanced Antenna System listening system backup design. Consequently, analytical work of a hybrid nature is being

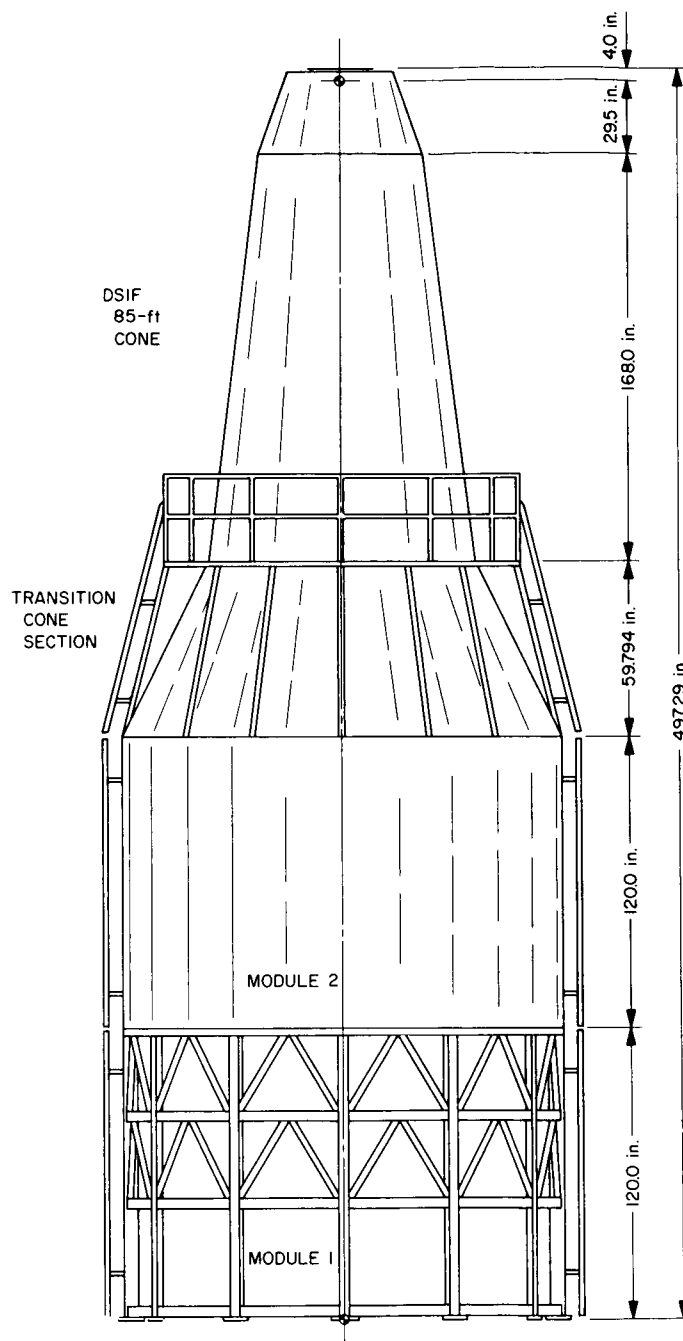Fig. 6. New cassegrain feed cone assembly configuration for the Advanced Antenna System

conducted. The synthesis program is being used to generate a prescribed subreflector surface and a prescribed feed-horn radiation pattern. The IBM 7094 computer scattering program is then used, with input describing the previously synthesized subreflector surface, but with illumination by a dual-mode horn rather than the ideal synthesis pattern.

SUPPORTING ACTIVITIES

V. Quality Assurance and Reliability

A. Parts Reliability

1. Qualification Testing of Crystal-Can Nonlatching Relays

a. Introduction. Of the designs of the more than 40 manufacturers presently producing microminiature relays, six crystal-can nonlatching relay configurations were selected for qualification testing. The selection of Babcock Electronics Corp.; Clare & Co.; Filtors, Inc.; General Electric Co.; Leach Corp.; and Sigma Instruments, Inc., and their designs (BR-12-675-B9, F-RP-10383, BRJ-

26A1H6-AS1, 3SAF1218, M201-E2-112, and 33RJP-800-VW-6SP, respectively) was based on experience with these products and on assessments made during plant evaluation tours where design, processes, quality control, and other factors were investigated.

The designs selected for qualification testing were ostensibly the manufacturers' best parts from their standard lines. It is acknowledged that some ratings of these parts (Table 1) are below expected spacecraft requirements; however, these designs represent the present state-of-the-art. Application of these parts is, therefore,

Table 1. Manufacturers' ratings for relays

Parameter	Babcock	Clare	Filtors	General Electric	Leach	Sigma
Contact resistance, mΩ	50	50	50	50	—[a]	50
Pickup at 25°C	12.5 v	13.5 v	13.5 v	14 v	13.5 v	16 ma
Operating time, msec	5	5	5	—[a]	5	3[b]
Insulation resistance, MΩ	10^4	—[a]	10^4	10^4	—[a]	10^4
Dielectric strength, v rms	10^3	10^3	10^3	10^3	10^3	0.7×10^3
Contact rating, amp	3	3	2	3	2	0.5
Coil resistance, Ω	675	675	800	675	600	800
Vibration (70–2000 cps), g peak	30	25	30	30	15	30
Shock, g	50	65	150	50	50	100
Temperature, °C	−65 to 125	−65 to 125	−65 to 125	−65 to 125	−65 to 125	−65 to 125

[a] Not specified.
[b] Excludes bounce.

necessarily limited by the manufacturers' ratings. Prequalification evaluation was performed at JPL to determine failure levels for critical environments.

b. Scope and objectives of tests. Various ordered environmental tests followed by a life test of either dry-circuit, resistive load, or inductive load were conducted on 96 parts from each manufacturer. The objectives of the tests were as follows:

(1) To demonstrate capability of relays to withstand standardized screening environmental stresses and to determine failure rates per 10,000 operations of the surviving samples when subjected to the three life tests (failure criteria to include both parametric and catastrophic failures).

(2) To determine the effects of each environment and of the various sequences of environments by a multiple linear regression analysis of parametric changes.

(3) To verify or refute statistical assumptions concerning the failure distribution of relays (conformance to exponential and Weibull distributions to be tested).

The environmental stresses and life-test conditions were as follows:

Thermal shock: 2 hr at an ambient temperature of −65°C, followed by 2 hr at an ambient temperature of 125°C; this cycle repeated three times.

High-temperature operation: 2 hr at an ambient temperature of 125°C, with relay coil in energized state at rated power.

Low-temperature operation: 2 hr at an ambient temperature of −65°C, with relay coil in unenergized state.

Vibration: 30-g-peak sinusoidal vibration swept uniformly from 75 to 2000 cps for 5 min.

Shock: Relays shocked four times in each direction in each of three mutually perpendicular axes; shock pulse was 100 + 10, −15 g square wave, with rise and fall times of 1.5 ±1 msec measured at the 10 and 90% amplitude points and a total pulse-width of 11 msec.

Dry-circuit life test: Coil voltage of 28 v dc; contact load of 10 μamp at 10-mv-dc resistive; operation at 1 cps for a maximum of 10⁶ cycles; room ambient conditions.

Resistive life test: Coil voltage of 28 v dc; contact load of 3 amp at 28-v-dc resistive; operation at 1 cps for a maximum of 10⁶ cycles; temperature cycled as follows: −65 ±3°C for 30 min, 25 ±3°C for 15 min, 125 ±3°C for 30 min, and 25 ±3°C for 15 min.

Inductive life test: Coil voltage of 28 v dc; contact load of 0.5 amp at 28-v-dc steady state, with 1.2-henry inductive load added for inductive characteristic; ambient temperature of 125°C.

c. Environmental test results. Prequalification evaluation testing of vibration and shock revealed excessive failures of the Leach relay at the test levels (30-g-peak vibration and 100-g shock); therefore, these relays were removed from the test. The results of the vibration and shock tests for the other five types of relays are given in Table 2. All testing was performed with the relays unenergized.

d. Effects of environments on parameters. A regression analysis method was used to determine the influence of environmental stresses on the five relay parameters: contact resistance, operate and release times, and bounce operate and release times. Measurements were taken at room ambient conditions before and after each environment, and the changes due to each environment were thereby detected and used as inputs to the regression analysis. The results were as follows:

Babcock relays. The regression analysis predicted an average increase in operate time of 0.25 msec when Babcock relays are subjected to a temperature of 125°C for 2 hr.

Clare relays. A sensitivity of the Clare relays to the vibration environments was indicated and took the form of an average increase of 4.12 mΩ in contact resistance.

Table 2. Failure summary for vibration and shock tests

Manufacturer	Number of failures[a]	
	Vibration tests	Shock tests
Babcock	1	5
Clare	8	6
Filtors	2	1
General Electric	0	5
Sigma	8	0

[a] Failure defined here as either a contact opening of the normally closed contacts for an interval in excess of 10 μsec or armature transfer to the normally open contacts.

Filtors relays. These relays showed a sensitivity to both shock and vibration environments in the form of increased contact resistance. The regression equation predicted a mean change in contact resistance of 4.27 mΩ due to vibration and 3.87 mΩ due to shock.

General Electric relays. Relays from this manufacturer showed sensitivity in more parameters and to more environments than did any of the other relays. There were three parameters showing sensitivity to environments: release time, bounce release time, and bounce operate time. The regression analysis predicted: (1) decreases of 0.28, 0.31, and 0.29 msec in release time when the relays are subjected to vibration, thermal shock, and high temperature, respectively; (2) increases of 0.42, 0.46, and 0.48 msec in bounce operate time when the relays are subjected to the same three environments; and (3) increases of 0.37 and 0.44 msec in bounce release time when the relays are subjected to vibration and thermal shock, respectively.

Sigma relays. The Sigma relays showed no significant effects due to environmental stresses.

e. Life-test results. A summary of life-test results is given in Table 3. It is obvious that the failure rates determined do not reach the goal of <1%/10⁴ cycles. However, the point estimate of mean time to failure and the failure rates are both based on the exponential assumption. In establishing the statistical assumptions of failure distributions, it was found that there were insufficient data to confirm either the exponential or the Weibull assumption. Since it is reasonable to expect relays to have a wear-out mechanism which is increasing with life, the validity of using a constant failure rate in these calculations is highly questionable. Accordingly, the summary

in Table 4 was prepared as a means for reviewing the relative performance of the relays in the over-all test program.

2. Failure-Mode Study of Power Wirewound Resistors

a. Test objectives and description. Power wirewound resistors operated under low-power application (i.e., 1- to 15-w resistors operated in the range of 1 to 50 mw) in ambient humidity have failed catastrophically. Limited investigation has revealed that the failure is the result of

Table 4. Relative performance[a] of tested relays

Test	Babcock	Clare	Filtors	General Electric	Sigma
Thermal shock	10	10	5	6	10
High-temperature operation	9	10	8	6	10
Low-temperature operation	10	10	8	6	10
Vibration	9	6	8	6	10
Shock	9	6	8	6	10
Vibration contact chatter	9	2	8	10	2
Shock contact chatter	5	4	9	5	10
Mechanical life	5	3	1	10	7
Dry-circuit life	9	9	9	8	10
Resistive-load life	9	0	8	6	3
Inductive-load life	0	2	4	1	5
Total	84	62	76	70	87

[a] Performance ratings were from 10 (exceptionally good) to 0 (exceptionally poor).

Table 3. Failure summary for life tests

Manufacturer	Mean time to failure, cycles × 10⁴			Failure rate[a], %/10⁴ cycles		
	Dry circuit[b]	Resistive load[c]	Inductive load[c]	Dry circuit[b]	Resistive load[c]	Inductive load[c]
Babcock	157.6	134.5	3.8	0.92	1.06	34.48
Clare	155.6	2.8	11.6	0.93	47.6	11.36
Filtors	162.2	84.9	22.2	0.89	1.61	5.92
General Electric	136.7	45.5	6.4	1.06	2.89	20.41
Sigma	210.1	20.0	30.4	0.72	6.58	4.33

[a] Failure rate given is the upper bound of a 90% confidence interval.

[b] Failure defined as a contact resistance value in excess of 100 Ω.

[c] Failure defined as a contact resistance value in excess of 100 mΩ.

corrosion, possibly caused by an electrolysis action. This could be a built-in failure mechanism resulting from the manufacturing process of all the constituent materials used in the manufacture, or it could be induced after the product is put into service.

A test was designed in an attempt to examine the exact nature of the failure, as well as the conditions under which it occurred. By subjecting the parts to a specific screening test and then applying power at 70% and 10% power levels in a controlled humidity of 95%, 35%, and room ambient (approximately 60%) relative humidity, it was intended to indicate the possible failure mode. The secondary purpose of the test was to subject resistors of the same type and family, but with different mandrels and processing, to the same environmental conditions to indicate possible material failures.

For the test, 3400 power wirewound resistors of five different types were selected, based on the following considerations: mandrel material, coating thickness, resistance wire diameters, and enclosures. One half of each group was screened. Three conditions of relative humidity were used for the humidity tests: room ambient, 35%, and 95%. Two levels of power were used at the latter two levels: one half of the test parts was operated at 10% of rated power, and the remaining half was operated at 70% of rated power. The test time for all humidity tests was 60 days.

b. Test results and conclusions. No failures resulted from a 60-day exposure to the 35% relative humidity condition; however, 23 catastrophic failures resulted from the 95% relative humidity condition: 18 when operating at 10% of rated power, three at 70% of rated power, and two when under a 100-v-dc polarization voltage. The two units which failed polarization were of the standard commercial type; the remainder were the specially produced types which have a considerably thinner insulating coat. Screening did not result in any measurably improved performance in this study.

Two different thicknesses of coating were used for the resistors. The group of resistors with standard coating thickness passed all tests, while the other group which had 50% less material had significant failures. The latter group of resistors was also divided into two types: the half of the group with a special Teflon jacket over the coating passed all tests. Mandrel material and wire diameter had no significant effect on the results.

The test indicated that, under high-humidity conditions, applying a relatively low percentage of rated power to a power resistor is more detrimental than applying a high percentage of rated power. Also, the test showed quite conclusively that it is only the coating's ability to seal out moisture that protects the unit from failure, regardless of the contaminants introduced into the resistance element prior to the coating application.

3. Transistor X-Ray Inspection

Reliability engineering techniques can be used to evaluate the inevitable workmanship defects in transistors and their effect on the performance and reliability of the devices. Interior gross mechanical defects are often overlooked during manufacture, even though it is presupposed that the manufacturer culls these defective parts because of their simple and obvious nature. Manufacturers perform in-process inspections, but on a sampling basis; therefore, these gross defects are of a random nature and are not lot-oriented. Many of the fabrication operations could constitute culling points; however, due to the volume production requirements, these inspections are quite cursory. Some users of high-reliability components do require additional comprehensive in-process inspection; however, the transient which this introduces into the production system tends to decrease the process reliability.

One means for detecting workmanship defects is X-ray inspection. A few examples of X-ray rejects are shown in Fig. 1. These pictures were taken for verification reasons by X-ray TV. The apparent case distortions were caused by the TV system.

Fig. 1(a) is our "Martian" transistor. The antenna in this transistor is made up of the gold lead bond wires formed during the lead to post-to-post attachment. The failure to remove the excess lead material was caused by momentary inattention of the operator. This transistor was further processed through a rinse station, a high-temperature vacuum bake station, and a capping station. These three stations are usually run by different operators who handle each part individually.

This obvious defect is a reliability hazard because: (1) the extra wires are connected to the base and emitter and could short either to each other or to the case, which is connected to the collector; and (2) these cantilevered structures have a high probability of breaking free and causing noise or momentary shorts during the shock and vibration of a spacecraft launch.
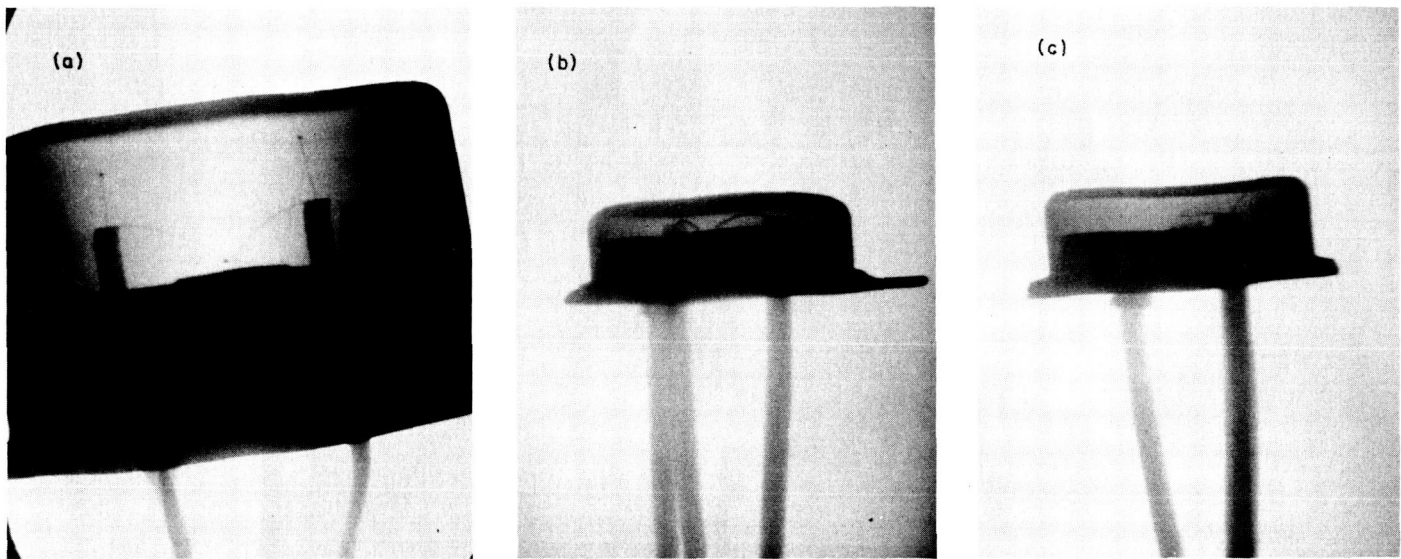
Fig. 1. Examples of transistor workmanship defects

Fig. 1(b) illustrates slack lead wires creating minimal spacing between the leads and the case. The clearance shown is on the order of 0.5 mil between the emitter lead and the case, which is electrically connected to the collector. Further displacement of these 1.5-mil gold wires resulting from handling, shock, or vibration will result in an electrical catastrophic failure. This particular type of transistor case is also susceptible to case deformation during encapsulation.

Fig. 1(c) illustrates a buildup of the gold preform around the silicon chip. The silicon chip is nearly invisible to X-rays. The gold preform is used to solder the silicon chip to the header. To assure mechanical adhesion, the silicon chip is scrubbed into the molten preform. Improper technique causes the buildup of material. This buildup is fragile and can become free within the case, causing noise and shorting in the transistor. This transistor also has a supernumerary wire emanating from the emitter post.

The devices shown in Fig. 1 are from different manufacturers. Workmanship standards of manufacturers vary, and, in all cases, defective parts are inevitable from time to time. A survey conducted on evaluation samples revealed that 53% of the lots examined contained X-ray rejects, and 26% of these were rejectable because of an inordinate number of difficulties or problems with them. X-ray inspection is admittedly a test of limited sensitivity. Experience to date has been that, even with this limitation, a sufficient number of defects have been found to render this test valuable. The X-ray inspection can be performed within 4 hr and usually adds only 5% to the device cost.

VI. Environmental Testing Facilities

A. Vibration Testing

1. Multi-Shaker System Study Program

A study program will be undertaken by JPL during fiscal year 1965 to generate an understanding of the multi-shaker test equipment and test methods. It will be a joint effort involving the Applied Mechanics, Environmental Requirements, and Environmental and Dynamic Testing Sections. Through this program, it is hoped to:

(1) Control and/or make uniform the vibration input to the spacecraft. It is expected that cross-axis motion will be reduced and fixture errors minimized.

(2) Increase the effectiveness of the vibration force input. Currently, the vibration fixtures weigh as much as, and sometimes more than, the space-craft. Reduction of fixture weight will result in a more effective application of the vibration force.

(3) Reduce fixture costs and fixture lead times. Fixtures will be simple; therefore, fixture costs and lead times will be reduced.

A theoretical analysis will be made of the interactions of a multi-degree-of-freedom system with multiple inputs, i.e., a simple beam connected to three vibration exciters. A test will be run using this same type of system. Interactions of the electromechanical system will be measured, and the theoretical analysis and test results will then be compared.

The analysis and test program will then be repeated using three vibration exciters connected to a spacecraft (*Ranger* proof test model). The experimental results from the tests will be compared with those from previous spacecraft tests which used only one large vibration exciter.

SPACE SCIENCES

VII. Lunar and Planetary Instruments

A. Advanced *Surveyor* X-Ray Diffractometer Sampler

Sampling system. Sampling systems are being designed and developed on the basis of sequential and/or simultaneous operations necessary to obtain required surface and sub-surface material specimens for presentation to the X-ray diffractometer. Two basic system schemes to categorize these operations are being studied:

(1) *Continuous sampling.* All particles collected and acquired by the extractor are transported to and through the X-ray diffractometer. However, it is not the intent to analyze each and every segment of the continuous flow of particulate surface and processed bedrock materials. X-ray diffractometer analysis operations will be conducted on segments of the continuous flow at a specified time to be controlled by a sensing device which will indicate if and when the required specimens are positioned over the viewing window.

(2) *Discrete sampling.* Only required specimens will be received at the extractor delivery station and transferred to the X-ray diffractometer viewing station.

All other extracted materials will be discharged out to the environment. This scheme necessitates the positioning of receiving containers alternately at the extractor delivery station and at the X-ray diffractometer viewing station whenever a discrete or specified specimen is to be analyzed.

Figs. 1 and 2 show block diagrams that indicate the operations to be accomplished under the two basic schemes. The operations will be performed by the mechanisms being designed and developed into the following subsystems:

(1) *Extractor subsystem.* This subsystem is designed to accomplish the following operations:

(a) *Rock drilling.* An impactor-type mechanism will provide the motion to a bit-cutter for cutting bedrock.

(b) *Sample preparation.* This is the sequence involved in processing the rock to powder form by crushing and pulverizing. The mechanism must be capable of preparing the sample to the required diffractometer sample specification.
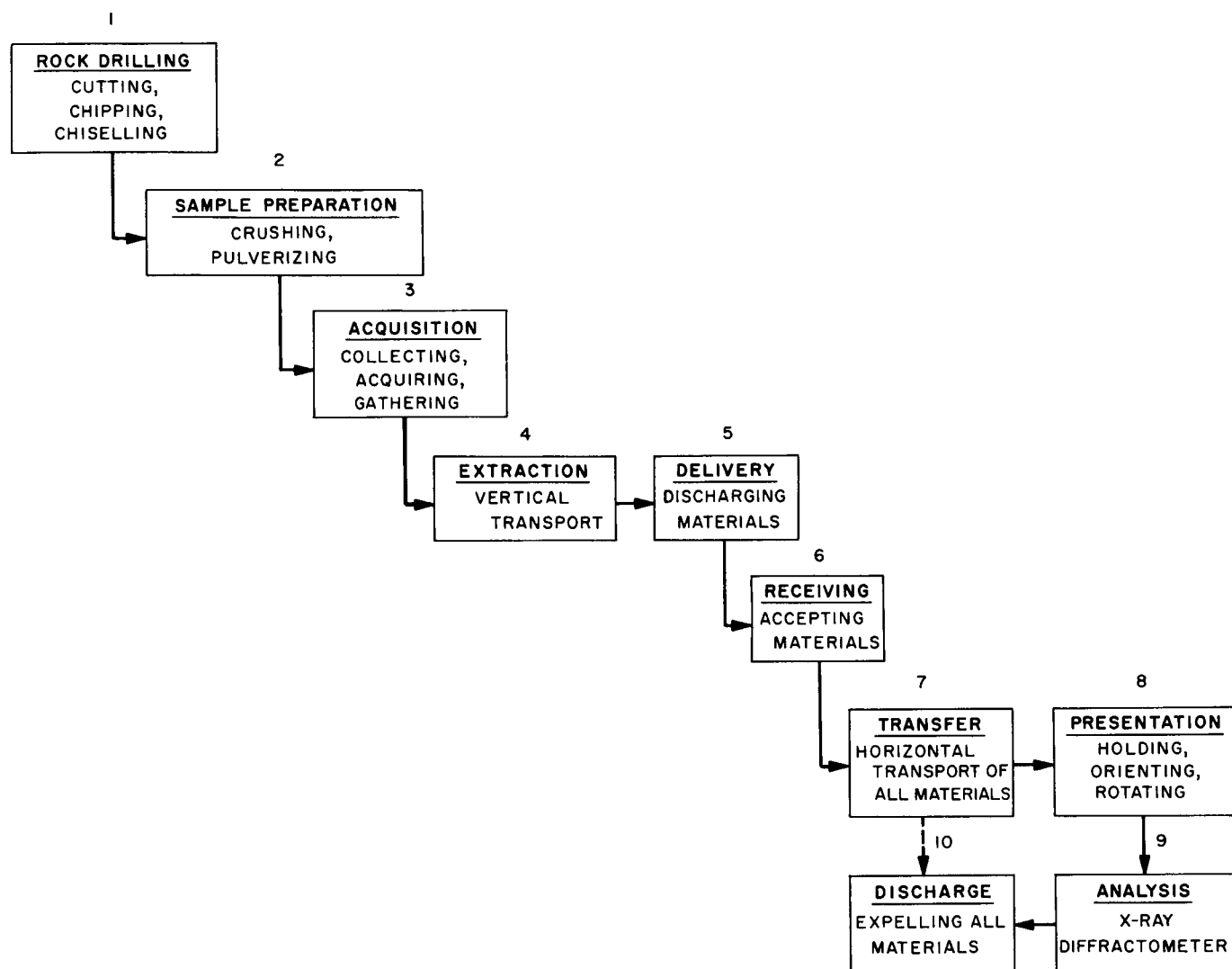
Fig. 1. Block diagram of operations in the lunar material sampling system (continuous sampling scheme)

(c) *Acquisition.* The prepared sample must be collected and gathered into the transport device.

(d) *Extraction.* Vertical transportation of the prepared samples from the hole to the X-ray diffractometer "level."

(e) *Delivery.* Discharging of transported material to a receiving medium which will transfer the sample to the X-ray diffractometer analysis station.

(2) *Transfer and presentation subsystem.* The following operations will be accomplished by this subsystem:

(a) *Receiving.* Accepting of samples delivered from the extractor subsystem.

(b) *Transfer.* Transporting the delivered sample from the extractor delivery station to the X-ray diffractometer viewing station.

(c) *Presentation.* Holding the sample to be analyzed and orienting this to the required rotational range for diffractometer analysis.

Discussions pertaining to the design and development of the mechanisms in the two subsystems follow. It should be emphasized that verification of the potential use of the mechanisms should be made by running tests on simulated lunar soils in an ultra-high vacuum (10^{-12} mm Hg).

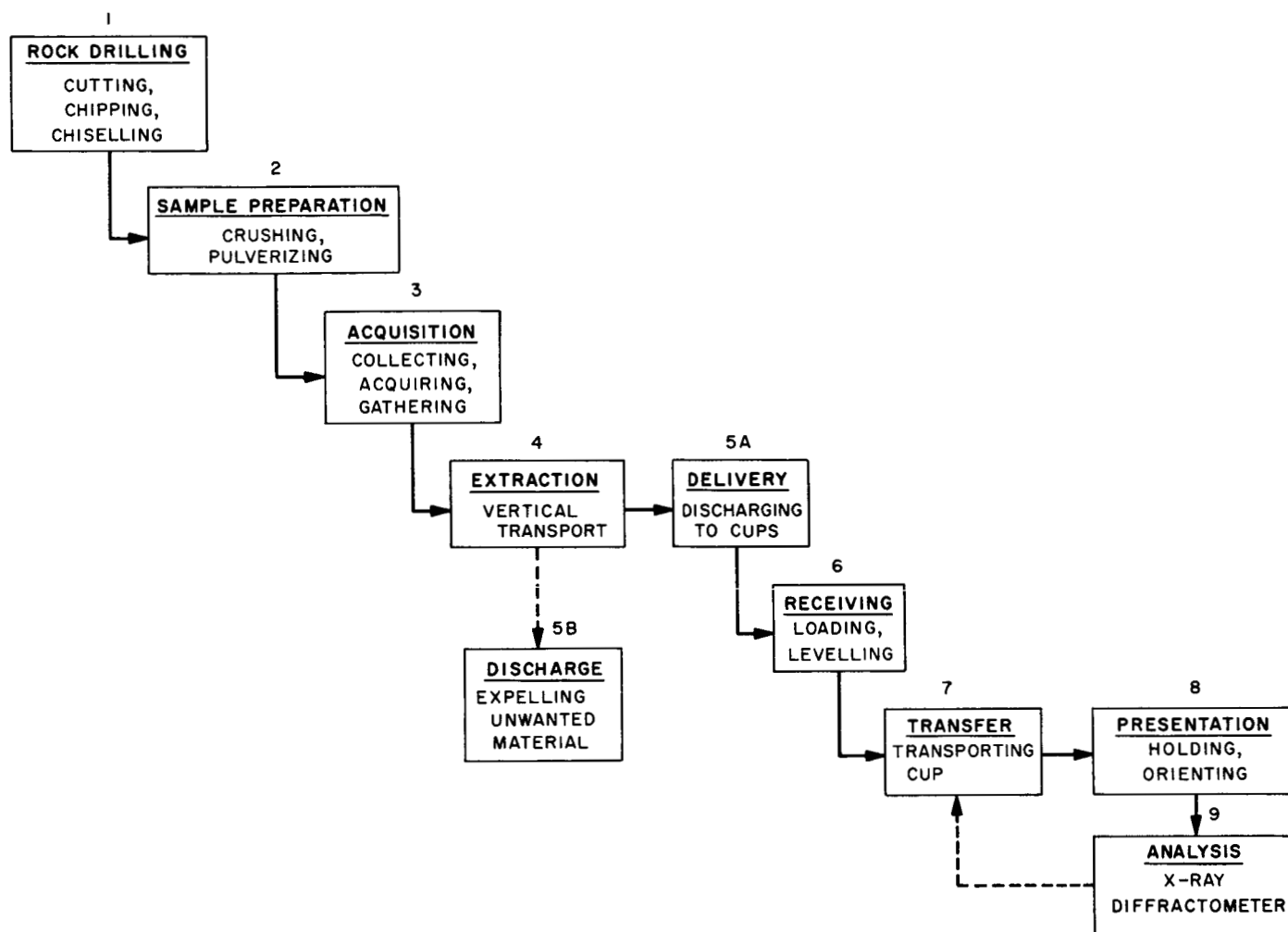*Extractor subsystem.* The extractor subsystem mechanism test rig designed to investigate the problems of

```
  1
┌─────────────────┐
│ ROCK DRILLING   │
│    CUTTING,     │
│    CHIPPING,    │
│   CHISELLING    │
└─────────────────┘
        │
        │        2
        │  ┌───────────────────┐
        └─▶│ SAMPLE PREPARATION│
           │     CRUSHING,     │
           │    PULVERIZING    │
           └───────────────────┘
                   │
                   │        3
                   │  ┌──────────────┐
                   └─▶│ ACQUISITION  │
                      │  COLLECTING, │
                      │   ACQUIRING, │
                      │   GATHERING  │
                      └──────────────┘
                            │
                            │       4                5A
                            │ ┌──────────────┐  ┌──────────────┐
                            └▶│  EXTRACTION  │─▶│   DELIVERY   │
                              │   VERTICAL   │  │  DISCHARGING │
                              │  TRANSPORT   │  │   TO CUPS    │
                              └──────────────┘  └──────────────┘
                                    ┊                  │          6
                                    ┊               ┌─────────────────┐
                                    ▼  5B           │   RECEIVING     │
                              ┌──────────────┐      │    LOADING,     │
                              │  DISCHARGE   │      │   LEVELLING     │
                              │   EXPELLING  │      └─────────────────┘
                              │   UNWANTED   │             │        7              8
                              │   MATERIAL   │      ┌──────────────┐  ┌──────────────┐
                              └──────────────┘      │   TRANSFER   │  │ PRESENTATION │
                                                 ──▶│ TRANSPORTING │─▶│   HOLDING,   │
                                                    │     CUP      │  │  ORIENTING   │
                                                    └──────────────┘  └──────────────┘
                                                           ▲                 │      9
                                                           ┊          ┌──────────────┐
                                                           ┊          │   ANALYSIS   │
                                                           └──────────│    X-RAY     │
                                                                      │ DIFFRACTOMETER│
                                                                      └──────────────┘
```

Fig. 2. Block diagram of operations in the lunar material sampling system (discrete sampling scheme)

synchronizing the sample acquisition and vertical transport sequences with the motion required for cutting into bedrock and processing (pulverizing) the cut rock into powder form to satisfy requirements of the X-ray diffractometer sample specifications has been assembled and is being subjected to extensive testing and evaluation.

It is the design and functional intent of this subsystem mechanism to use the principle of the vibrating "helical conveyor," which has been demonstrated as an effective mechanism for sample acquisition and vertical transport. The conveyor mode is synchronized with the rotary-impact type of motions found effective for hard rock drilling and pulverizing. Synchronization of the motions required to accomplish the objectives of the extractor subsystem will obviously eliminate the need for separate

drive mechanisms, achieve the objectives with a minimum number of parts and, hence, will minimize trouble spots and increase the reliability of the system.

The major sub-components of the extractor subsystem mechanism test rig (Fig. 3) are:

(1) *Modified Syntron electric hammer drill.* Electrically, the hammer is still a "self-contained" unit, meaning it has its control (selenium rectifier) built into it. The modification consisted of separating mechanically the hammer body from the handle and trigger switch assembly which also houses the rectifier. The trigger switch is set to the "on" position and a separate line "on-off" switch was incorporated for ease of power control.
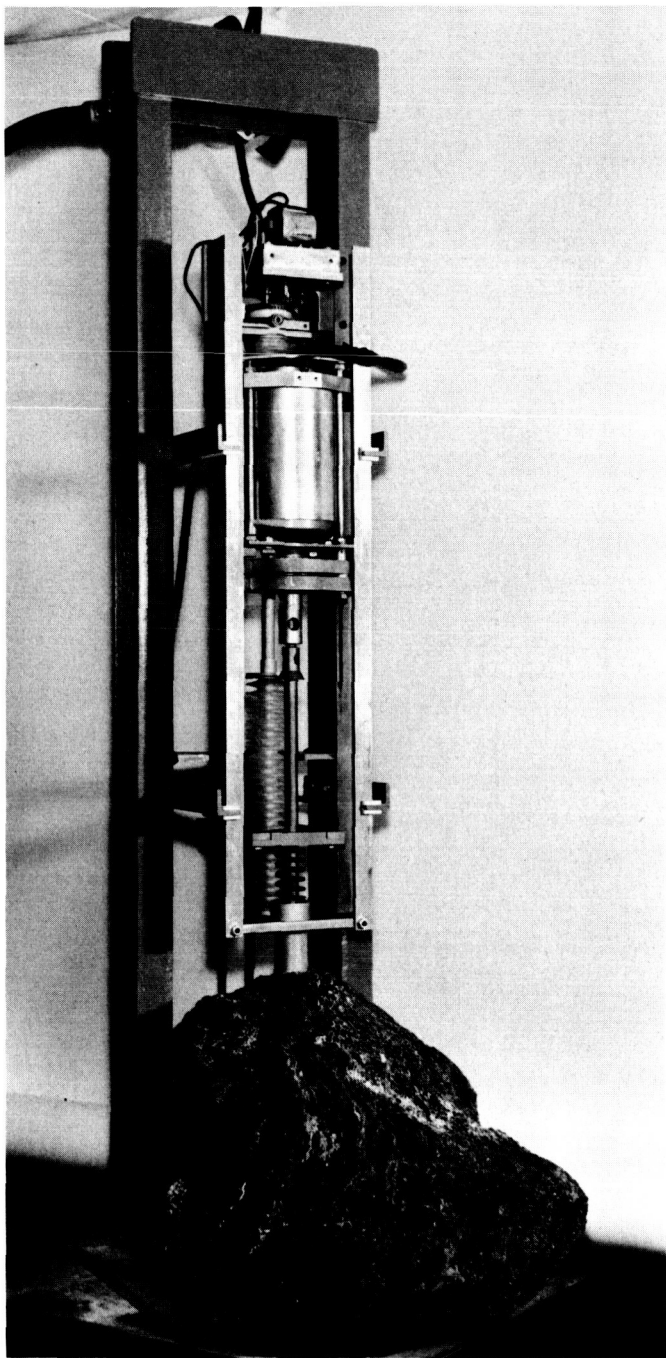
Fig. 3. Extractor subsystem test rig

(2) *Extractor bit-cutter assembly.* This is an improved version of the "helical conveyor" mechanism described previously in SPS 37-31, Vol. VI, pp. 49–53. Basically, the mechanism is the same vibrating "helical conveyor." However, this assembly has been equipped with: (1) a conical deflector for the delivered sample particles in order to minimize

delivery losses between the extractor outer sleeve and the sample particle receiving medium; (2) a tapered shank designed to fit into the *Syntron* hammer chuck; (3) exposed auger flutes at the lower end in order to readily collect and acquire the powdered particles; and (4) a bit-cutter capable of cutting into hard rock (Figs. 4 and 5).

(3) *Feed drive motor and cam assembly.* This provides the linear feed (for the hammer-extractor assembly) into the particulate surface material and into the bedrock. The cam is shaped to provide the sequential operations of rock cutting, processing, sample acquisition, and vertical transport. The feed rate defined by the shape and drive speed of the cam is commensurate with the rate of cutting of the rock. The feed rate therefore becomes a function of the hardness of the rock.

(4) *Feed screw.* The hammer-extractor bit assembly travels axially by rotation of the feed screw which is directly controlled by the feed drive motor and cam assembly. The screw is enclosed in a sleeve and dust bellows assembly to protect the threads.

(5) *Guide chassis.* This serves as guide rails for the hammer-extractor bit assembly.

(6) *Support frame.* The spacecraft will provide this function.

The subsystem mechanism test rig is also designed to be used in investigating the entire sampling system since it is designed to accept the sample transfer and presentation subsystem of the continuous sampling scheme.

Tests have been started on hard granitic rock and soft pumice rock. Preliminary observations noted are:

(1) *Granite rock sampling.* Cutting and drilling is satisfactory. The initial run was made at a feed rate of 0.12 in./min. Sample delivery from the extractor openings commenced at a drill depth of approximately 1.0 in. At a depth of 2.5 in., the total sample delivered from the extractor outlet was approximately 2.2 cm³. Visual examination of the delivered sample showed that the particles were of uniform, finely pulverized size (finer than 15 μ). No rubbles or chunk-size particles were observed. X-ray diffractometer analysis of a sample obtained from this test indicated a very satisfactory pattern and no degradation.
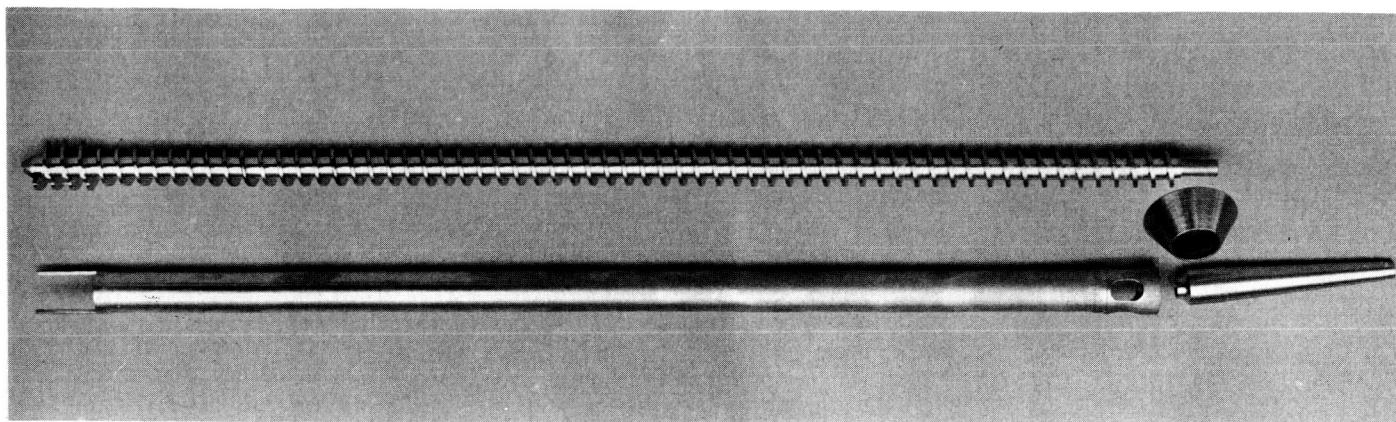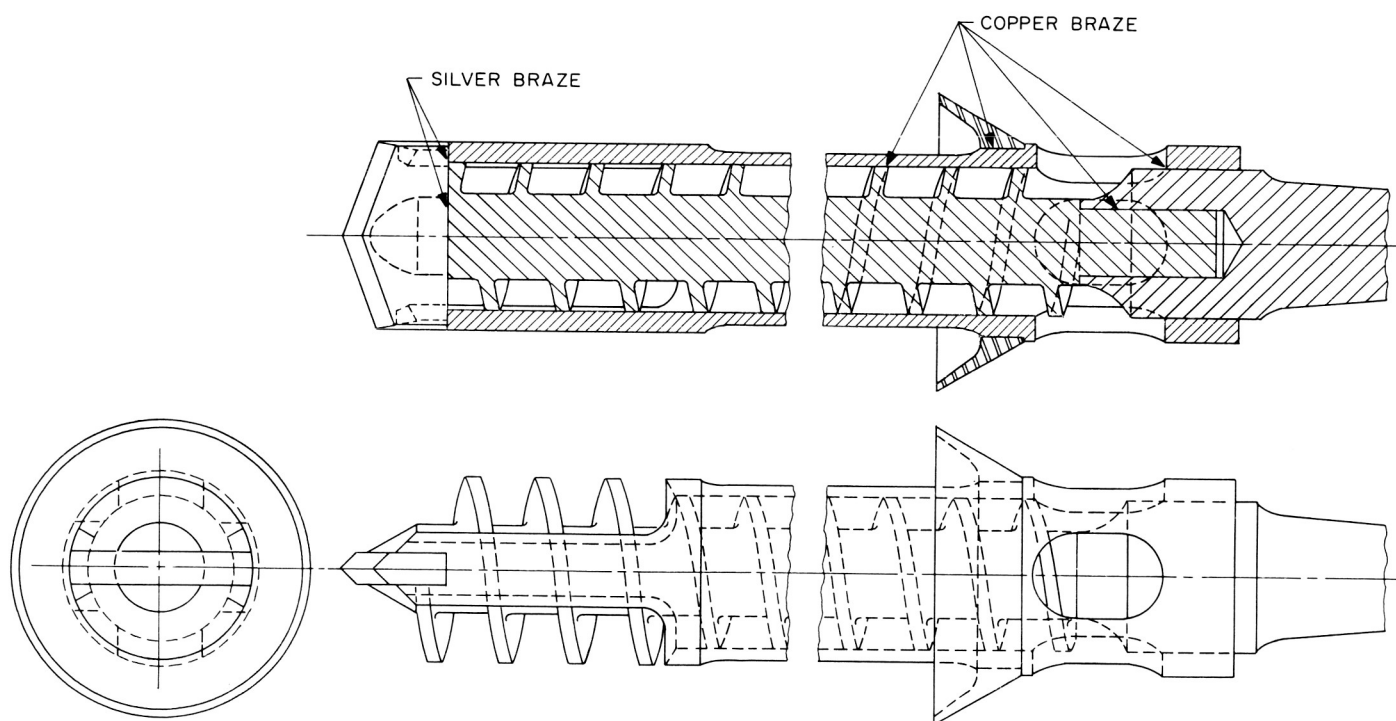
Fig. 4. Extractor bit-cutter components

Fig. 5. Extractor bit-cutter assembly cross section

(2) *Pumice rock sampling.* Cutting and drilling is very satisfactory. Sample delivery from the extractor openings commenced at a depth of 1.0 in. The quantity of samples delivered averaged through three runs indicated an average depth of approximately 1.5 cm³/in. and a recorded maximum amount delivered of about 6 cm³ through a depth of 3.0 in. Visual examination of all samples extracted showed a mixture (unfractionated) containing a small amount of flakes and chunks (minute but noticeable) interspersed in pulverized particles of finer than 15-μ size. X-ray diffractometer analysis of two samples obtained from separate holes but from the same rock indicated very good patterns and satisfactory specimen quality. There was no outstanding difference in quality between the two specimens analyzed.

Transfer and presentation subsystem. Concurrently with the investigations into means of bedrock cutting,

processing, and sample extraction, a development program is being conducted to produce the mechanisms for the transfer and presentation subsystem, which will accomplish the following:

(1) Receive the processed rock and particulate surface material specimens from the extractor.

(2) Transfer the specimens to the sample station of the X-ray diffractometer.

(3) Support the specimen and permit specimen orientation by goniometer drive mechanism.

Various approaches have been and are being studied. This article, however, discusses only one mechanism under each of the two basic schemes, continuous sampling and discrete sampling.

Continuous sampling. The design of the mechanism is based on the principle of the vibrating tray for particle conveyance. The tray is designed to receive and convey all the powdered rock and particulate surface material extracted. It will also serve as the sample holder for the X-ray diffractometer and, hence, is designed to have the capability of being rotated to the required angular range for diffractometer viewing. The vibratory motion imparted to the tray must convey the particles, provide adequate cleaning of tray surfaces in order to prevent (or maintain at a very low level) contamination between phases of the continuous flow of extracted material, and cause zero fractionation in mixtures of different density and/or size specimen particles.

A simple device consisting of a spring-mounted tray and driven by a solenoid was initially used for the preliminary feasibility investigations and study of the problems of contamination and fractionation. All tests conducted on this device relied entirely on visual observations using samples of 20/30-mesh sand and 15-μ quartz. These tests have shown that the vibrating tray principle is a potential means for sample transfer from the extractor delivery station to the X-ray diffractometer viewing station, even at the 15-deg possible spacecraft tilt. Visual observations revealed that fractionation (in mixtures of 20/30-mesh sand and 15-μ quartz) and contamination between phases of a continuous flow are minimal for low-amplitude vibratory conditions. Insufficient friction between the 20/30-mesh sand particles and the metal surface is observed at high-amplitude vibration, so much so that these particles are not conveyed when the tray is
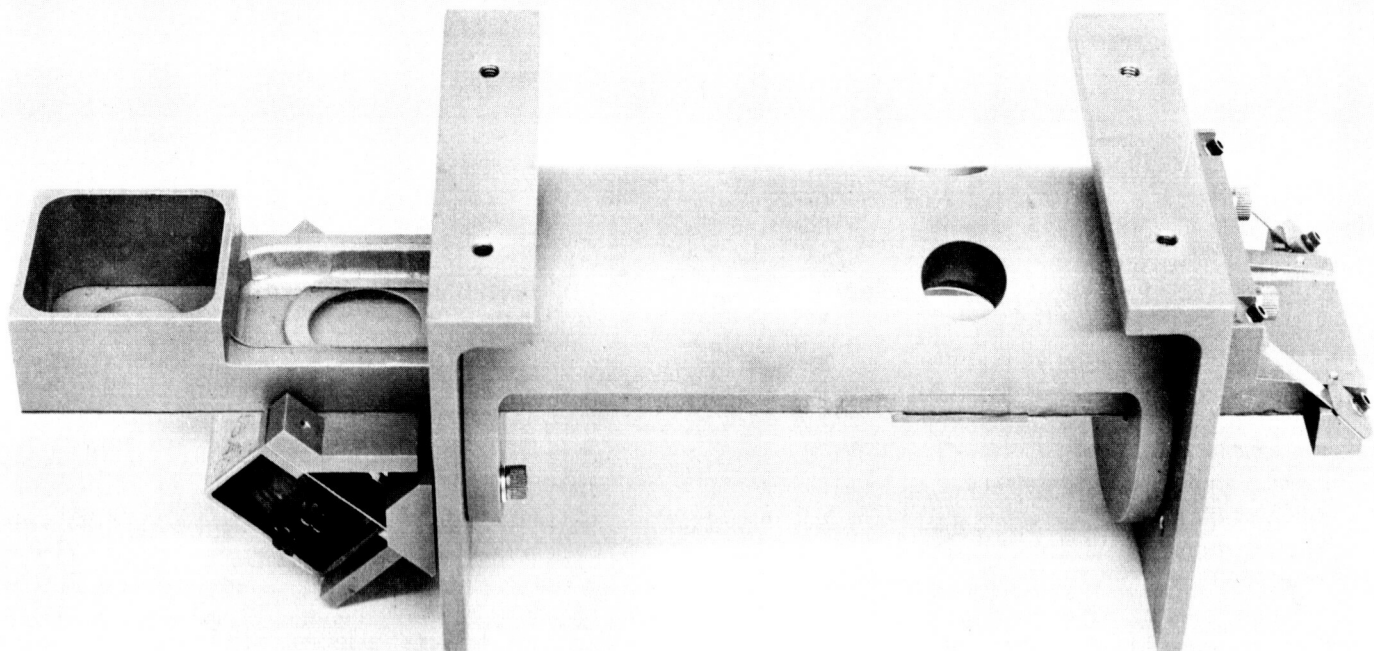

Fig. 6. Transfer and presentation subsystem

tilted to the 15-deg inclination. The very fine powdered specimens are satisfactorily conveyed over a wide range of amplitudes; however, these fine particles may be subject to the contamination and agglomeration problems with high-amplitude low-frequency vibration patterns. This simple rig is not versatile enough to be able to demonstrate the degree of effectiveness and reliability of such a scheme in view of the lack of control and inadequate matching of the springs and the solenoid driver. However, it is felt that this rig satisfied the intent to show partial feasibility and give an indication of the extent of fractionation and contamination, if any, to be expected. Moreover, this rig was satisfactory as a means of revealing problems which would require further investigations in the development of this scheme and of making it worthwhile to proceed with further evaluations using a more complete subsystem assembly.

The complete subsystem mechanism assembly embodying the vibrating tray philosophy, in addition to all the required modes, has been assembled and is being prepared for extensive testing both as a separate subsystem and as an integral part of the entire sampling system. The mechanism (Figs. 6 and 7) consists of the basic tray (box section) with its vibrator drive, spring mounted on rotatable blocks, and fitted with the required X-ray diffractometer viewing window (beryllium foil). The rotatable mounting blocks are designed to orient the tray and, hence, the specimen on the viewing window to the specified 2θ range of the diffractometer optics. Initially, the rotation will be under manual operation; however, it is intended to have this motion coupled to the goniometer drive mechanism of the X-ray diffractometer when the complete diffractometer tests are made.

The main problems apparent at this time, and which will be the principal subjects of the investigation, are:

(1) Collection of adequate sample on the beryllium window—the quantity of sample and the sample density over the window area at all possible spacecraft orientations. Results of the tests will show whether or not the need exists for some means to confine the sample.

(2) Contamination between samples of a continuous flow of powdered rock.

(3) Fractionation of mixtures of different densities and/or sizes during the transfer sequence.

(4) Agglomeration of very fine particles.
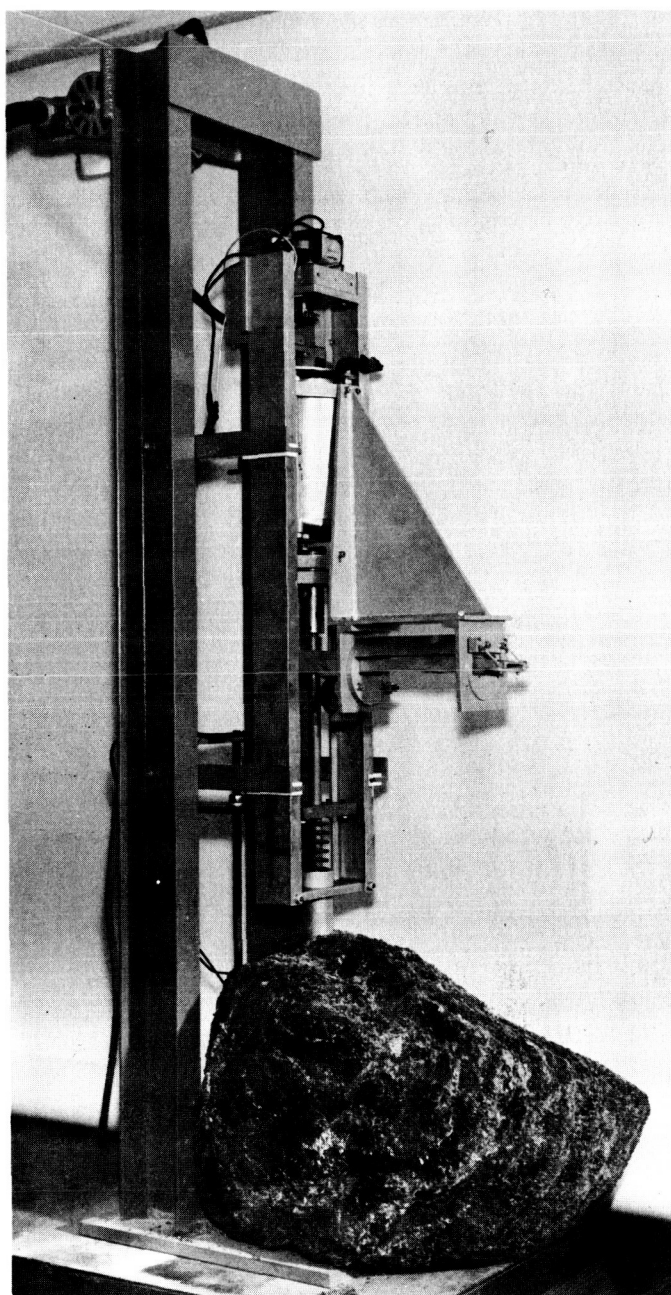
(5) Carrying and presentation of Earth standard sample.

Fig. 7. Complete sampling system test rig

(6) Synchronization of the required motions for transfer and presentation with those motions of the extractor subsystem mechanisms.

(7) Accuracy of sample presentation to the X-ray diffractometer.

Discrete sampling. The basic philosophy underlying the scheme of discrete sampling is to be able to obtain separate samples without intermixing of subsequent

specimens. The mechanism envisioned in this scheme will consist of separate receiving containers for the Earth sample, bedrock pulverized specimen, and the naturally particulate surface material specimen.

A system is being designed presently to demonstrate the idea. The mechanism has a containment device equipped with three separate compartments, two of which are open compartments for the lunar material samples. The third compartment, which is sealed, will contain the Earth sample carried for "before and after" calibration and check runs. This containment device is coupled to the goniometer drive mechanism for the presentation phase; however, a secondary mechanism drive for the transfer phase is incorporated in order to position each compartment alternately at the extractor delivery station and the X-ray diffractometer viewing station. It may be found necessary to include a linear vibrator in conjunction with the transfer drive as a means

of spreading the delivered sample particles over the viewing window. A schematic of the discrete sampling transfer and presentation subsystem is shown in Fig. 8.

This mechanism does not appear to have the problems of fractionation and contamination. As in the case of the continuous sampling mechanism, this device will require some redesign of the X-ray diffractometer and goniometer drive components, but it is felt that these are minor changes to accommodate the functions required of the transfer and presentation subsystem. Accuracy should not be a serious problem either, since essentially the changes consist of replacement of the sample holder assembly designed into the X-ray diffractometer goniometer assembly.

It is realized that this scheme will require exhaustive study and evaluation before it is ready for consideration as the transfer and presentation subsystem of the lunar material sampling system.
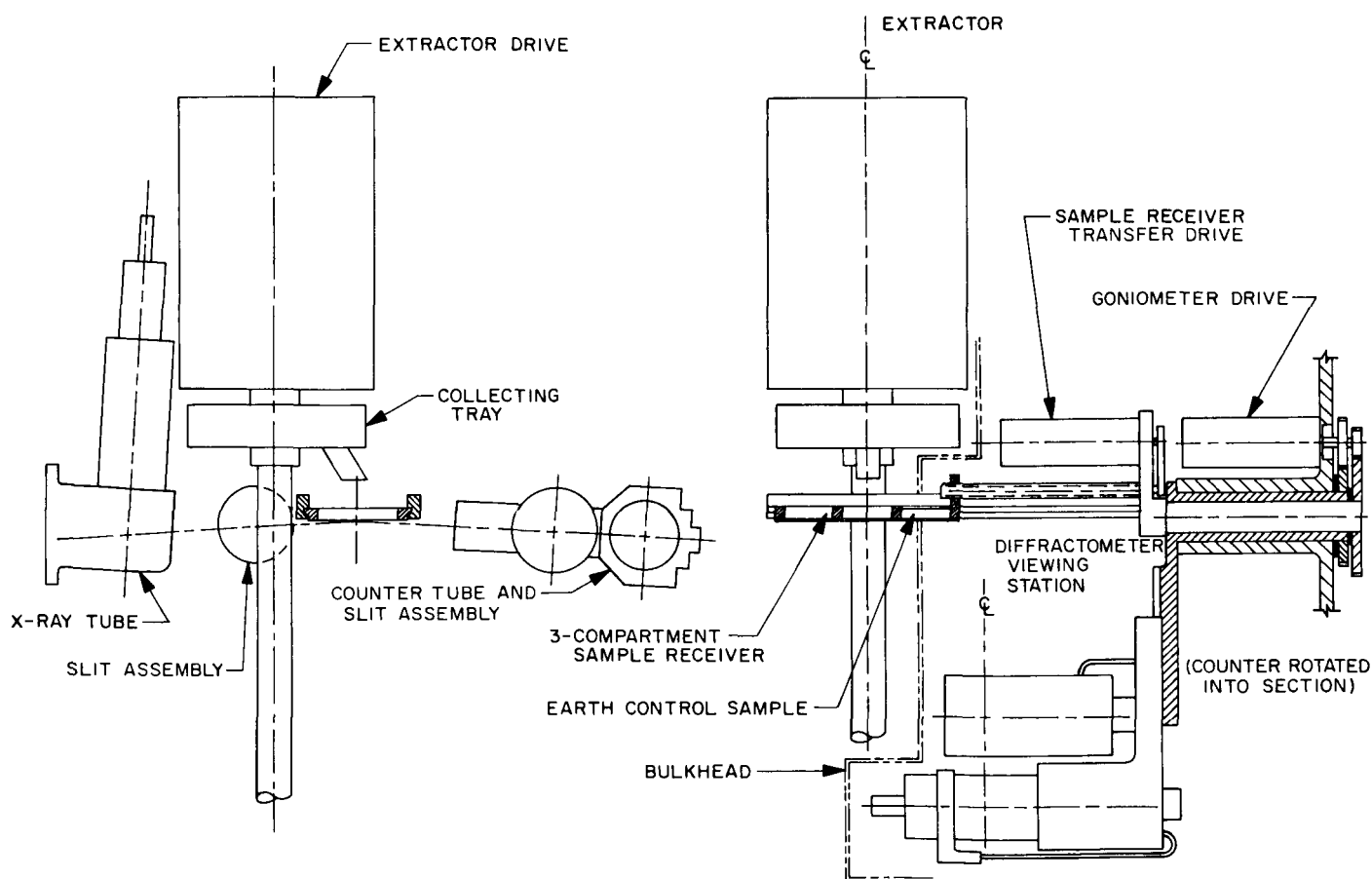

Fig. 8. Transfer and presentation subsystem schematic (discrete sampling scheme)

VIII. Space Instruments

A. *Mariner C* TV Field Support Operations

1. Introduction

A science field support operation for the TV subsystems was set up at the Air Force Eastern Test Range (AFETR) during the launch operations phase for the *Mariner C* (*Mariner* Mars 1964) spacecraft. The primary purpose of the operation was to ensure that the four TV subsystems were flight-ready at launch time. The areas of operation were:

(1) Subsystem calibration.

(2) Supporting spacecraft testing operations.

(3) Interpretation and review of testing data.

(4) Component retrofitting.

(5) Special testing and troubleshooting.

A sizable quantity of equipment was shipped to the AFETR for this operation. One full set of TV development support equipment (DSE) described in *SPS 37-25*, Vol. VI, pp. 43–46, was shipped. The main DSE console (Fig. 1) includes the following equipment required for the operation and data display of the TV subsystem: data

automation system (DAS) simulator, digital-to-analog converter, 2400-cps power supply, Conrac slow-scan TV monitor and scope camera, patch and test-point panel,
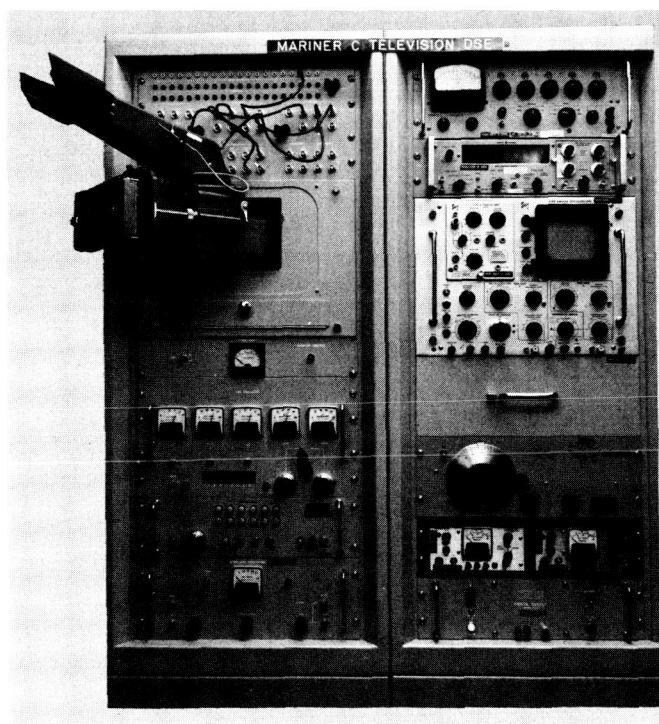

Fig. 1. Main DSE console

and oscilloscope. In addition, the main console also contained standard test equipment for subsystem analysis and troubleshooting. Fig. 2 shows the video film recorder, one of which was shipped. Calibration equipment consisting of two collimators (9- and 40-in. effective focal length), spot photometer, color meter, and a light standard was also shipped. Bench-test hardware consisting of optical benches and carriages was required. A partial bench setup with the TV camera head is shown in Fig. 3. A temperature chamber and assorted analysis and troubleshooting equipment such as meters, bridges, and oscilloscopes were

Fig. 2. Video film recorder

shipped to the AFETR for the operation. The equipment was set up in an assigned area in the science laboratory.

2. Subsystem Calibration

The main purpose for the large quantity of equipment was to support the detail subsystem calibrations. The calibration procedure has been described in SPS 37-28, Vol. VI, pp. 43–48. A detail calibration had been performed on each TV subsystem at JPL. A detailed calibration of each subsystem was also planned at the AFETR for verification of the first calibration and as a recheck after the shutter retrofitting.

It had been initially planned to perform the final calibration of the TV subsystems aboard the spacecraft. The complexity of the calibration procedure, as well as the new mode of spacecraft operation that would be required, caused the plans to be changed. The subsystems were calibrated in the TV operations area of the science laboratory. The camera head was mounted on an optical bench facing a collimator as shown in Fig. 3. The DSE console was used to operate the subsystem. The digital data were processed and recorded on magnetic tapes by the PDP-4 (Programmed Data Processor 4) computer. Film recordings were made of the reconstructed digital data by the video film recorder.

A calibration verification was performed prior to shutter retrofit. This was a short-form calibration for comparison with the original JPL calibration of the response of each subsystem to a flat-field illumination. After the shutter retrofit, a complete detailed calibration of each subsystem was conducted. It was during the calibration that the basic performance of each subsystem was carefully noted and used as a guide for data interpretation of the spacecraft tests. Each subsystem had its own operating characteristics (e.g., different signal-to-noise ratios, different color sensitivity, tube blemishes, and shading), which were also noted during the spacecraft testing.

3. Spacecraft Testing Operations

All spacecraft testing operations that involved the operation of the TV subsystems were carefully monitored. Previous experience with spacecraft testing operations at JPL had shown that on-the-spot monitoring gave the best indication of TV operation, normal or abnormal. The digital printout data received the day after the test, though very valuable, would sometimes be misleading, due to errors in processing or computer programming.
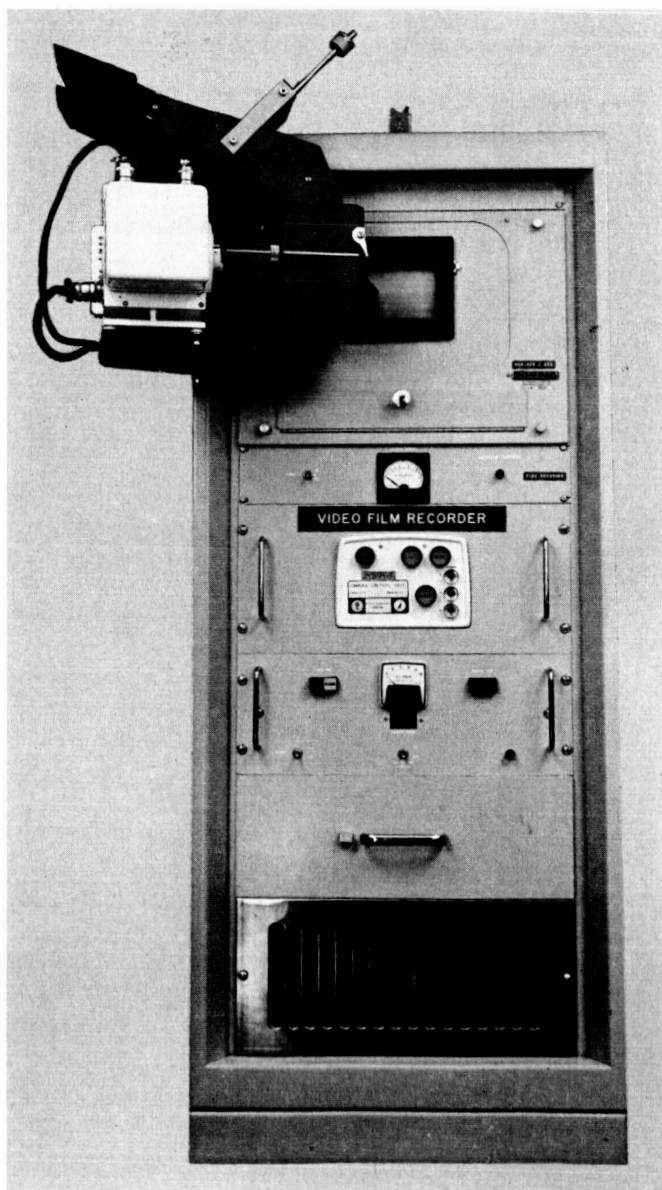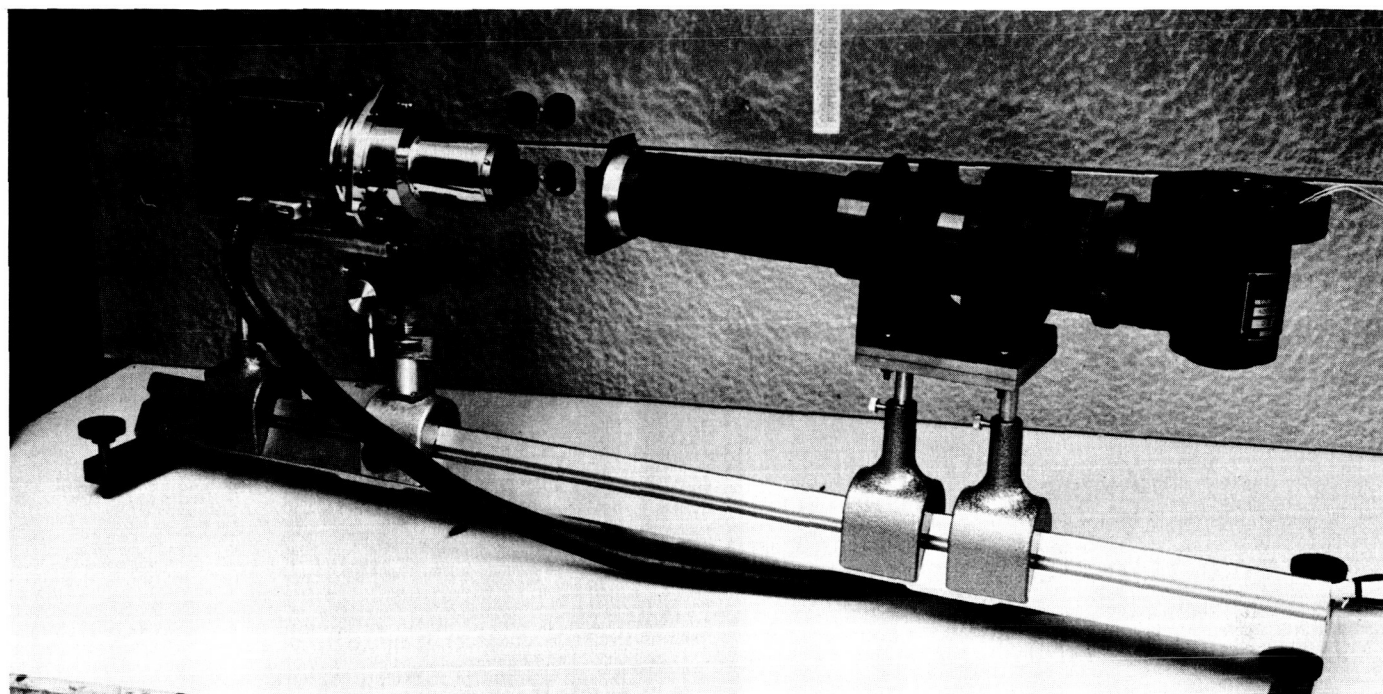
Fig. 3. Collimator and camera head

Three pieces of data display equipment from the science operational support equipment (OSE) were used for observing the performance of the TV subsystems. This equipment was the Conrac slow-scan TV monitor, the oscilloscope, and the real-time data translator (RTDT) printer and electric typewriter. The science OSE was described in SPS 37-24, Vol. VI, pp. 77–84.

The Conrac slow-scan TV monitor presented a full picture display of the TV data. Analog video from the TV subsystem prior to digital encoding, reconstructed 83.3-kc digital video from the TV subsystem, or reconstructed 10.7-kc digital video from the DAS could be displayed on the monitor. The DAS 10.7-kc data were usually displayed, and polaroid pictures were taken for a permanent record.

The OSE oscilloscope was used for continual monitoring of the A-trace display of the three data modes previously described. Experience gained during the design, development, and testing phases of the TV subsystems has shown that the A-trace display was the most valuable method of data display for indicating performance of the TV subsystem. The signal amplitude, signal-to-noise ratio, and shading were best determined from the display.

The RTDT printer and electric typewriter displayed the real-time (RT) data. Three octal words of the RT data

provided the outputs of the telemetry circuits in the TV subsystem:

(1) Word 31 indicated the vidicon control grid (G_1) voltage.

(2) Word 39 indicated the video signal voltage reference.

(3) Word 41 indicated the gain state and amplitude of the TV subsystem, the shutter exposure time, the color-filter wheel position, and the presence of the planet-in-view signal.

Some of the Word 41 data was interpreted from the A-trace display which provided a check on the telemetry circuits and the RT data.

The test monitoring methods described above were used during all spacecraft testing. During the AFETR operations, each spacecraft underwent two systems tests. Each systems test procedure contained a minimum of four encounter sequences in which the TV subsystem was operated. The first three encounter sequences used small pin lights located in the science platform cover, known as pad lights, as the illumination source for the TV camera. An all-white or gray picture was the TV subsystem output for these sequences, as shown in Fig. 4. A complete analysis of the total performance capabilities of the subsystem could not be made from these sequences, but normal or abnormal performance of the subsystem could be judged.
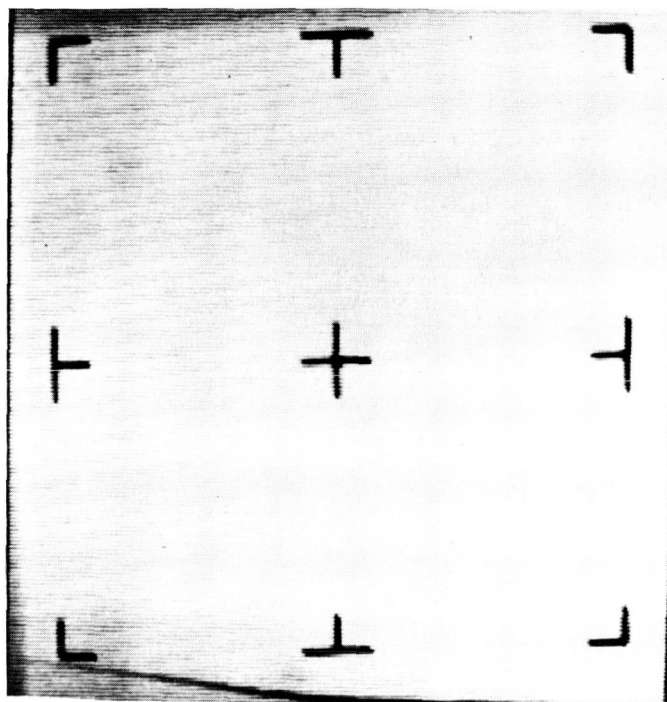
Fig. 4. Pad-light picture

Fig. 5. Shades-of-gray picture

The complete testing of the TV subsystem was performed during the collimator encounter sequence. The science cover was dropped and a collimator was mounted on the spacecraft to provide illumination to the TV camera. The collimator was aligned by a procedure consisting of:

(1) Inserting a test slide and using low illumination, about 200 ft-L.

(2) Observing the A-trace and monitor displays.

(3) Directing the adjustment of the collimator mount for optimum display.

The collimator illumination was then set for 800- to 900-ft-L illumination and a gray slide for checking the planet-in-view operation was inserted. The encounter sequence was started by a planet-in-view signal initiated from the TV subsystem. The second slide was moved into position after Word 41 in the RT data indicated a planet-in-view and Word 39 indicated a change in G_1 voltage. The second slide provided five shades of gray to give a simple test of the contrast capabilities of the TV subsystem. A picture taken of the monitor with this slide is shown in Fig. 5. After 11 frames, a third slide was moved into position. This slide contained a resolution pattern to test the resolving capabilities of the subsystem. Fig. 6 shows a picture taken of the video display from the resolution pattern. At the end of the normal 22 pictures per
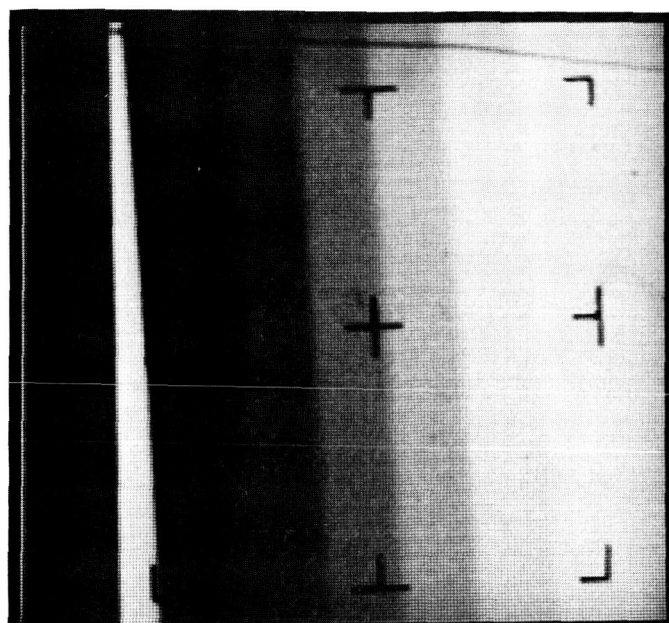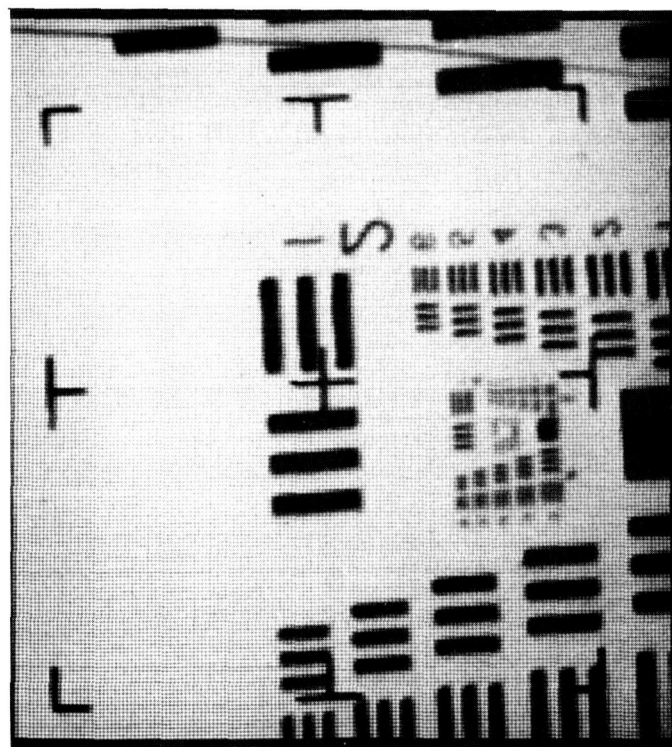

Fig. 6. Resolution-pattern picture

sequence, a fast shutter and gain stepping exercise was conducted. The illumination of the collimator was raised to the point greater than 900 ft-L where the subsystem exposure time changed to 80 msec. The illumination was

then lowered to approximately 50 ft-L. The subsystem gain stepped up to the maximum and the subsystem switched back to normal exposure time. Successful operation in the collimator encounter ensured complete performance of all TV subsystem functions.

The pad lights were used as the illumination source for all other spacecraft testing. The Explosive Safe Facility (ESF) electrical tests and the on-pad checks were carefully monitored to determine the TV subsystem operation in those environments. The Day-1 tests were conducted slightly differently due to the importance of that testing. There were two stations of observation, one on the test complex with the OSE equipment and the other in the science data room. During the encounter sequence, the A-trace display was carefully watched for the slightest deviation from the normal. The monitor pictures were also carefully reviewed. The RT data were observed on a remote printer in the data room and a plot of the TV data was made during real-time. After a comparison of the data observed at both stations, the decision was made that the TV subsystem was qualified for launch.

4. Data Interpretation

Digital printout data were received from each spacecraft test where a TV subsystem was in operation. All data were analyzed and compared with what had been observed from the monitoring of the test. In some cases, 83.3- and 10.7-kc data for the same test were received and these were compared for exactness on a random sampling basis. The video storage playback data were compared word for word with their 10.7-kc data counterpart. The data from pad-light tests were checked for fiducial mark location, bit errors, shading, spots, noise and black mask location. The data from the collimator encounters were checked for contrast, resolution, and saturation in addition to the items checked in pad-light tests. The data were then booked and kept for reference to other tests. The calibration digital printout data were used many times as a reference for analysis of data from the spacecraft tests.

5. Mechanical Operations

Because of shutter wear problems, it had been planned to retrofit shutters into the TV subsystems at AFETR. The field operations were set up for this support. A clean room was provided and the operation was conducted under optimum conditions. A shutter was removed from each subsystem, sent back to JPL for rebuilding, returned, and reinstalled in a subsystem. A careful check was made of the color filters to ensure that they were reinstalled on the same subsystem.

The data displays observed during spacecraft testings in some cases showed spots that were not apparent during calibration. These spots were analyzed and determined to be dust particles on the vidicon face plate. In the clean room, the telescope and shutter were removed and the vidicon face plate cleaned. Data observed during tests after the cleaning process showed that the spots had been removed.

6. Special Operations

Sufficient equipment had been shipped to the AFETR to handle any situations that might arise. It was necessary at one time to perform a thermal calibration on the camera head of one subsystem. The camera head was mounted in a temperature chamber and the temperature controlled from -30 to $50°C$.

The prototype TV subsystem was sent to AFETR for support of OSE checkout and other checkout requirements as needed. The prototype was used for checkout of video cabling from the launch pads and ESF building. Some troubleshooting was required on this subsystem when a component failure occurred. The component was replaced and the prototype put back in operation and tested.

The TV field support operation was terminated with the launch of the second spacecraft. The objective of ensuring that the four subsystems were 100% flightworthy had been accomplished.

B. Mariner C Magnetometer: Development of Modified Helium Lamps and Cells

Failure of helium lamps and cells, both in component testing and in unit testing, indicated the need for a program to increase the reliability of these devices. New lamps and cells of improved design were developed and fabricated at JPL, and the sensor modification required to employ the modified units was authorized under Engineering Change Requirement 7472.

The experimental work that led to an understanding of the failure mechanism and to continuing research work

on helium lamps and cells for an advanced version of the helium magnetometer will be covered in detail in a future *SPS*. This article deals with a qualitative description of the failure mechanism in helium lamps and cells, the operating characteristics of these devices, and the corrective steps taken to extend their lifetime.

In the grossest sense, a failure of either a lamp or cell results from such a loss of helium gas that a glow discharge can no longer be sustained.

Failure of a lamp or cell can be induced by running the unit at a high power level. However, after a unit has failed, it can be revived by applying intense heat (400°C) for 1 hr. This recovery process indicates that the gas has not leaked out of the glass container, but is trapped in the glass near the inside surface of the container. Heating the glass drives the gas back out of the glass. Detailed testing was performed to determine the rates at which gas is lost. Fig. 7 shows an experimental curve representing the gas lost to the glass walls as a function of time, with a helium lamp being discharged at the same level (1-w RF power) as flight lamps. The lamp was run for a number of hours and then evacuated. The lamp volume was then sealed off from the vacuum system, and the lamp was baked out to recover and measure the amount of occluded helium. Curve fitting indicates that, after a very fast initial occlusion rate, the gas is lost to the wall at a rate equal to
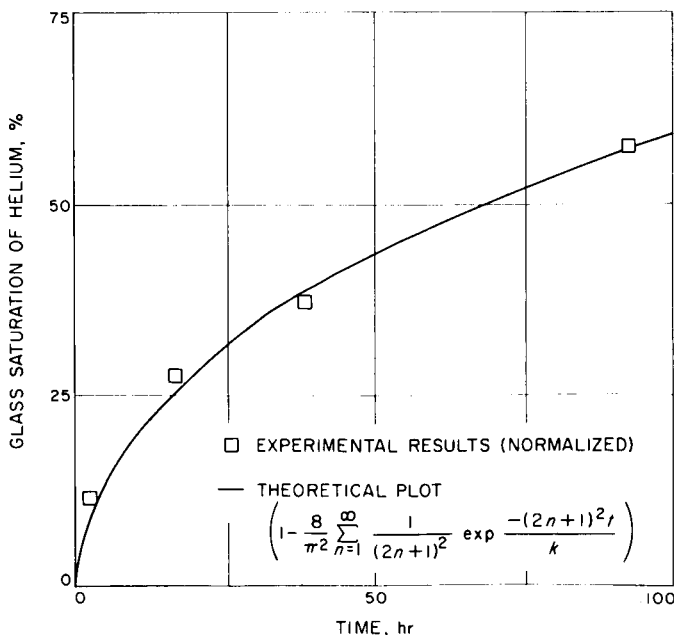
e^{-kt}, where the saturation is approximately half complete at the end of 3-days running time.

Based on the experimental results on the rate of gas loss, a decision was made to increase the volume of the lamp (no space was available in the sensor to increase the volume of the cell) and to increase the pressure at which the lamps and cells were filled. It was necessary to run a series of tests to determine the operating characteristics of both the lamp and the cell versus pressure to establish what increases in pressures could be tolerated.

1. Helium Lamp Characteristics

The two lamp parameters of significance to magnetometer system operation are the intensity of the 1.083-μ light from the lamp under RF discharge, and the ignition potential. The data shown in Fig. 8 were taken by operating a lamp on a vacuum system and varying the lamp pressure. The intensity of the 1.083-μ light was measured, using an interference filter and an infrared light detector. The data indicate that the lamps will operate satisfactorily in the system when filled as high as 10-mm pressure. The ignition voltage indicates that a pressure drop of a factor of 2 can be tolerated.

2. Cell Characteristics

The data shown in Fig. 9 were obtained by operating a breadboard magnetometer in a flux tank adjacent to a vacuum system. The cell in the breadboard sensor was
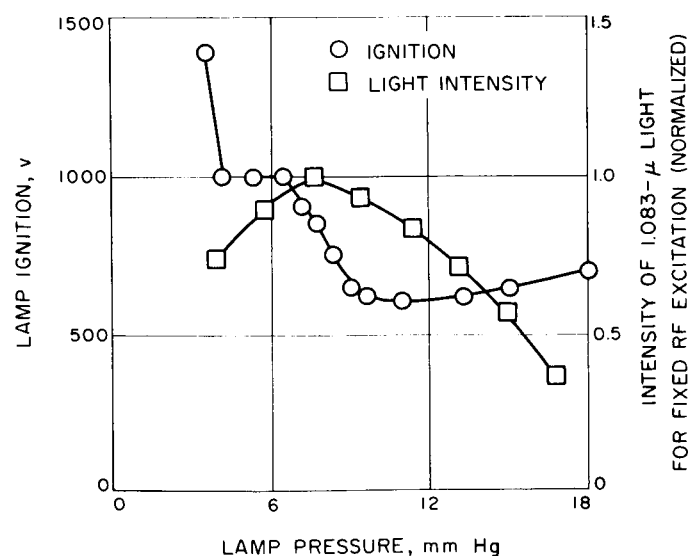

Fig. 7. Loss rate of helium into glass

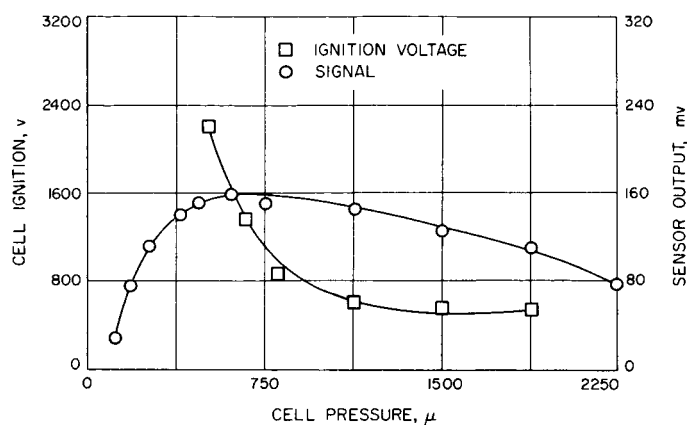**Fig. 8. Lamp ignition potential and light intensity versus pressure**

Fig. 9. Cell ignition potential and sensor signal versus pressure

attached through a long glass tube to the vacuum system, and the pressure in the cell was varied while the magnetometer was operating in a low magnetic field.

3. Modified Lamp Design

The conclusion from lamp tests was that the pressure could be increased to 10 mm over the 8-mm pressure used by Texas Instruments in fabrication of the original lamps. In addition to this pressure increase, a new glass envelope was designed to increase the volume of the helium reservoir by a factor of 3. Since the glass used by Texas Instruments (Corning 1723 Alumino Silicate) has excellent properties for containing helium, no significant improvement could be made by changing glass types. Prior to sealing off the helium lamps from the glass system, the lamps were operated at a discharge level higher than would be used in the magnetometer for 72 hr to saturate the glass with helium. When the lamps were sealed off from the vacuum system, additional glass was added to the tipoff region to ensure a tight seal. Prior to installation in the magnetometer sensor, the lamps were leak-tested and were all found to have measured leaks less than 6×10^{-11} standard cm^3/sec, which would correspond to a loss of gas by mechanical leakage of less than 2% per year.

The helium lamp mounting in the sensor was modified so that the ground electrode was thermally and electrically attached to the aluminum housing of the magnetometer sensor. The RF electrode was wired to the RF matching network with a No. 12 bus wire. The large wire ensured the removal of heat from the glass. With this mechanical installation technique, the temperature of the lamp with 1 w of RF power applied is only 10°C higher than the chassis temperature in vacuum operation.

The design problem of the helium cell is substantially different, since only 100 mw of power are applied to the cell, and with the much greater surface area of the cell compared to the lamp, heating problems are much less severe. However, the mechanical leak rates through glass are proportional to the surface area and inversely proportional to the wall thickness. The low-permeation glass used in the lamp design is not available in the size necessary for fabrication of the helium cell, so Pyrex was used for cell fabrication. The redesign of the helium cell included an increase in glass thickness from 1 to 2 mm to reduce losses by permeation, as well as modified glass seals to allow addition of glass to the tipoff to seal any tunnels that might be formed when the cell is removed from the vacuum system. In addition to these mechanical changes, the data in Fig. 9 indicate that sensor signal is not appreciably degraded by operating at pressures twice as great as the peak operating point, whereas the ignition potential is greatly diminished. The Texas Instruments lamps were filled at 500 μ, which was slightly lower than the peak performance pressure. However, when the glass was heated during the sealing operation, the gas was also heated, but the pressure remained relatively constant because of the buffer volume of the manifold from which the cells were removed. The actual pressure of the gas after the cell was sealed off and cooled to room temperature would be less than the filling pressure, and this would vary from cell to cell. This pressure drop from the sealing of the cell is the most probable explanation for the failure of cells. A slight modification in the magnetometer sensor allowed the use of a long glass tube to seal off the cell, so that heating the glass to seal off the cell did not heat the main body of gas. The leak rates of all cells fabricated represented less than 4% loss per year.

After installation of redesigned lamps and cells in all the *Mariner C* magnetometer sensors, the instrument lamp and cell ignition potentials were monitored to evaluate performance characteristics of these new components. This test does not give absolute information on the helium pressure because, when the units are sealed off, impurities are driven out of the glass, and these impurities affect the ignition potential. It is, however, a good figure of merit, and it is encouraging to note that the most stable units for ignition tests conducted from the time of installation to final testing at the AFETR were those in the *MC-3* (*Mariner IV*) spacecraft. It should also be noted that, by pressurizing both the lamp and cell above the optimum operating pressures, initial degradation in the lamps and cells will enhance system operation.

IX. Space Instrument Systems

A. Methods of Determining the Characteristics and Performance of Radiation Detectors Used in the *Mariner* C Planetary Scan Subsystem

When the mission design and development requirements of the planetary scan subsystem are considered, it follows that one of the most important factors affecting subsystem performance is the operation of the radiation detector. It is not enough for the detector to merely collect radiation from the planet; it must also be capable of transforming the radiant energy into electrical energy efficiently in order to obtain signals indicating both the relative position of the planet and the amount of radiation received. The basic requirements imposed on the detector for the subsystem are:

(1) A definite spectral range of sensitivity corresponding to the assumed spectral radiance characteristics of the planet.

(2) The achievement of a high radiant-to-electrical energy conversion efficiency through the proper combination of characteristics of the optical system and detector.

(3) A definite relationship between the detector electrical output and the magnitude and relative position of the radiation source.

In this article, some methods of relating these requirements in mathematical forms are presented. These methods allow the determination of the characteristics and performance of the detector by defining the various parameters of the detector and subsystem.

1. Carrier Collection and Spectral Response

It is known that the performance characteristics of a p-n junction detector are dependent upon its fabrication material, physical geometry, and electronic parameters. An analysis of the effects of these parameters (*SPS 37-27*, Vol. IV, pp. 92–97) showed that the carrier collection efficiency and relative spectral response of the detector, $\eta_c(\lambda)$, is given by

$$\eta_c(\lambda) = \eta_n(\lambda) + \eta_p(\lambda) \tag{1}$$

where

$\eta_n(\lambda) = p$-layer efficiency

$$= \frac{1}{h(\lambda)\left\{1 - \left[\frac{1}{L_n h(\lambda)}\right]^2\right\}} \left\{\frac{\beta_n}{L_n} \exp\left(\frac{a}{L_n}\right)\right.$$

$$= \frac{\gamma_n}{L_n} \exp\left(-\frac{a}{L_n}\right) - h(\lambda) \exp\left[-h(\lambda)a\right]\right\} \tag{2}$$

$\eta_p(\lambda) = n$-layer efficiency

$$= \frac{1}{h(\lambda)\left\{1 - \left[\frac{1}{L_p h(\lambda)}\right]^2\right\}} \left\{\frac{\beta_p}{L_p}\exp\left(\frac{a}{L_p}\right)\right.$$

$$\left. - \frac{\gamma_p}{L_p}\exp\left(-\frac{a}{L_p}\right) - h(\lambda)\exp[-h(\lambda)a]\right\} \tag{3}$$

$$\beta_n = \frac{[\delta + h(\lambda)]\exp\left(-\frac{a}{L_n}\right) - \left(\delta + \frac{1}{L_n}\right)\exp[-h(\lambda)a]}{\left[\delta + \frac{1}{L_n}\right]\exp\left(\frac{a}{L_n}\right) - \left(\delta + \frac{1}{L_n}\right)\exp\left(-\frac{a}{L_n}\right)}$$

$$\gamma_n = \frac{\left[\delta - \frac{1}{L_n}\right]\exp[-h(\lambda)a] - [\delta + h(\lambda)]\exp\left(-\frac{a}{L_n}\right)}{\left(\delta + \frac{1}{L_n}\right)\exp\left(\frac{a}{L_n}\right) - \left(\delta - \frac{1}{L_n}\right)\exp\left(-\frac{a}{L_n}\right)}$$

$$\beta_p = \frac{h(\lambda)\exp-\left[\frac{a}{L_p} + h(\lambda)d\right] - \frac{1}{L_p}\exp-\left[\frac{d}{L_p} + h(\lambda)a\right]}{\frac{2}{L_p}\cosh\left[\frac{d}{L_p} - \frac{a}{L_p}\right]}$$

$$\gamma_p = \frac{-h(\lambda)\exp\left[\frac{a}{L_p} - \frac{h(\lambda)}{d}\right] - \frac{1}{L_p}\exp\left[\frac{d}{L_p} - h(\lambda)a\right]}{\frac{2}{L_p}\cosh\left[\frac{d}{L_p} - \frac{a}{L_p}\right]}$$

$$\delta = \frac{e}{SKT}\mu_n$$

$L_n = $ diffusion length of the free electrons, cm

$L_p = $ diffusion length of the free holes, cm

$S = $ surface recombination rate, cm-sec^{-1}

$h(\lambda) = $ absorption coefficient as a function of incident wavelength λ (SPS 37-27, Vol. IV, pp. 92–97)

$\mu_n = $ mobility of electrons, cm^2-v^{-1}-sec^{-1}

$\mu_p = $ mobility of holes, cm^2-v^{-1}-sec^{-1}

$d = n$-layer thickness, cm

$a = p$-layer thickness, cm

$K = $ Boltzmann constant

$T = $ temperature, °K

$e = $ electronic charge

It is seen from Eq. (1) that proper values for the various parameters can be selected reasonably to match the spectral response of the detector to that of the radiation source. Such a detector is considered capable of converting the incident energy most effectively. Accordingly, Eq. (1) was solved for a number of cases using the IBM 7094 computer and by substitution of the proper numerical values for the various parameters of a silicon detector in each of the cases. These results have already been presented in the above SPS. As a result of the analysis, the numerical values chosen for the various detector parameters were:

$L_n = 1.0 \times 10^{-4}$ cm $\mu_n = 1200$ cm^2-v^{-1}-sec^{-1}

$L_p = 2.5 \times 10^{-2}$ cm $\mu_p = 500$ cm^2-v^{-1}-sec^{-1}

$d = 5 \times 10^{-2}$ cm $S = 2 \times 10^4$ cm-sec^{-1}

$a = 0.7\,\mu$ $\delta = 300$ cm^{-1}

2. Total Radiation Collection and Detector Spectral Response

In order to establish the over-all radiation collection efficiency for the detector, a number of factors need to be considered. When the radiation is incident upon the detector, some of it is reflected. Also, when the photons absorbed have more energy than is necessary for the generation of electron-hole pairs, the excess energy contributes to lattice vibration and is dissipated as heat. The energy needed for the photon-electron interaction is a function of the energy gap of the material. For every value of the energy gap, an absorption band edge is obtained beyond which the photon energy is not sufficient to create electron-hole pairs and the detector will be transparent to these photons. With the various factors taken into consideration, the over-all radiation collection efficiency is

$$\eta(\lambda) = [1 - r(\lambda)]\left\{1 - \exp[-h(\lambda)d]\right\}\eta_c(\lambda) \tag{4}$$

$$r(\lambda) = \frac{(n-1)^2 + \left[\frac{\lambda \cdot h(\lambda)}{4\pi}\right]^2}{(n+1)^2 + \left[\frac{\lambda \cdot h(\lambda)}{4\pi}\right]^2} \tag{5}$$

where

$r(\lambda) = $ relative reflectivity as a function of incident wavelength λ

$n = $ refractive index of the detector

$\left\{1 - \exp[-h(\lambda)d]\right\} = $ factor accounting for incomplete radiation absorption

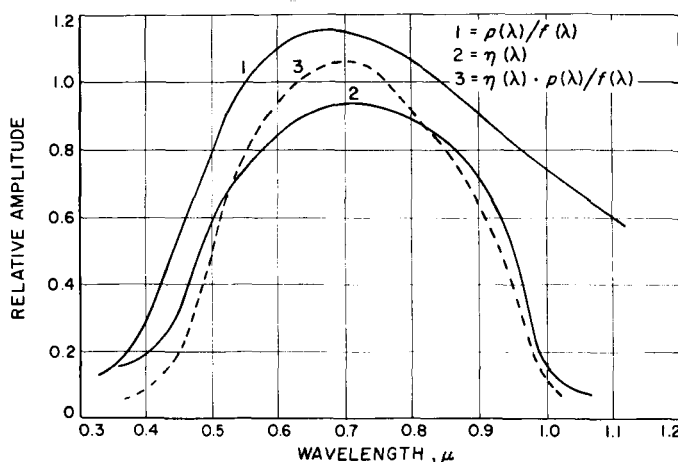$\eta_c(\lambda) = $ carrier collection efficiency as shown in Eq. (1)

Fig. 1. $p(\lambda)/f(\lambda)$ **and** $\eta(\lambda)$ **as functions of wavelength**

$\eta(\lambda)$ in Eq. (4) was calculated and plotted as Curve 2 on Fig. 1. This curve was generated with $\gamma(\lambda)$ as the reflectivity curve having the value of 4.1% at 0.5 μ, 0% at 0.7 μ, and 6.5% at 1.0 μ. Since $\eta(\lambda)$ is plotted as a function of the incident energy wavelength, the shape of the curve represents the over-all spectral response of the detector. It is seen from Fig. 1 that, when the numerical values of the parameters of the detector were properly chosen, the detector spectral response was reasonably matched with the spectral response of the source for high-energy collection efficiency.
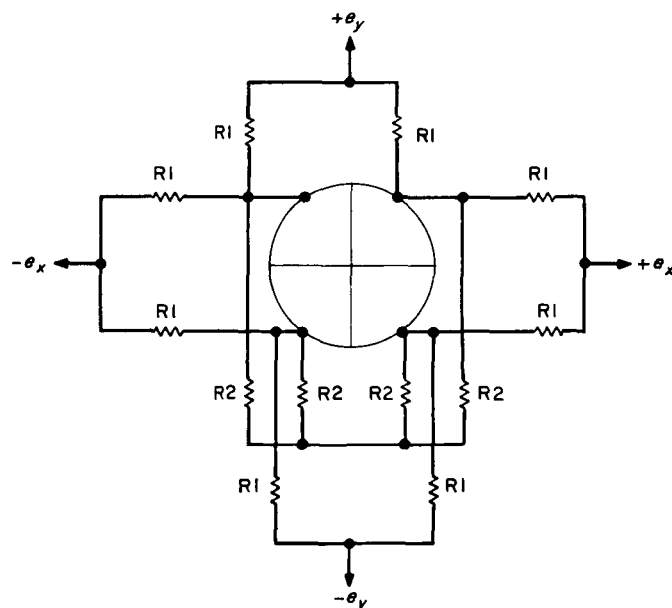

Fig. 2. Detector output

3. Physical Description and Detector Output Characteristics

The detector was fabricated to have a useful area 1.000-in. in diameter with an over-all diameter of 1.125 in. and was chemically etched to form four quadrants of equal area. The depth of the etch was such that the top p-layer, including the detector junction, was separated from the bottom n-layer to form four electrically isolated quadrants. To form a two-axis device, two differential output pairs, e_x and e_y, were formed as shown on Fig. 2, and an optical lens system having a circular field-of-view of 50 deg was used to focus the planet image on the detector surface. The output of the detector can be related to the various parameters by Eq. (6).

$$e_x, e_y = [1 - R(\theta)] \cdot [\Delta A(\theta, \beta, \phi)] \cdot \delta(\theta)$$
$$\times E(r, \alpha, \lambda) \cdot K(I_s, V_0, Z_s, Z_h) \qquad (6)$$

where

$$R(\theta) = \frac{1}{2} \left\{ \left[\frac{n^2 \cos\theta - (n^2 - \sin^2\theta)^{1/2}}{n^2 \cos\theta + (n^2 - \sin^2\theta)^{1/2}} \right]^2 \right.$$
$$\left. + \left[\frac{\cos\theta - (n^2 - \sin^2\theta)^{1/2}}{\cos\theta + (n^2 - \sin^2\theta)^{1/2}} \right]^2 \right\} \qquad (7)$$

= Fresnel coefficient of reflection for unpolarized incident energy as a function of incident or planet position angle θ.

$$\Delta A(\theta, \beta, \phi) = \frac{1}{\pi} \left[k_1^2 \cos^{-1}\frac{y}{k_1} + \cos^{-1}(k_2 - y) - 2\cos^{-1}k_2 \right]$$
$$- \frac{1}{\pi} \left[y(k_1^2 - y^2)^{1/2} + (k_2 - y) \right.$$
$$\left. \times [1 - (k_2 - y)^2]^{1/2} - 2k_2(1 - k_2^2)^{1/2} \right] \qquad (8)$$

= factor relating planet angular semidiameter β, optical angular half field of view ϕ, and planet position angle θ.

$$y = \frac{k_1^2 + k_2^2 - 1}{2k_2}; \quad k_1 = \frac{\tan\phi}{\tan\beta}; \quad k_2 = \frac{\tan\theta}{\tan\beta}$$

$$\delta(\theta) = [1 - \sin 2\theta]$$

= factor relating the fractional illuminated planet and optical geometry to planet position θ.

$E\ (r,\ \alpha,\ \lambda)$, the input energy from the planet, can be calculated by assuming the planet has the spectral radiance property of $p\ (\lambda)/f\ (\lambda)$ as shown on Curve 1 of Fig. 1.

$$E\ (r,\ \alpha,\ \lambda) = \frac{E_v \cdot \phi\ (\alpha) \cdot K\ (\alpha) \cdot A \cdot \tau}{\Delta^2 \cdot r^2} \int_{\lambda_1}^{\lambda_2} \frac{p\ (\lambda)}{f\ (\lambda)}\ \eta\ (\lambda)\ d\ (\lambda) \tag{9}$$

where

E_v = monochromatic energy flux at λ = 0.55 μ corresponding to visible albedos $r = 1$, $\Delta = 1$

= 1.52×10^{-11} w-cm^{-2}-μ^{-1}

$\phi\ (\alpha)$ = phase function at the phase angle of α (Sun-planet-detector angle)

= 0.406 when α = 60 deg

A = aperture area of the optics

= $\pi d^2/4$ = 1.32 cm^2 for d = 1.3 cm

τ = transmission efficiency of the optics

= 0.80 or 80%

$K\ (\alpha)$ = illuminated fraction of the planet at phase angle of α

= $\frac{1}{2}(1 + \cos \alpha)$

r = distance from planet to the detector in astronomical units

Δ = mean distance from planet to Sun in astronomical units = 1.524

$p\ (\lambda)$ = assumed planet spectral reflectivity

$f\ (\lambda)$ = spectral energy function of solar radiation

λ_1, λ_2 = cutoff wavelength of the radiation gathering system

$\eta\ (\lambda)$ = over-all spectral response of the detector as shown in Eq. (4)

$K\ (I_s, V_0, Z_s, Z_h)$ = detector responsivity as a function of short-circuit current, open-circuit voltage, series and shunt impedance
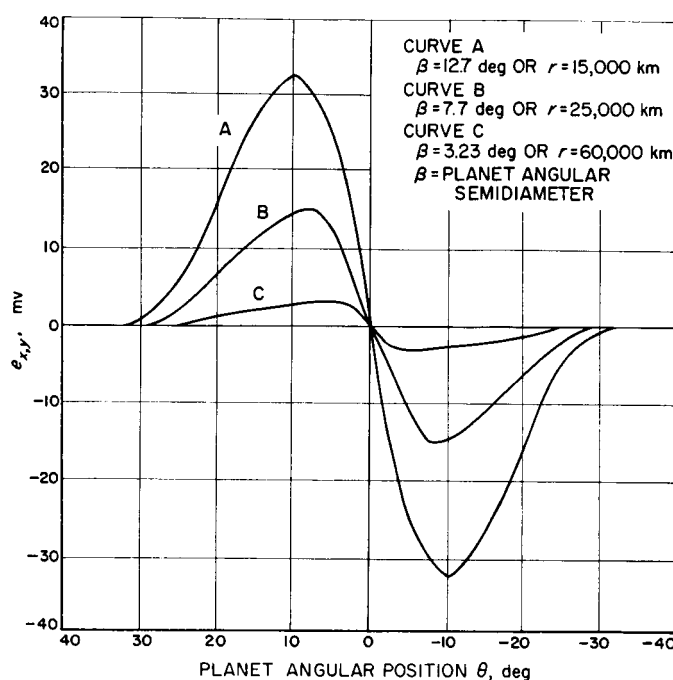
= 750 $\mu v/\mu w$

Fig. 3. Calculated detector output as a function of planet angular position

To show the effects of the various parameters on the detector of x- or y-axis output, $e_{x,y}$ was plotted as a function of the planet position angle θ with the planet angular semidiameter β as the parameter (Fig. 3). It is seen from the figure that the magnitude and polarity of $e_{x,y}$ can be used to determine the position of the planet image with respect to the detector axis, and the magnitude of $e_{x,y}$ can be used to determine the amount of energy received at a distance at which the planet is considered to have an apparent angular semidiameter of β. Accordingly, e_x was used as an error signal for planet tracking, and e_y was used to indicate the planet position in terms of θ, the angle between the direction toward the center of the planet and the optical line-of-sight.

To evaluate the performance of the actual detector, tests were performed on a subsystem using a planetary simulator (SPS 37-25, Vol. VI, pp. 56–58). The output of the detector y-axis, e_y, was amplified and converted from a bipolar to a unipolar signal, V_y. Fig. 4 shows the measured V_y (in solid line) when the subsystem was operating at various conditions. The calculated y-axis outputs are shown in dashed lines on the same figure. These calculated curves were obtained by multiplying the detector output e_y of Eq. (6) by the closed-loop amplification factor of the subsystem y-axis electronics for each operating condition. It is seen from these curves that the y-axis output can be used to determine the relative position of the
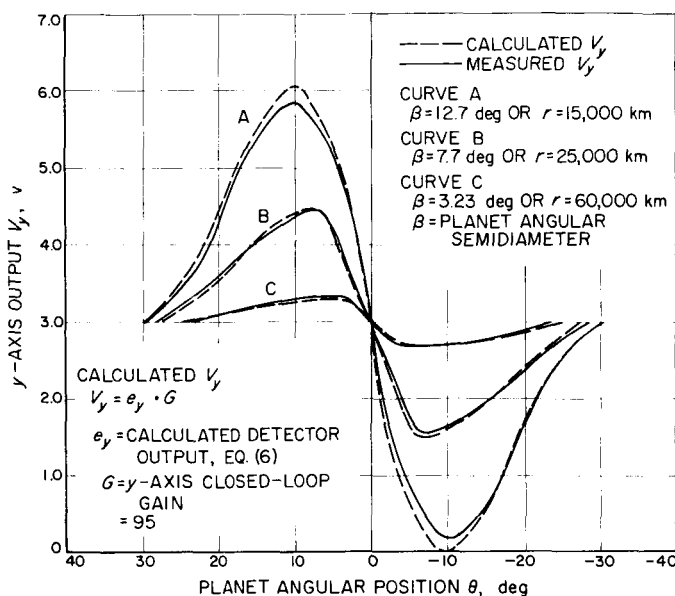
Fig. 4. y-axis output as a function of planet angular position

planet by the magnitude and the sign of the slope of these curves.

It is also seen from these curves that the measured values tended to deviate from the calculated values as β increased. Although a detailed analysis has not yet been performed, it is likely that these deviations resulted from a combination of the following: (1) the numerical solution from Eq. (9) becomes less accurate as the value of β becomes large, and (2) the detector output was calculated by Eq. (6). In this equation, the detector's responsivity was assumed to be constant over the entire input energy range. To a certain extent, therefore, the deviation in Fig. 4 can be used to indicate the amount of nonlinearity in the detector's responsivity as a function of input energy.

4. Discussion

The presence and relative position of the planet may be detected and determined through the detection of either the planet's blackbody radiation in the far infrared spectrum range of 10 to 40 μ or the planet's reflected solar energy in the visible and near infrared spectrum range of 0.4 to 1.5 μ. A study has been made on the characteristics of various detectors capable of performing the tasks. A detector sensitive in the far infrared region can be utilized for this purpose, but predetection modulation of the infrared signal, usually by mechanical chopping, is required for effective detector operation. At

present, infrared detectors of practical application also require active cooling to achieve the desired responsivity. Detectors of the photoconductive type can be used to detect radiation in the visible and infrared regions. For precision planet-position and intensity indications, such detectors require highly regulated power supplies to provide bias for their operation. Thermocouple detectors with the proper filters can also be used to sense radiation in the visible and infrared regions, but complications arise in the design of the electronic circuitries required to handle the extremely small output signal from the thermocouple. To overcome some of these difficulties, the p-n junction type of detector was selected for the subsystem, since the outputs of this type of detector are self-generating and no bias supply or other external devices are required for its operation.

A study has been made on a lateral junction detector capable of generating a pair of voltages e_x and e_y proportional to the radiation spot displacement on its surface. The linear dependence of the output signal upon the radiation spot displacement is desirable, since it is relatively easy to interpret the position of the radiation source from the linear relationship with the output voltage. Analysis (*SPS 37-22*, Vol. IV, pp. 270–275) indicated that the sensitivity of this detector was highly dependent on the layer resistivity. A detector with adequate sensitivity would have had to be fabricated from material with resistivity on the order of 1500 ohm-cm or higher, and the fabrication of sufficiently uniform silicon detectors of such high resistivity was found to be impractical. This article described some methods of determining the characteristics and performance of a p-n junction silicon detector made of material having low resistivity. This detector has been successfully developed and incorporated in the *Mariner C* planetary scan subsystem as the radiation-sensing element to detect and track the planet, so that the planetary experiment instruments are correctly oriented for making encounter measurements.

Additional information can also be obtained from the y-axis output as shown on Fig. 3. The slope of these curves at $\theta = 0$ is a function of the planet angular diameter. Since the detector-to-planet distance is related to the angular diameter by the known optical geometry, the approximate distance can be calculated from the value of the slope at $\theta = 0$ or

$$\left.\frac{dv_y}{d\theta}\right|_{\theta=0}$$

where v_y is related to θ by Eq. (6).

B. Advanced *Mariner* Data Automation System Development

1. Introduction

This task was started for the *Mariner* 1966 Project in FY 1964. It was part of the over-all task to design a data automation system (DAS) for the acquisition of data from several planetary scanning instruments on a flyby mission. These instruments were:

(1) Infrared (IR) interferometer

(2) Ultraviolet (UV) spectrometer

(3) Mars scanner

When the *Mariner* 1966 mission effort was discontinued, the DAS design and development task was continued on a reduced basis. The purpose in continuing the DAS effort was to develop and improve the capability for handling data from scanning instruments on future planetary flyby or orbiter missions.

Several areas of work were considered basic to this task. These areas and their objectives were:

a. Circuit design. A digital logic family was to be developed, incorporating design improvements over existing logic circuits and undergoing a computer worst-case analysis. The standardization of interface circuits was to be investigated and accomplished wherever possible.

b. Packaging. New and more reliable approaches to the packaging of discrete components in a welded cordwood module and methods of module interconnection to optimize the number of circuits and modules per tray were to be investigated.

c. Logic. The UV spectrometer was considered typical to demonstrate the logic design of a scanning instrument. The design would utilize any new logic circuits developed and would eventually be breadboarded with actual flight circuits wired on small plug-in cards.

d. Buffer memory. Investigation of small-capacity buffer storage devices was to be undertaken. The *Mariner C* buffer would be reviewed, as well as other state-of-the-art techniques. Packaging and peripheral electronics were to be a major consideration.

e. Tape recorder. A tape recorder of approximately 10^6-bits capacity was required for storing the data from such a scanning instrument as the UV spectrometer. While other projects require a central bulk-storage device capable of storing data from several instruments, there are some circumstances which indicate a need for an independent recorder. This task would make use of existing designs such as the Kinelogic "Iso-Elastic" drive recorder system (*SPS 37-25*, Vol. IV, pp. 217–226). The primary objective here is to make the necessary modification of the existing design.

2. Circuits

a. Objectives. Due to the extensive amount of circuitry required to process and multiplex the scientific data into the single, serial, binary data channel used for communication at planetary distances, low power consumption (a few milliwatts per circuit) is more important than extreme microminiaturization. Silicon integrated circuits have a potential for better reliability than circuits using discrete components; however, present designs consume too much power for many of our applications. Techniques for decreasing the power consumption are promising, but reliability sufficient for an interplanetary mission will not be demonstrable for some time. Work must continue

Table 1. Digital logic family circuit specifications

Circuit	Maximum frequency, kc	Typical power, mw	Fan-out[a], unit loads	Fan-in, number of inputs	Flip-flop load[a], mw (enable)	(trigger)	Noise immunity, v
Nand gate	500	5.2 (output) 6.1 (input)	9	9	—	—	> 0.5
Flip-flop	500	11.2	9	—	0.5	2.5	> 0.5
Flip-flop	65	7.1	9	—	0.25	1	> 0.5

[a]The nand gate input is considered a unit load.

ALL TRANSISTORS 2N914
ALL DIODES FD643

VALUES FOR 65-kc OPERATION

R5 & R6	R9 & R10	R11 & R12
39.2K	100K	39.2K

Fig. 5. 500-kc logic flip-flop

CR1, CR2, CR5: FD643
CR3, CR4: FD306
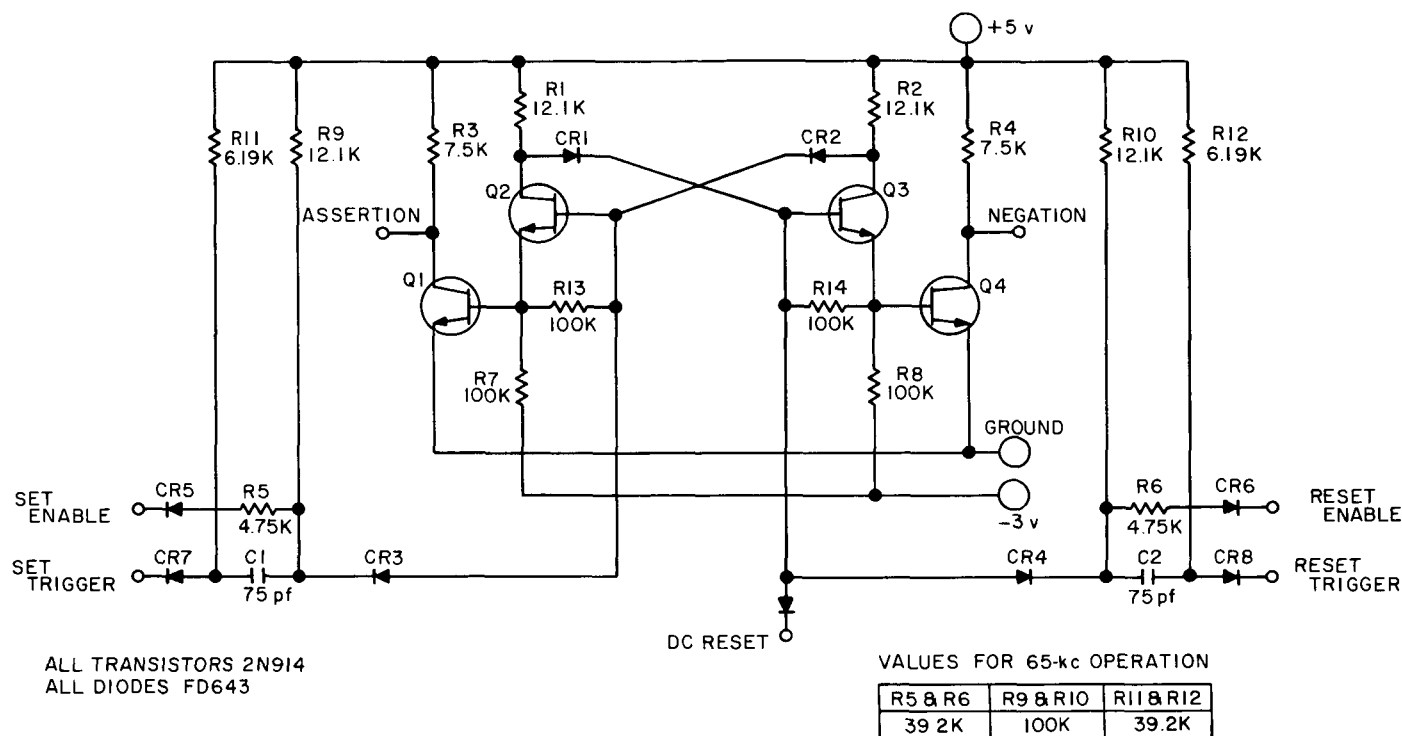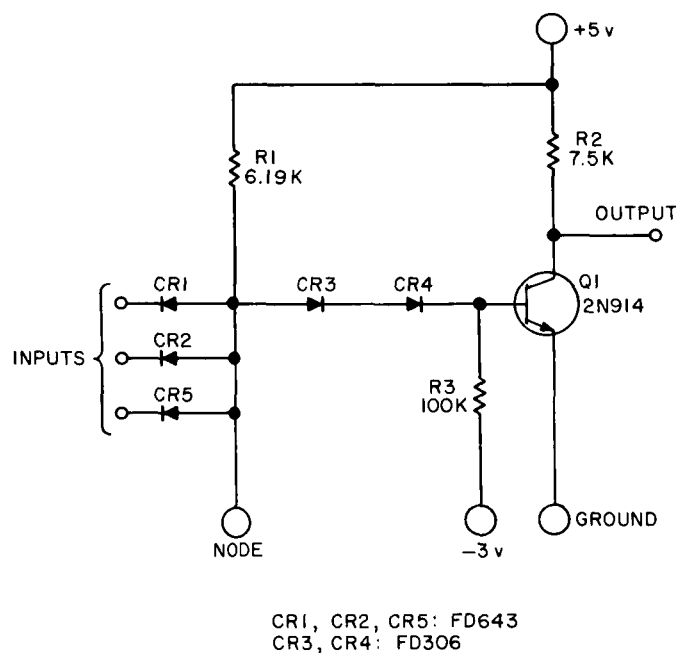
Fig. 6. Expandable *nand* gate

on discrete component designs in parallel with the evaluation of integrated circuits. The diode-transistor *nand* gate was selected for examination and refinement because of its potential for low power consumption, reasonable

speed, and good noise margins. Furthermore, the same factors apply to the choice of logic for low-power integrated circuits.

The state-of-the-art in worst-case design and testing concepts was to be utilized and advanced. The circuit designs should be compatible with the packaging design (discussed later in this article).
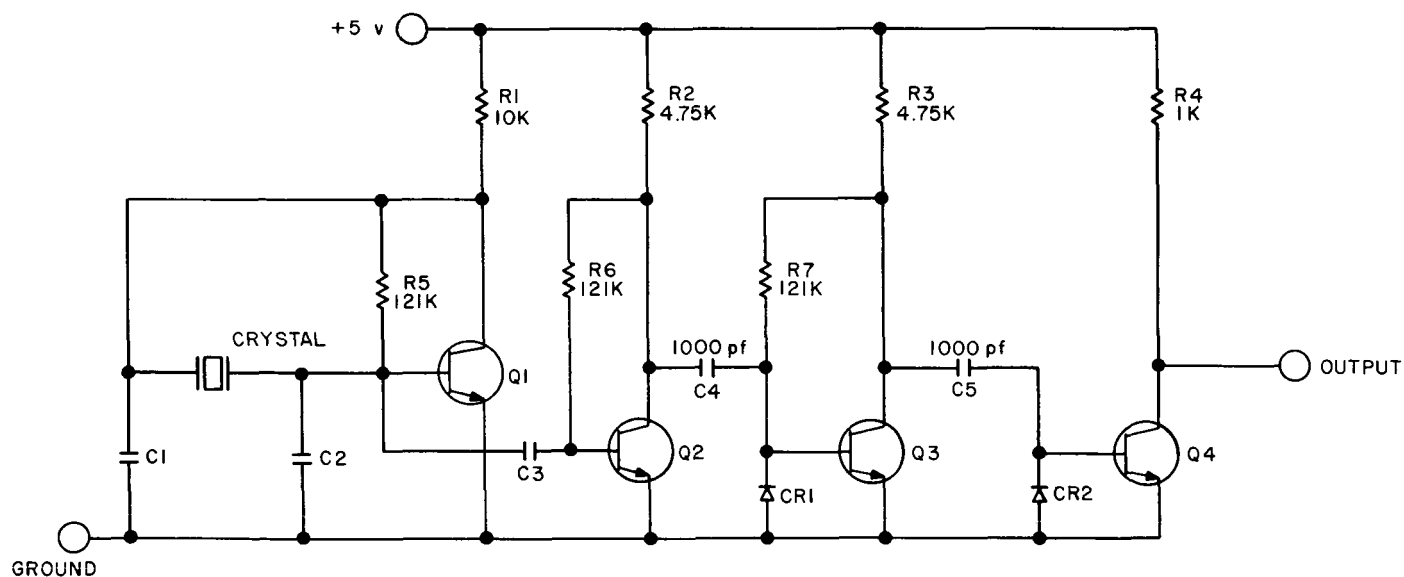
b. Design. The development of a digital logic family for the DAS was undertaken by the design and worst-case analysis of the digital circuits shown in Figs. 5 and 6. The General Electric Company at Valley Forge, Pa., performed the worst-case analysis using the SPARC method and a Recomp II computer (Ref. 1). The design of these circuits was accomplished exclusively with components from the JPL Hi-Rel or Preferred Parts List. Some of the more pertinent worst-case logic rules and typical power consumptions are listed in Table 1.

A noninverting logic driver capable of driving up to fifty loads has also been designed. This driver will be subjected to a worst-case analysis similar to that of the flip-flop and *nand* gate. Fig. 7 shows the circuit diagram of the driver.
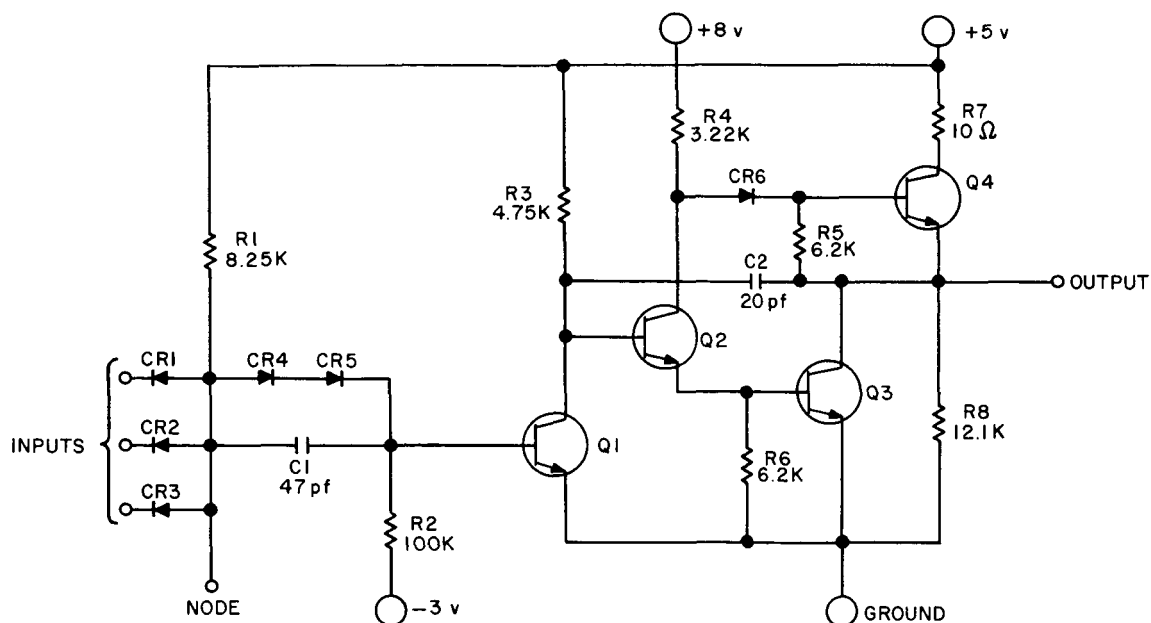
Fig. 7. Noninverting logic driver

ALL DIODES: FD643
ALL TRANSISTORS: 2N914

Fig. 8. Crystal-controlled Pierce oscillator

ALL DIODES: FD643
ALL TRANSISTORS: 2N914

The crystal oscillator shown in Fig. 8 has been designed for a wide range of DAS applications. Among these is the requirement for a stable clock for the analog-to-digital conversions. The oscillator is the Pierce configuration; it has undergone a manual worst-case analysis for oscillator frequencies from 50 to 500 kc. Applications for using two such oscillators in synchronism are being investigated. Such a mode of operation could be used

to increase the oscillator reliability through redundancy. Analysis and laboratory measurements indicate that synchronization is practical.

An improved version of the *Mariner C* analog-to-pulse width (A/PW) converter (*SPS 37-24*, Vol. IV, pp. 84–87) has been designed and packaged at JPL. Fig. 9 shows the welded cordwood construction of the new A/PW converter module. Some of the improvements include:

(1) Bipolar analog input.

(2) Improved linearity.

(3) Improved temperature stability.

(4) Transformer-coupled output.

General specifications are found in Table 2.

3. Packaging

New packaging ideas for discrete components in welded cordwood modules have been under investigation since FY 1964. The investigation has been aimed at improvements in several problem areas which previous DAS packaging has experienced. Some of these areas are:

a. Module interconnection. A new method for increasing the circuit density per tray without increasing intermodule wiring congestion is a fundamental problem related to the ease of repairing a system.

b. Flexibility. Changes in the scientific instruments are often desired at a later date. The packaging scheme

Fig. 9. Bipolar A/PW converter module

Table 2. Bipolar A/PW converter specifications
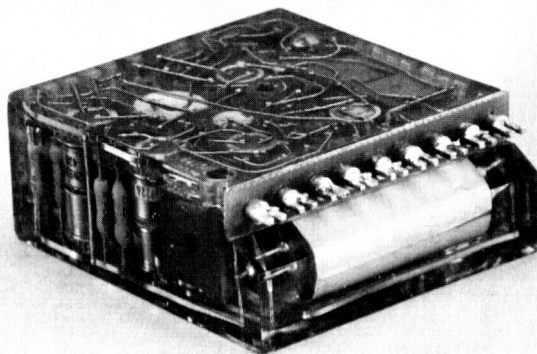
Analog input	$+6$ to -6 v
Data output	The data output is the time difference measured between two voltage pulses occurring on separate output lines. The polarity of the analog input is determined by noting the order in which the pulses occur. A full-scale output from several hundred microseconds up to approximately 10 msec is attainable through proper component selection during the fabrication process.
Conversion accuracy	$\pm 0.05\%$ of full-scale
Conversion stability	$\pm 0.3\%$ of reading ± 2.5 mv over the temperature range -10 to $+80°$C
Linearity	0.05%
Supply voltage	$+15$ and -15 v $\pm 10\%$ tolerances
Power consumption	75 mw
Operating temperature	-10 to $+80°$C
Sample rate	500 samples/sec (max)
Component count	74

should be able to accommodate mandatory changes without serious schedule or reliability consequences.

c. Logic module simplification. The need for module simplification is important. The fewer the module types and the more universal their applications, the simpler the fabrication, testing, and reworking; the greater the reliability.

In considering the module simplification problem, the number of different types of basic logic circuits has been held to a minimum. In this instance, the logic is restricted to the use of a single *nand* gate, one reactive-triggered flip-flop (two versions: 65 and 500 kc) and a noninverting driver. With these basic circuits, it has been demonstrated that 90% of the UV DAS logic can be implemented.

It is obvious in most logic systems that many logic elements share common inputs and outputs or are grouped together in common circuit functions. An example of this would be the flip-flops in a shift-register stage or a group of gates in a decoding matrix. Intramodule wiring congestion can be reduced by making good use of this fact. If these circuits, sharing common functions, are chosen to be contained within the same module, then prewiring of the module can be accomplished to eliminate later external connections. To avoid manufacturing a large

number of such special modules, the design of a utility module has been undertaken. This module is a standard module of a fixed configuration and employs a fixed number of gates or flip-flops. The modules would be fabricated, potted, and then tested as a single module type. The utility concept is introduced by leaving input and output functions exposed on the top side of the module. When system requirements are known, the modules can be programmed to perform a specific function by the appropriate welding or soldering of the exposed connections on the top side of the module.

Figs. 10 and 11 show two programmable modules that have been designed to handle the *nand* gate and flip-flop discussed in the circuits section of this article. The module of Fig. 10 is shown prior to encapsulation. This module is designed to fasten to a master printed-circuit board by soldering the twenty leads to forked terminals mounted on the opposite side of the board. Holes are provided in the master printed-circuit board for feeding the leads through. The side of the module facing the front of the picture is the programmable side. After intramodule connections are made, the wires would be clipped.

The module of Fig. 11, called Wirecon, utilizes a molded header housing thirty connector terminals and leads. Most of the terminal leads extend to the back of the module for intramodule programming. This module and associated header were designed and developed by the Electro-Mechanical Engineering Section at JPL.

Fig. 12 shows the contents of the Wirecon gate module. It is possible, with this assignment of gate legs and

diode clusters, to implement almost all of the DAS gating functions with little or no loss of gate utilization. In most cases, there will be diode clusters and/or gate inputs available in each module for future system expansion or last-minute system changes. The feasibility of the utility module has been demonstrated by assigning logic functions from past, present, and proposed DAS's to the module and noting the application of programmability and gate usage.

The modules discussed here are still in the developmental stage and are thus subject to further evaluation. It is worth noting, however, that the use of the utility module shows promise for improvement in the packaging problem areas previously discussed:

(1) Module simplification. Fewer different module types are possible, resulting in easier fabrication, testing, and reworking.

(2) System interconnection. The programming feature reduces considerably the congestion of intermodule wires by making the connections an integral part of the module.

(3) Flexibility. The ability to accommodate a large number of system changes is enhanced. In some instances, a module can be completely reprogrammed without altering the system cabling. In
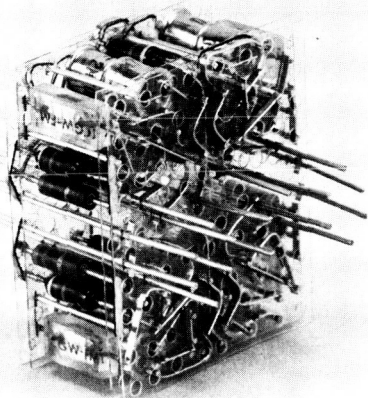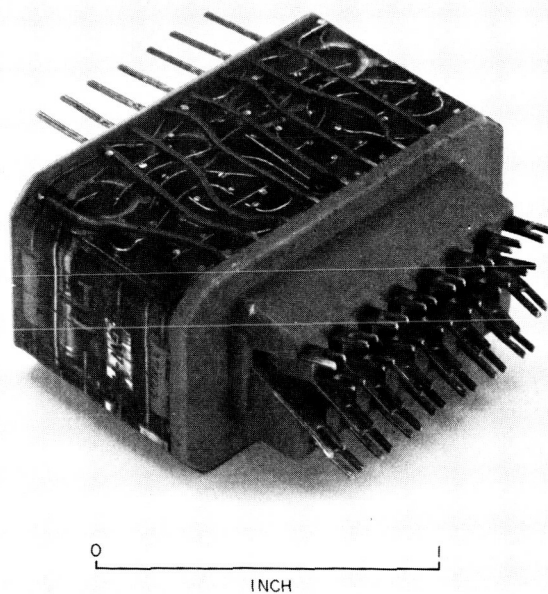

Fig. 10. Programmable flip-flop module

0   1
INCH

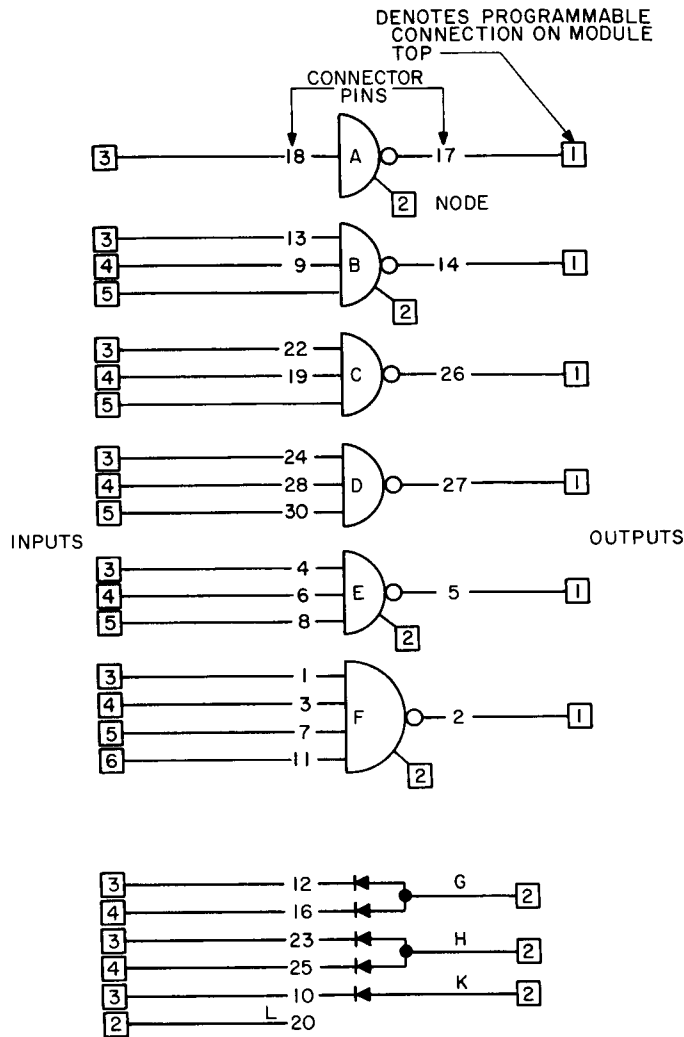Fig. 11. Programmable Wirecon flip-flop module

Fig. 12. Programmable Wirecon gate module

other instances, spare gate legs and diode clusters can be used to accommodate a system change.

Further feasibility of the module packaging concepts discussed here will be demonstrated by mocking up a 6- × 6-in. tray from portions of the UV spectrometer DAS logic diagram. Full utilization will be made of the programmable features of the modules.

4. Logic

The logical design of the DAS for the UV spectrometer instrument is essentially complete. In achieving the logical design, several constraints were imposed in an attempt to cope better with the special problems associated with a DAS. These constraints (design goals) and related discussion are listed herewith:

a. Logic circuit constraints. The logical design was restricted to the use of three basic logic elements. These are the *set-reset* flip-flop, *nand* gates, and noninverting driver described in the circuits section of this report.

b. Mission independence. Although the logic was designed specifically for the UV instrument, the generation of timing and control signals was extended to include all possible subperiods of a DAS frame with fixed length. In effect, this allows for instruments of unknown timing requirements to be added at a future date. It turns out that the capability of providing these additional timing functions does not significantly increase the hardware required to control only the UV spectrometer instrument.

c. Synchronous logic. Clocked memory elements were used wherever possible. This arrangement reduces the constraints of critical races and hazards when the logic elements are used within their design capabilities.

The choice of logic techniques used for scaling, counting, shifting, etc., was governed primarily by the restriction of logic element types and the need to minimize hardware, where possible. As a result, feedback shift registers (Ref. 2) are used in most scaling, counting, and shifting operations. The serial nature of the DAS data lends itself quite well to the use of this type of shift register.

An electrical breadboard of the UV spectrometer DAS is being assembled. The breadboard includes a modified *Mariner C*, discrete core, buffer pair with a capacity per buffer of 1320 bits. Also included will be a Kinelogic tape recorder capable of storing more than 10^6 bits. The entry and retrieval of data from the recorder is based on the system described in *SPS 37-27*, Vol. IV, pp. 101–107. The logic is being breadboarded, using actual flight circuits wired on small plug-in cards. All the logic circuits mentioned earlier have been laid out on these cards, giving the logic designer valuable breadboarding capability. The card shown in Fig. 13 is a flip-flop card containing four circuits, all of which are fabricated with flight-qualified components. Other cards available include:

(1) Expandable *nand* gate card.

(2) Power amplifier (driver) card.

(3) Crystal oscillator card.

Enough cards are being fabricated to breadboard a system containing 100 flip-flops, 100 *nand* gates, and 50 drivers.
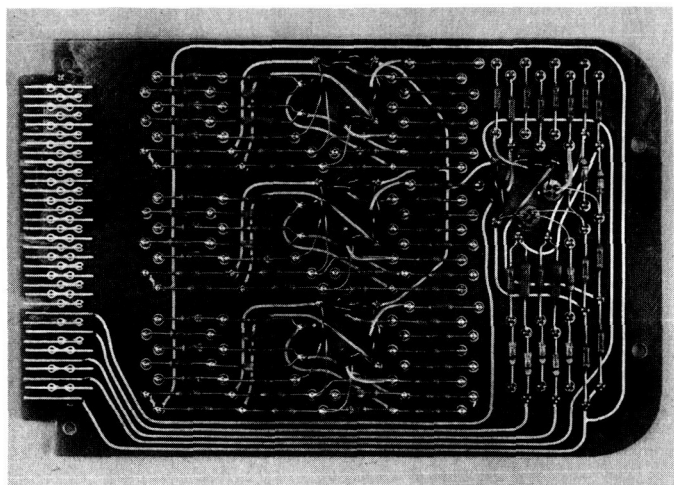
Fig. 13. Flip-flop logic card

To complete the breadboarding capability for this task, a logic applications manual is being compiled that will completely specify all the logic circuits with regard to fan-in, fan-out, capacitive loading, etc. Any special logic rules, such as how to avoid logic hazards, etc., will be included. The objective is to supplement the circuit design and logic cards with sufficient documentation to enable a logic designer to design a system with a minimum amount of effort.

5. Buffer Memory

A survey is presently being conducted to explore the applicability of the many memory techniques to the data-handling problem. Considerations include packaging, shock, sterilization, etc. The results of this survey will be the subject of a later report.

6. Tape Recorder

Many items of the necessary supporting technology are covered by mission-independent SRT (supporting research and technology) tasks and by the spacecraft central bulk-storage tasks. The items specifically supported by the *Mariner* 1966 task and its extension are listed below:

(1) Modification of an obsolete recorder to serve as part of the UV DAS breadboard is in process.

(2) A subcontract has been let to the Kinelogic Corp. to design and fabricate a recorder which will bene-

fit from other studies being conducted by JPL and which will exhibit state-of-the-art reliability characteristics. The basic design is the reel-to-reel, "Iso-Elastic" drive principle developed by the Kinelogic Corp.

(3) A study of drive belts, including the development of fatigue-life curves and information concerning belt fabrication necessary to predict fatigue life, is 80% complete at the Kinelogic Corp.

(4) An electrical analog of the tape transport mechanism used in items (1) and (2) above has been developed and is currently being used to aid in the understanding of transport phenomena (contract assistance by Kinelogic). An extensive environmental test program has been applied to the Rocket-radar recorders. Tests include type-approval vibration and thermal-vacuum (*Mariner C* levels) tests, operational life tests, and dormancy tests. A significant discovery to date is that defective manufacturing techniques are the major deterrent to operating life and that, once these are eliminated by proper quality assurance procedures, the recorders tend to run more or less indefinitely.

(5) When operating at elevated temperatures, tape-head contact develops some problems involving friction or sticking. A study of head and tape materials is in process at the Applied Magnetics Corp.

(6) The development of documentation for the procurement of future flight recorders is under way. This effort will include inputs for a request for proposal, especially quality assurance requirements, and would also provide a potential contractor with all of the design data and testing procedures developed by JPL and its study contractors. This effort is about 5% complete.

7. Future Activities

In addition to completing the projects described herein, additional tasks will be undertaken in the remaining months of FY 1965 to further the development of data-handling capabilities. These activities will include: circuit failure-mode analysis, system failure-mode analysis, the generation of module screening test procedures, and further evaluation of packaging techniques.

References

1. *Digital Logic Family Study Final Report*, Document No. 64-SD-4331, General Electric Co., Valley Forge Space Technology Center, Philadelphia, Pa., August 1964.

2. Chow, P. E. K., and Davies, A. C., "The Synthesis of Cyclic Code Generators," *Electronic Engineering*, pp. 253–259, April 1964.